Modeling of chlorosomal light-harvesting antennae: molecular control of self-assembly of chlorins, resolved by MAS NMR

Boer, Ido de

Modeling of chlorosomal light-harvesting antennae: Molecular control of self-assembly of chlorins resolved by MAS NMR

PROEFSCHRIFT

ter verkrijging van
de graad van Doctor aan de Universiteit Leiden,
op gezag van de Rector Magnificus Dr. D.D. Breimer,
hoogleraar in de faculteit der Wiskunde en
Natuurwetenschappen en die der Geneeskunde,
volgens besluit van het College voor Promoties
te verdedigen op woensdag 1 december 2004
klokke 16.15 uur

door

Ido de Boer

geboren te Heerlen

in 1976

Promotiecommissie

Promotor:	Prof. dr. H. J. M. de Groot
Referent:	Prof. dr. A. P. M. Kentgens, Radboud Universiteit Nijmegen
Overige leden:	Dr. T. J. Aartsma
	Prof. dr. ir. J. G. E. M. Fraaije
	Prof. dr. J. Reedijk
	Prof. dr. H. Tamiaki, Ritsumeikan University, Kusatsu, Japan

Modeling of chlorosomal light-harvesting antennae:

Molecular control of self-assembly of chlorins resolved by MAS NMR

Contents

Contents

List of abbreviations

1D (*n*D)	one-dimensional (*n*-dimensional)
BChl	bacteriochlorophyll
CD	circular dichroism
Chl	chlorophyll
cif	crystallographic identification file
CP	cross polarization
CSA	chemical shift anisotropy
DFT	density functional theory
FWHM	full width at half maximum
IUPAC	international union of pure and applied chemistry
LG	*Lee Goldburg*
MAS	magic angle spinning
MCD	magnetic circular dichroism
NMR	nuclear magnetic resonance
PMLG	phase modulated *Lee Goldburg*
rf	radio frequency
RFDR	radio frequency-driven dipolar recoupling
TPPI	time-proportional phase incrementation
TPPM	two pulse phase modulation
VACP	variable amplitude cross polarization
WISE	wideline separation

Preface

In the photosynthetic apparatus of green bacteria the light-harvesting is performed by chlorosomes, vesicles attached to the inner side of the membrane. The tubular elements filling the chlorosomes are the light absorbing antennae. The structure of these antennae is controlled by self-assembly of BChl *c* molecules. This is of interest from a biological point of view, since it is an example of how fundamental physical and chemical principles can determine the make-up of a biological function. To understand the relation between the molecular building blocks and the resulting suprastructure it is essential to resolve the driving factors behind the assembly process. This is also of great interest in the materials and nanotechnology field, where supramolecular assemblies are constructed for novel functionalities. The structures that can be built by manipulating all atoms or molecules individually are practically limited. On the other hand, by changing the properties of the constituting molecules a variety of suprastructures can be generated in a self-assembly process. The chlorosomes, for example, constitute a biological light concentrator that may inspire the construction of future photovoltaic devices.

This thesis presents a study of self-aggregates of modified chlorophylls. The suprastructures are models that help to elucidate the molecular mechanisms steering the self-assembly in the chlorosomal antennae. The structures of these self-assemblies are resolved by solid-state Magic Angle Spinning (MAS) NMR, which is a rapidly emerging technique to determine the structure of ordered systems without long-range translation symmetry, and its suitability for resolving structure of chlorophyll assemblies has been demonstrated recently. To improve upon the existing methodology for 3D structure determination and to establish the necessary MAS NMR tools for the aggregate studies, a substantial part of this thesis has been devoted to the development of novel MAS NMR techniques. First, a 2D experiment was implemented to detect intermolecular structural restraints that serve to reduce the number of ways that a space-filling structure can be realized in a modeling step. Second, the ring current shifts that arise in aromatic systems are very sensitive to the supramolecular structure. Calculations are performed to

reproduce the observed ring currents quantitatively by taking into account long-range effects up to ~24 Å. In this way the 3D model of the structure and the suprastructure can be validated. In a converging process, a local crystal structure is determined.

With the help of the structures of the model aggregates obtained with the MAS NMR, key molecular factors steering the self-aggregation *in vivo* can be resolved and validated. On the one hand, the local structural organization is constrained by a strong intermolecular bonding network. This produces bottom-up control over the suprastructure by the molecular building blocks. On the other hand, the modeling studies suggest that terms in the free energy balance associated with larger distances, leading to the formation of tubular micelles, are also an important factor for the supramolecular organization. In an upward causal process, the elementary biological building blocks interact to generate functionality at a higher organizational level. This is constrained by the environment in which the smaller elements operate in a downward causal or feedback process. The balance between these two forms a regulating mechanism that is essential to provide a robustness of the biological system against various perturbations. Hence in a broader biological context, the simple chlorosome system provides insight on how physicochemical interactions between different levels of hierarchical complexity can lead to stability in the living world.

Chapter
1

Introduction§

1.1   The chlorosomes

Chlorosomes are found in photosynthetic green bacteria as ellipsoid vesicles of about 100-300 nm in length attached to the inner surface of the cytoplasmic membrane (Fig. 1.1), where they provide a large cross-section for the absorption of sunlight [1, 2]. The chlorosomes contain rod-shaped elements of 5 nm in diameter for *Chloroflexus* and 10 nm for *Chlorobium* as visualized by electron microscopy [4, 5]. The assumption that the rods are formed by protein-pigment complexes, as found in other photosynthetic
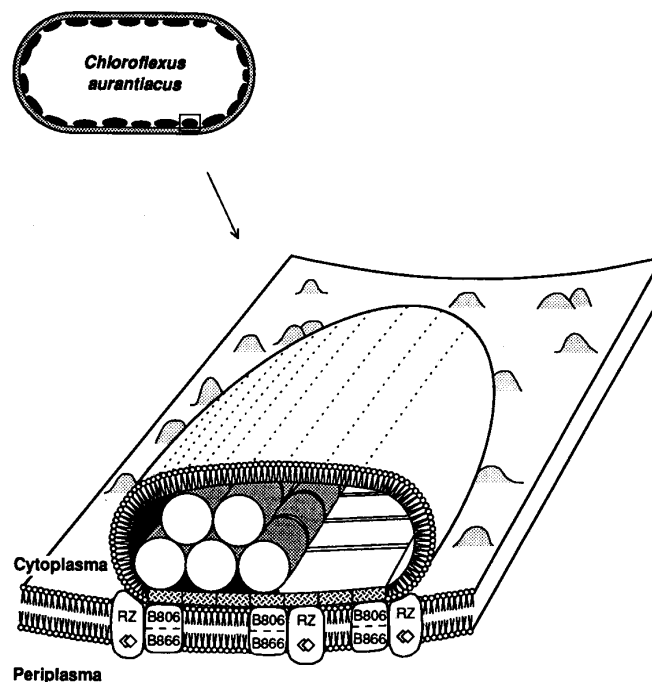

Fig. 1.1. Schematic representation of the chlorosomes in Chloroflexus aurantiacus with the enlarged picture showing the antennae [3].

§This chapter has been accepted in part for publication in *Chlorophylls* (*2ⁿᵈ ed.*) (H. Scheer, Ed.), Kluwer.

elements, has been challenged by increasing evidence that self-organized BChl *c* (Fig. 1.2) is responsible for the shape and function of the antennae [2, 4-9]. The crucial evidence is that the *in vitro* aggregation of BChl *c* leads to similar structures and spectroscopic properties as occur in the natural system (for review, see *e.g.* ref. [10]). Small-angle neutron scattering studies have indicated cylindrical shaped micelles for aggregates prepared in organic media [6]. In addition, various spectroscopic methods suggest a highly ordered structure of both aggregated BChl *c* and the chlorosomes [8, 11, 12]. Molecular modeling has also been used to explain the structural features of the cylindrical micelles [13]. For the chlorosomes, an intermolecular bonding network has been proposed, where the 3^1-hydroxy group of BChl *c* coordinates to the central metal of a neighboring BChl *c* molecule and also hydrogen bonds with the 13^1 carbonyl-oxygen of yet another BChl molecule [13, 14].

1.2 Aggregated Chl *a*/H$_2$O as a model for MAS NMR technology development

In the past, NMR has contributed significantly to the study of chlorophyll chemistry in solution, which was reviewed extensively (see *e.g.* ref. [15]). Two different routes have been worked out to use NMR data for structure determination in uniformly ^{13}C-labeled chlorophylls in the solid state. First, the chemical shift assignment obtained from correlation experiments can provide information about the spatial structure. This is
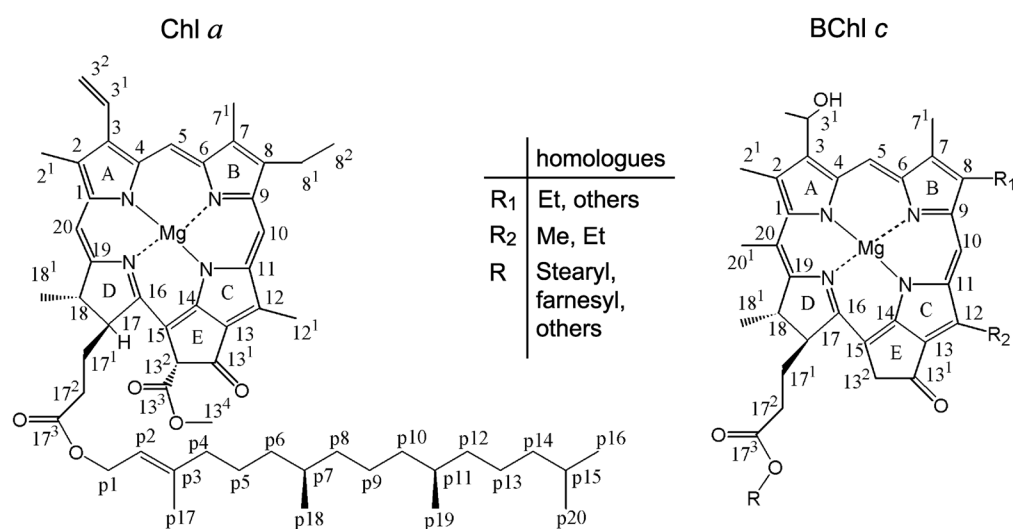
Fig. 1.2. Chemical structures of Chl a and the BChl c homologues.

consistent with the early analyses of the stacking in small chlorophyll aggregates from ring current shifts [15]. In particular, ^{1}H aggregation shifts are important for the purpose of structure determination. The chemical shift of ^{1}H is relatively insensitive to electronic perturbations, while shifts induced by ring currents are large on the ^{1}H shift scale of 10-15 ppm. In a similar way, the ring current shifts are indispensable for structure elucidation in the solid state. Second, structural information in the solid state may be obtained from the measurement of distance restraints revealing close contacts between molecular moieties.
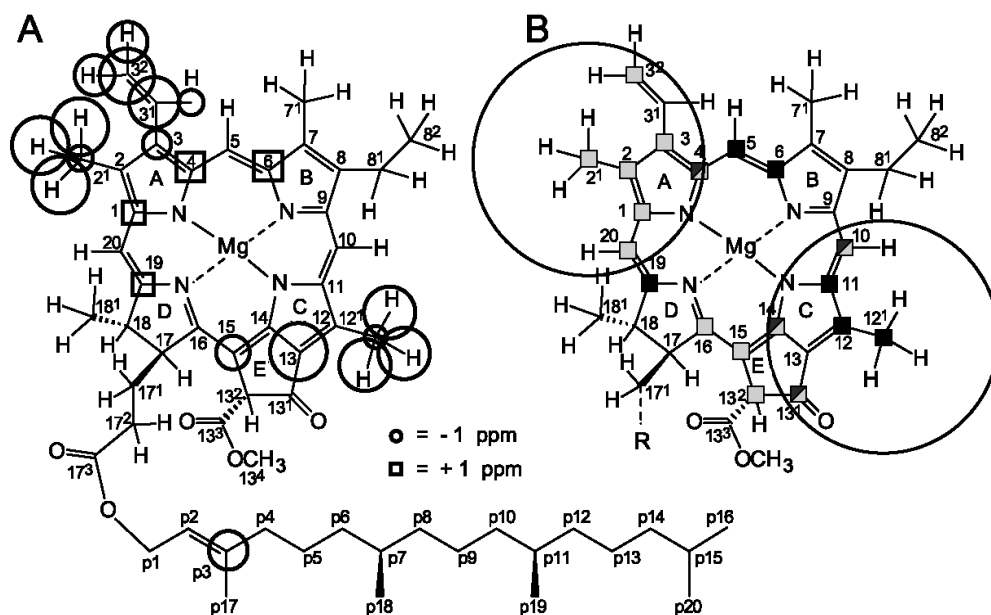
Fig. 1.3. (A) Visual representation of the carbon and proton aggregation shifts (Δσ) for aggregated Chl a. The circles around the carbon and hydrogen atoms represent upfield aggregation shifts, squares represent downfield shifts. The sizes of the circles and squares reflect the magnitude of the aggregation shifts. (B) Schematic representation of the assignment of heteronuclear correlations involving the 2^1-H₃, which are shown in shaded grey or the 12^1-H₃, which are solid black. For the 4-C, 10-C, 13^1-C and 14-C the correlations with proton signals are assigned to transfer from both methyl groups. The ranges for intramolecular transfer for the two methyl groups are indicated with the circles. Intramolecular correlations involving the 3^1-C and 13-C could not be assigned. Reprinted from ref. [19].

Much of the MAS NMR methodology was first tested using a Chl a/H$_2$O aggregate and then applied in a second step to study the structure of the chlorosomes. The Chl a/H$_2$O aggregate is very suitable to develop and evaluate novel pulse sequences. As a moderately-sized molecular system, it represents an intermediate between small model compounds, such as the tyrosine HCl salt, that are frequently used for a demonstration of principles of pulse techniques, and larger systems of genuine biological interest. The aggregation of Chl a and the Chl-water interaction in Chl a/H$_2$O micelles has been extensively studied in the past [16]. Chl a can only form solid aggregates by incorporation of H$_2$O, which is believed to coordinate the central magnesium atom and form hydrogen bonds with the carbonyl functions of surrounding molecules. Recent MAS NMR results suggest a close homology between the structure of Chl a/H$_2$O and crystalline ethyl-chlorophyllide a, with two water molecules forming the bridging network [17-19].

Complete ^{1}H and ^{13}C assignments were obtained in a field of 14.1 T using the ^{13}C-^{13}C RFDR and ^{1}H-^{13}C LG/CP methods [19]. The ^{13}C line widths are small (120-200 Hz) revealing a rigid and well-ordered structure. The ^{1}H and ^{13}C shifts of the monomer in solution were used to estimate the aggregation shifts (Fig. 1.3). Upfield aggregation shifts
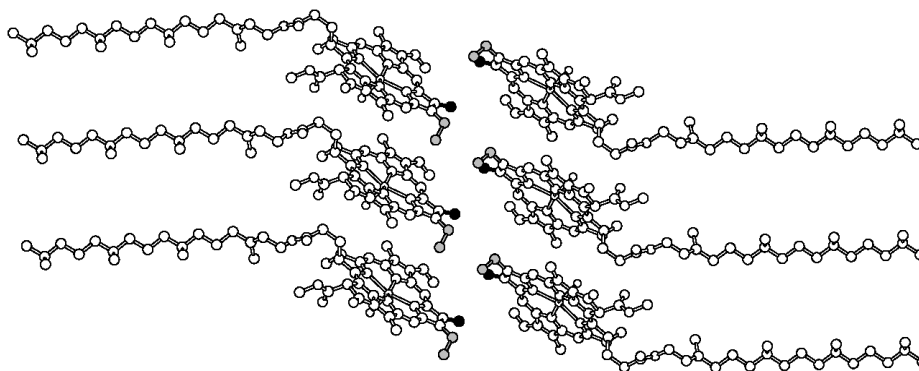
Fig. 1.4. Schematic representation of a bilayer formed from two sheets of microcrystalline aggregated Chl a/H$_2$O [19]. The two sheets consist of stacks of Chl a perpendicular to the paper. The 7-Me and 8-Et moieties are shown in black and grey, respectively.

up to ~5 ppm are observed, mostly induced by ring currents. The shift pattern is in agreement with models for the Chl a/H_2O aggregates that assume strong overlap between the ring A and the rings C and E of adjacent molecules forming stacks [6]. In addition, in a 2D ^{13}C-^{13}C RFDR spectrum recorded with a long mixing time of $\tau_m = 10$ ms, several cross-peaks are observed that can be attributed to intermolecular transfer [17].

Heteronuclear ^{1}H-^{13}C spectra were recorded with long LG-CP times to generate intermolecular correlations [19]. For a LG-CP time of 2 ms, a maximum transfer distance (d_{max}) of ~4.2 Å was estimated from an analysis of the correlations involving the 2^1-H_3 and 12^1-H_3 protons. Weak transfer was observed from the 2^1-H_3 protons to the 10, 13^1, 13^2, 14, 15 and 16 carbons at the opposite side of the molecule (Fig. 1.3B), which was assigned to intermolecular contact over distances ~4 Å. Similarly, weak correlations between the 12^1-H_3 protons and the 4, 5, 6 and 19 carbons indicate intermolecular transfer. They confirm the 2D arrangement of the Chl a in sheets (Fig. 1.4).

Finally, ^{1}H signals, correlating with similar bridging moieties in the heteronuclear MAS NMR spectra, could be assigned to structural water similar to ethyl-chlorophyllide a. In addition, a small doubling of the 7-C, 7^1-CH_3 and $8^{1,2}$-C was resolved. This provides evidence for two marginally different well-defined molecular environments at the interface between two layers (Fig. 1.4).

1.3 Self-organization of BChl is the main structural feature of the chlorosomal antennae

A complete ^{13}C assignment was made for the NMR response of the chlorosomes and various BChl c homologues from the uniformly ^{13}C labeled chlorosomes of *C. tepidum* [7]. 2D ^{13}C-^{13}C RFDR dipolar correlation spectra of solid BChl c aggregated in hexane and the chlorosomal antennae are depicted in Fig. 1.5 [7, 20]. Many peaks are resolved in the spectra, and the two spectra are almost identical. The predominant component of the MAS NMR signals in the chlorosomes is from BChl c. Only a minor fraction is observed in the chlorosomes that is not present in the aggregate. These peaks are attributed to lipids

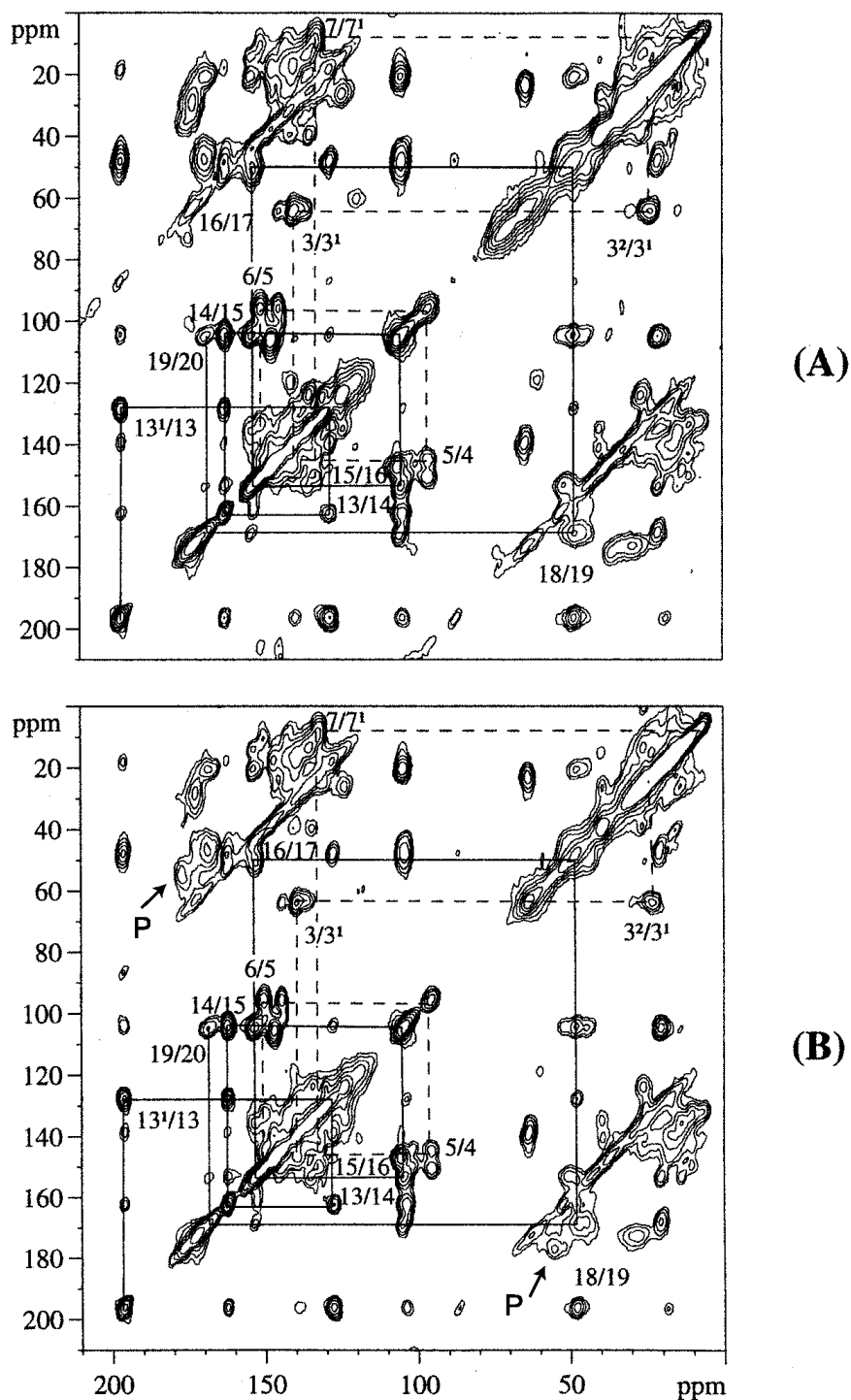*Fig. 1.5. Contour plots of 2D MAS NMR dipolar correlation NMR spectra of uniformly ^{13}C labeled BChl c aggregates (A) and ^{13}C labeled chlorosomes (B), recorded in a magnetic field of 9.4 T. The MAS rate was 11 kHz and a CP time of 1 ms was used. The lines indicate sequences of nearest neighbor correlations. A small protein fraction in (B) is indicated with P. Reprinted from ref. [20].*

and proteins in the chlorosomes. Correlations between the carbonyl and α carbons of a small protein component are indicated in Fig 1.5.

The 2D response of the BChl *c* in intact chlorosomes is virtually indistinguishable from the data collected from the *in vitro* aggregate with respect to chemical shifts, line widths and relative intensities of the cross-peaks. This demonstrates that the minor fractions of proteins and lipids are not an integral part of the BChl *c* assembly [7, 20]. In this way, the NMR data provide conclusive evidence that self-assembly of BChl *c* is the structural basis for the BChl *c* organization *in vivo*, without the intervention of proteins.

In earlier 1D MAS NMR experiments, solid BChl *c* was also compared with the chlorosomes, providing the first evidence for the same aggregated forms [21-23]. The T_{CH} and $T_{1\rho}^{H}$ values were also comparable for both samples, which corroborates the structural correspondence between the aggregate and the natural system.The observation that a biological function can be realized without active participation of protein can be considered anomalous, since the central dogma of molecular biology states that all function originates from the DNA code via protein: DNA $\rightarrow$ RNA $\rightarrow$ protein $\rightarrow$ function. In a chlorosome, the biological function of the antennae is based on self-assembly steered by the physicochemical properties of the constituting molecules and top-down control from higher levels in the biological hierarchy. Other examples of this principle have been encountered in the past, such as biomineralization of inorganic matter into a morphology controlled by the organism [24]. For instance, the magnetite crystals in the magnetosomes of magnetobacteria correspond to single magnetic domains of 40-120 nm, and allow the bacteria to orient themselves using the earth magnetic field.

The self-organization of BChl *c* may be of interest for artificial photosynthesis. Although the actual application of artificial molecular solar energy converters may still be years away, elucidation of the concepts behind nature's efficient energy converting system will be of use to photovoltaics and molecular electronics research. In particular, the discovery of natural light-harvesting systems without proteins may be of help to indicate novel routes in photovoltaics research.

To produce aggregates resembling the chlorosomes, the solvent used in the process is essential. In particular, the effect of different solvents to form solid aggregates of $[3^1R]$ BChl *c* was recently studied [25]. Various techniques including ^{13}C CP/MAS were applied to investigate the size and order of the aggregates formed after drying in diethyl ether, CH_2Cl_2, CCl_4 or CH_2Cl_2 in an excess of hexane. From the MCD spectra, the aggregates treated with CCl_4 and hexane were estimated to be larger than those with diethyl ether and CH_2Cl_2. The CD spectra show differences between the CH_2Cl_2-treated aggregates and the diethyl ether and CCl_4-treated samples, indicating a different molecular arrangement. In addition, the BChl *c* treated with CH_2Cl_2 is weakly diffracting by X-ray, similar to methyl-BChlide *c* formed in hexane. This suggests that the tails leave the stacking of the BChl *c* intact. In addition, recent MAS NMR experiments revealed two distinct sets of resonances for a CH_2Cl_2-treated uniformly ^{13}C and ^{15}N labeled $[3^1R]$ BChl *c* aggregate, which are attributed parallel and antiparallel stacking, based on model studies for closed dimers of BChl *c* [26].

1.4   A 3D model for the structure of the chlorosomal antennae

The structure of the chlorosomal antennae of *Chlorobium tepidum* was recently investigated with 2D and 3D MAS NMR. The ^{13}C shifts of BChl *c* assigned from the 2D RFDR experiments provided the first step to a structural model [7]. The relatively large ^{13}C line widths contrast with the microcrystalline Chl *a*/H_2O aggregates and reveal significant disorder down to the microscopic level. Large ring current shifts are detected in the regions of rings A, C and E (Fig. 1.6). [13]C-^{13}C RFDR experiments were performed, using long mixing times of 5-10 ms [20, 27]. Correlations between the 13^1-carbon and the 19-, 20-, 1-, 2- and 3-carbons were attributed to intermolecular transfer and appear to confirm the layer structure. In addition, rotational resonance experiments show that the $C3^1$-$C13^1$ distance is similar to the $C20$-$C3^1$ distance, in accordance with hydrogen bonding between the 3^1 and 13^1 groups [23].

Introduction

The ¹H shifts of the BChl *c* were determined in a 3D experiment using rapid MAS in combination with a high magnetic field. Under these conditions, it was shown that proton shifts can be determined. Intermolecular heteronuclear correlations as well as hydrogen–bonding characteristics can already be determined with simple pulse schemes such as the WISE technique [28]. Since the chlorosome response is considerably inhomogeneously broadened, a 2D ¹³C-¹³C RFDR experiment was extended in a straightforward fashion by a third ¹H WISE dimension to construct a 3D ¹H-¹³C-¹³C MAS NMR experiment [9]. As a result, all ¹H resonances of the chlorosomes could be assigned. The ¹H aggregation shifts (Fig. 1.6) are consistent with the ¹³C pattern. Two fractions **I** and **II** are observed in the NMR dataset. In both fractions, two regions with pronounced upfield shifts are visible around ring A and C/E. In addition, for fraction **II**, large upfield shifts for the 5-C and the 7-Me are detected. This suggests the existence of two distinct structural arrangements, related to the rod-like suprastructure in the chlorosomes.
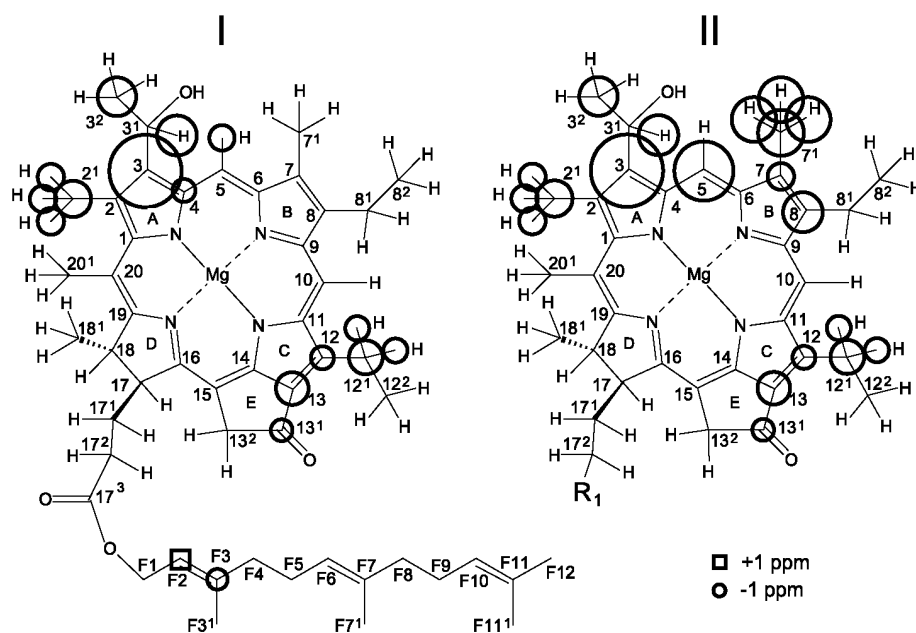
*Fig. 1.6. Carbon and proton aggregation shifts $|\Delta\sigma_i| \geq 1.5$ ppm of BChl c with $\Delta\sigma_i = \sigma_i - \sigma_{liq}$. The NMR response comprises two components, denoted **I** and **II**. The circles around the carbon and hydrogen atoms represent upfield aggregation shifts, the squares downfield aggregation shifts. The size of a circle or square is proportional to the magnitude of the aggregation shift. Reprinted from ref. [9].*

The chemical shift data were used to refine the structural model for the chlorosomes. First, the molecular structure was optimized by quantum chemical calculations for the $(3^1\ R)$ or $(3^1\ S)$ stereoisomers using methanol as a fifth ligand. The Mg ion can be positioned at the same side of the porphyrin plane as the 17^1-C (*syn*) or at the opposite side (*anti*). The two energetically most favorable forms are the $(3^1\ R)$-*anti* and the $(3^1\ S)$-*syn* combinations. Stacks of molecules of the *syn* or *anti* type can be formed by successive
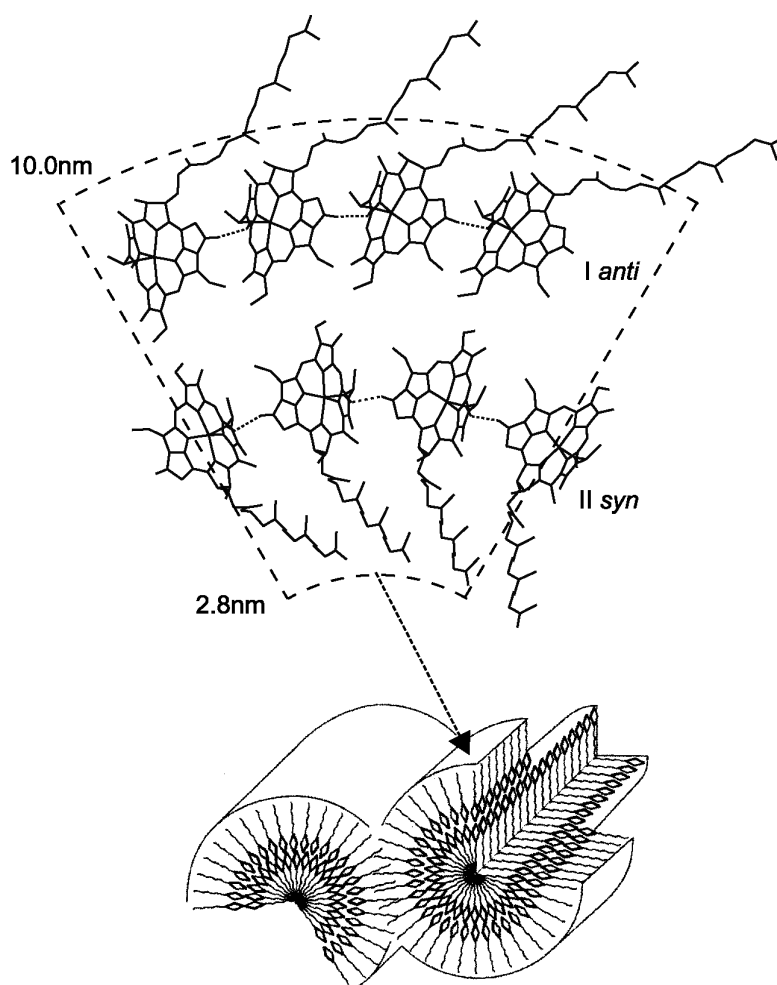
*Fig. 1.7. Schematic representation of a radial wall section of a bilayer tube formed from curved 2-D sheets of anti (**I**) and syn (**II**) stacks. The chlorin rings are completed with the farnesyl tails, which were not included in the ab initio calculations. The curvature leads in a natural way to the dimensions determined with electron microscopy. The direction of the stacks is perpendicular to the plane of the paper. The dotted lines indicate hydrogen bonds between 13-C=O and 3^1-OH of adjacent stacks. In reality, the interface between the outer and inner tube is expected to be more dense than in this schematic representation, to account for the aggregation shifts of the 7^1 methyls*

coordination of the 3^1-OH to the Mg of the next molecule (Fig. 1.7). From model studies, it was concluded that the ratio between the two stereoisomers can vary considerably. Provided a minor fraction of either form is present, the rods can be formed [29]. This suggests that both species can be accommodated in a stack by rotating the 3-side chain.

The stacks can be combined to form layers by hydrogen bonding between the 3^1-OH groups of one stack with the 13-C=O of a neighboring stack. Heteronuclear transfer was observed in a 2D ^{1}H-^{13}C dipolar correlation experiment to the 13-C=O that may originate from the 3-moiety [9]. Evidence for this has also been found from the CP build-up of the 13^1 carbon signal in the chlorosomes of *Chloroflexus aurantiacus* and in the hexane treated aggregate. It was concluded that the 13^1 carbonyl is hydrogen bonded, probably to the hydroxyethyl group at the 3 position [21].

Based on the NMR results, a bilayer tube model was proposed for the chlorosome rods in *Chlorobium tepidum*, where a predominantly *syn* layer forms the inner tube with the tails filling the center, while a layer of *anti* character constitutes the outer tube with the tails pointing away from the surface (Fig. 1.7) [9]. In the *anti* conformation, the layer of BChls corresponds to the model of Holzwarth et al., where the tails are directed outward [13]. The layer formed from *syn* stacks has an opposite curvature with the tails directed inward. The existence of two different parallel chain stacks with *syn* and *anti* configurations has also been detected by NMR in solution [30]. The two different layers (Fig. 6) have virtually identical aggregation shifts. Evidently, the overlap in both cases is similar and induces the same ring current shifts. The bilayer model is supported by electron microscopy, since the rod-shaped structures with an outer diameter of 10 nm and an internal hole of 3 nm can be formed easily from the bilayer tube inferred from the MAS NMR data. Calculations of optical spectra based on a single outer layer can explain the measured spectra satisfactorily, and refinements including the bilayer are expected [32, 33].

For the bilayer tubes, an intensity ratio between components **I** and **II** of approx. 3:2 is observed [9]. The splitting of the chemical shift pattern was explained by an interaction

between *syn* and *anti* layers yielding a different electronic environment. The component **I** in the NMR spectra was attributed to a (3^1R) *anti* structure and the component **II** to a (3^1S) *syn* structure. The upfield shifts around the 7-CH$_3$ in component **II** may reflect a different structural arrangement for the 7-Me groups at the interface of the layers leading to an extended overlap for this component only. Finally, comparison of the proton responses of the farnesyl chain of BChl *c* with the phytyl chain of self-aggregated Chl *a*/H$_2$O reveals significant excess line broadening of the BChl *c* proton signals, suggesting that the farnesyl chain may exhibit some random folding. On the other hand, it was demonstrated that the NMR relaxation parameters of the farnesyl chain are highly similar to those of the rigid ring system, from which it was concluded that at least a substantial fraction of the farnesyl chains should be relatively immobile [34]. This is consistent with the bilayer tube model of Fig. 1.7, since it can be expected that at least the fatty tails on the inside will be rigidly held in place.

1.5   Thesis scope

Recent progress in resolving the nature of the chlorosomal antennae that has been acquired by MAS NMR studies has been discussed. In addition, the strategy for structure elucidation of chlorophyll aggregates using MAS NMR, which has been developed primarily on a Chl *a*/H$_2$O model system, was summarized. It has been found that the chlorosomes consist mainly of aggregated BChl that is indistinguishable from BChl *c* precipitated from hexane. Based on MAS NMR experiments, a bilayer tube model for the chlorosomes has been proposed. The next step, which is the main scope of this thesis, is to explain the self-assembly process.

With a combination of chemical shift data and intermolecular constraints, detailed information about the structure of chlorosomes and solid chlorophyll aggregates can be obtained. In this thesis, both routes to structural information will be further explored. **Chapter 2** provides an overview of the principles that were used for novel NMR methodology.

The intermolecular ^{1}H-^{13}C correlations provide direct structural information in terms of close contacts between molecules. A few contacts strongly reduce the number of possible space filling arrangements for the chlorophyll aggregates. **Chapter 3** presents a 2D MAS NMR experiment for the collection of intermolecular ^{13}C-^{13}C correlations in uniformly labeled systems. This experiment is first applied to the Chl *a*/H$_2$O aggregate, where it refines the structure of Fig. 1.4 in showing that the phytyl tails are stretched and interdigitating.

Access to the proton chemical shifts of aggregated chlorophylls allows accurate probing of ring current effects. This can be related to the stacking of the macrocycles. In **chapter 4**, it is demonstrated how a quantitative analysis of the ^{1}H ring current shifts, in conjunction with intermolecular distance restraints, can be used to establish a local crystal structure of a chlorophyll aggregate.

For the study of the chlorosomes, MAS NMR has been proved to be a valuable tool, and the model structure of Fig. 1.7 is increasingly accepted (see *e.g.* refs. [35-37]). MAS NMR in conjunction with other spectroscopic methods and microscopy provide converging evidence for the bilayer tube model of Fig. 1.7. One key remaining issue is to prove that specific side chains can steer the supramolecular structure through the aggregation process. In particular, the role of the [3^1*R*] and [3^1*S*] stereoisomers, the long ester tails and their interplay appears to be important. **Chapter 5** discusses the self-assembly of BChl *c* in the chlorosomes, and the key molecular factors controlling this process. This is accomplished by a MAS NMR study of two self-assembled chlorin systems that are modified with respect to the natural BChl *c*. Finally, the conclusion of this work and the future prospects are presented in **chapter 6**.

References

[1]   R.E. Blankenship, J.M. Olson and B. Miller, "Anoxygenic Photosynthetic Bacteria", Kluwer, Dordrecht (1995).

[2]   J.M. Olson, *Photochem. Photobiol.* **67**, 61-75 (1998).

[3] M.G. Müller. *Ph.D. Thesis,* Max-Planck-Institut für Strahlenchemie, 1991.

[4] L.A. Staehelin, J.R. Golecki, R.C. Fuller and G. Drews, *Arch. Mikrobiol.* **119**, 269-277 (1978).

[5] L.A. Staehelin, J.R. Golecki and G. Drews, *Biochim. Biophys. Acta* **589**, 30-45 (1980).

[6] D.L. Worcester, T.J. Michalski and J.J. Katz, *Proc. Natl. Acad. Sci. U. S. A.* **83**, 3791-3795 (1986).

[7] T.S. Balaban, A.R. Holzwarth, K. Schaffner, G.J. Boender and H.J.M. de Groot, *Biochemistry* **34**, 15259-15266 (1995).

[8] P. Hildebrandt, H. Tamiaki, A.R. Holzwarth and K. Schaffner, *J. Phys. Chem.* **98**, 2192-2197 (1994).

[9] B.J. van Rossum, D.B. Steensgaard, F.M. Mulder, G.J. Boender, K. Schaffner, A.R. Holzwarth and H.J.M. de Groot, *Biochemistry* **40**, 1587-1595 (2001).

[10] H. Tamiaki, M. Amakawa, A.R. Holzwarth and K. Schaffner, *Photosynth. Res.* **71**, 59-67 (2002).

[11] K. Griebenow, A.R. Holzwarth, F. van Mourik and R. van Grondelle, *Biochim. Biophys. Acta* **1058**, 194-202 (1991).

[12] K. Matsuura, M. Hirota, K. Shimada and M. Mimuro, *Photochem. Photobiol.* **57**, 92-97 (1993).

[13] A.R. Holzwarth and K. Schaffner, *Photosynth. Res.* **41**, 225-233 (1994).

[14] J. Chiefari, K. Griebenow, N. Griebenow, T.S. Balaban, A.R. Holzwarth and K. Schaffner, *J. Phys. Chem.* **99**, 1357-1365 (1995).

[15] R.J. Abraham and A.E. Rowan, in *Chlorophylls* (H. Scheer, Ed.) pp. 797-834, CRC Press, Boca Raton, FL (1991).

[16] J.J. Katz, M.K. Bowman, T.J. Michalski and D.L. Worcester, in *Chlorophylls* (H. Scheer, Ed.) pp. 211-235, CRC Press, Boca Raton (1991).

[17] G.J. Boender, J. Raap, S. Prytulla, H. Oschkinat and H.J.M. de Groot, *Chem. Phys. Lett.* **237**, 502-508 (1995).

[18] I. de Boer, L. Bosman, J. Raap, H. Oschkinat and H.J.M. de Groot, *J. Magn. Reson.* **157**, 286-291 (2002).

[19]   B.J. van Rossum, E.A.M. Schulten, J. Raap, H. Oschkinat and H.J.M. de Groot, *J. Magn. Reson.* **155**, 1-14 (2002).

[20]   G.J. Boender. *Ph.D. Thesis,* Leiden University, 1996.

[21]   T. Nozawa, S. Manabu, S. Kanno and S. Shirai, *Chem. Lett.* **1990**, 1805-1808 (1990).

[22]   T. Nozawa, M. Suzuki, K. Ohtomo, Y. Morishita, H. Konami and M.T. Madigan, *Chem. Lett.* **1991**, 1641-1644 (1991).

[23]   T. Nozawa, K. Ohtomo, M. Suzuki, H. Nakagawa, Y. Shikama, H. Konami and Z.Y. Wang, *Photosynth. Res.* **41**, 211-223 (1994).

[24]   E. Bäuerlein, *Angew. Chem.-Int. Ed.* **42**, 614-641 (2003).

[25]   M. Umetsu, Z.Y. Wang, J. Zhang, T. Ishii, K. Uehara, Y. Inoko, M. Kobayashi and T. Nozawa, *Photosynth. Res.* **60**, 229-239 (1999).

[26]   M. Umetsu, J. Hollander, Z.Y. Wang, T. Nozawa and H.J.M. de Groot, *J. Phys. Chem. B* **108**, 2726-2734 (2004).

[27]   B.J. van Rossum, G.J. Boender, F.M. Mulder, J. Raap, T.S. Balaban, A. Holzwarth, K. Schaffner, S. Prytulla, H. Oschkinat and H.J.M. de Groot, *Spectrochim. Acta* **A54**, 1167-1176 (1998).

[28]   B.J. van Rossum, G.J. Boender and H.J.M. de Groot, *J. Magn. Reson. Ser. A* **120**, 274-277 (1996).

[29]   D.B. Steensgaard, H. Wackerbarth, P. Hildebrandt and A.R. Holzwarth, *J. Phys. Chem. B* **104**, 10379-10386 (2000).

[30]   T. Mizoguchi, S. Sakamoto, Y. Koyama, K. Ogura and F. Inagaki, *Photochem. Photobiol.* **67**, 239-248 (1998).

[31]   D.L. Cruden and Stanier, *Arch. Microbiol.* **72**, 115-134 (1970).

[32]   V.I. Prokhorenko, D.B. Steensgaard and A.F. Holzwarth, *Biophys. J.* **79**, 2105-2120 (2000).

[33]   J. Psencik, Y.Z. Ma, J.B. Arellano, J. Hala and T. Gillbro, *Biophys. J.* **84**, 1161-1179 (2003).

[34]   B.J. van Rossum, B.Y. Van Duyl, D.B. Steensgaard, S.T. Balaban, A.R. Holzwarth, K. Schaffner and H.J.M. De Groot, in *Photosynthesis: Mechanisms*

and Effects (G. Garab, Ed.) Vol. I, pp. 117-120, Kluwer Academic Publishers, Dordrecht, the Netherlands (1998).

[35]   S.P. Brown and H.W. Spiess, *Chem. Rev.* **101**, 4125-4155 (2001).

[36]   J. Glaeser, L. Baneras, H. Rutters and J. Overmann, *Arch. Microbiol.* **177**, 475-485 (2002).

[37]   E.V. Vassilieva, V.L. Stirewalt, C.U. Jakobs, N.U. Frigaard, K. Inoue-Sakamoto, M.A. Baker, A. Sotak and D.A. Bryant, *Biochemistry* **41**, 4358-4370 (2002).

Chapter
2

Methodological background

2.1 Fast Magic Angle Spinning NMR in high magnetic field

Magic Angle Spinning (MAS) NMR structure determination of multispin labeled solids critically depends on both the resolution and the stability that can be obtained with the NMR spectrometer. In both aspects, important improvements have been realized in the past few years. The resolution was improved by fast MAS, high field and modern pulse technology. In particular, the recent realization of ultra high field spectrometer technology has boosted the development and implementation of novel structure determination methodology. The stability required to perform the new generation of experiments was achieved by improvements in the spectrometer electronics hardware, allowing fast, precise and coherent phase and frequency switching during the NMR experiment.

For a theoretical description of the NMR experiments, the Hamiltonian

$$H_S = H_{CS} + H_{II} + H_{IS} \qquad (2.1)$$

is used [1]. H_{CS} is the chemical shift term, H_{II} contains the homonuclear dipolar couplings and H_{IS} represents the heteronuclear dipolar couplings. Anisotropic spin interactions that are averaged to an isotropic part in liquids cause large NMR line broadening in solids. These are primarily the anisotropic part of the chemical shift and the dipolar spin-spin couplings. The chemical shift σ, for example, depends on the orientation of the chemical environment of the nucleus in the magnetic field.

The anisotropic interactions in solids can be eliminated by fast rotation of the sample around an axis at the magic angle $\theta_m \approx 54.74°$ with the static field [2, 3]. To calculate the effects of this rotation, a hamiltonian of anisotropic interactions is most conveniently expressed in irreducible spherical tensors as [4, 5]

$$H = \sum_k \sum_{q=-k}^{+k} (-1)^q A_{kq} \hat{T}_{k(-q)},$$ (2.2)

where the A tensors contain the spatial part, while the $\hat{T}$ tensors contain the spin terms. By rotation of the sample, the A tensors are transformed, which can be evaluated by applying the Wigner rotation matrices [4].

For the chemical shift, for example, Eq. [2.2] reduces in a strong magnetic field B_0 to

$$H_{CS} = A_{00}\hat{T}_{00} + A_{20}\hat{T}_{20},$$ (2.3)

with

$$\begin{cases} A_{00} = -\sqrt{3}\sigma_{iso} \\ \hat{T}_{00} = -\dfrac{1}{\sqrt{3}}B_0\hat{I}_z \\ A_{20} = \sqrt{\dfrac{3}{2}}(\sigma_{zz} + 2\sigma_{iso}) \\ \hat{T}_{20} = \sqrt{\dfrac{2}{3}}B_0\hat{I}_z \end{cases}$$ (2.4)

If the sample is rotated with frequency ω_r, only A_{20} becomes time dependent through σ_{zz}. A_{20} is transformed from the principal axis system to the laboratory system in two steps,

$$A_{20}^{PAS} \xrightarrow{R(\alpha,\beta,\gamma)} A_{20}^{Rotor} \xrightarrow{R(\varphi_0+\omega_r t,\theta_m,\psi)} A_{20}^{LAB}.$$ (2.5)

Methodological background

The first rotation is determined by the orientation of the chemical environment with respect to the rotor, while the second rotation introduces the spinning of the rotor. This yields

$$A_{20}^{LAB}(t) = \sum_{q=-2}^{2} A_{2q}^{PAS} \left[e^{-i\alpha q} d_{q0}^2(\beta) e^{-i\eta q} \right] \cdot \left[e^{-iq(\varphi_0 + \omega_r t)} d_{q0}^2(\theta_m) \right], \qquad (2.6)$$

where the d elements are defined by the Wigner transformation rules [1]. In case of fast rotation, this gives an average value of

$$\left\langle A_{20}^{LAB}(t) \right\rangle = \tfrac{1}{2}(3\cos^2\theta_m - 1) A_{20}^{PAS} = 0, \qquad (2.7)$$

and only the isotropic shift remains. As a result of MAS, the powder line shape associated with the CSA breaks up into a narrow center peak at the isotropic shift and spinning sidebands, a set of peaks positioned at multiples of ω_r from the center peak. From Eq. [2.6] it is clear that these sidebands originate from rotational echoes. For slow spinning the envelope of the peaks is the powder line. If ω_r is larger than the CSA, the sidebands disappear from the spectrum. If an intermediate value of ω_r is chosen, the CSA information can be extracted at high resolution from an analysis of the sideband pattern [6]. The CSA can be very informative about the chemical environment of the nuclear spin in a solid. In chapters 4 and 5 of this thesis, for example, it will be shown how the coordination of a ^{113}Cd ion is revealed by the CSA.

In Eq. [2.1] the chemical shift scales with B_0 according to Eq. [2.3], while the dipolar couplings are field-independent. In particular, if the spinning rate ω_r is not much larger than the strength of the anisotropic interactions, residual broadening effects occur. Thus, higher magnetic fields are generally desirable as the dispersion of the signals increases relative to the broadening effects of the dipolar couplings and the resolution is enhanced. In addition, high fields increase the sensitivity of the NMR experiments. Since the chemical shift anisotropy also scales with B_0, fast MAS is necessary in high fields. With

developments in instrumentation, MAS rates of ~15 kHz are now common practice and higher rates up to ~50 kHz are possible, although at the expense of smaller sample volumes [7, 8]. This is sufficient to reduce the chemical shift anisotropy as well as the homonuclear dipolar couplings between isotope labels such as ^{13}C.

Many of the standard cross polarization (CP) experiments can be applied or have been adopted for use with rapid MAS in high field. The CP technique exploits the high abundance, high sensitivity and short relaxation times of the protons by transferring transverse ^{1}H magnetization to another spin species [9]. The maximum enhancement for a ^{13}C signal compared to direct ^{13}C excitation is $g_{1H}/g_{13C} \approx 4$. In addition, the recycle delay required for the accumulation of the free induction decays is usually short. Overall, CP introduces a significant gain in sensitivity. During the detection of the signal, heteronuclear decoupling is applied to achieve a high resolution. The robust TPPM sequence is now widely used for this purpose [10]. It uses 180° pulses with alternating phases for efficient decoupling. The CP/MAS experiment with TPPM decoupling is the building block for more advanced techniques, such as two-dimensional correlation spectroscopy.

2.2   2D and 3D correlation spectroscopy

To resolve signals and for *de novo* structure determination of solids, correlation NMR spectroscopy of multi-spin labeled molecules is necessary. Here the homonuclear dipolar couplings, that are averaged by MAS to achieve a high resolution, are reintroduced during a mixing interval to generate correlated spin states [1, 11]. Two experiments that are widely used and important for the study of organic compounds are ^{13}C-^{13}C and ^{1}H-^{13}C correlation spectroscopy.

The sequence of the ^{13}C-^{13}C Radio Frequency-Driven Dipolar Recoupling (RFDR) MAS correlation experiment is shown in Fig. 2.1A [12]. The preparation step consists of the CP procedure. During t_1 and t_2, the ^{13}C spins precess under heteronuclear decoupling

to give a high resolution. During τ_m, however, the dipolar ^{13}C-^{13}C couplings have to be reintroduced to promote transfer of magnetization. The magnetization is first stored along z by a 90° pulse. The actual recoupling is achieved by a series of 180° pulses, which are synchronized with the rotor frequency. If a short mixing time τ_m of ~1 ms is used, only correlations between spins separated by one bond in an organic molecule are created, which is most beneficial for the assignment of the chemical shifts.
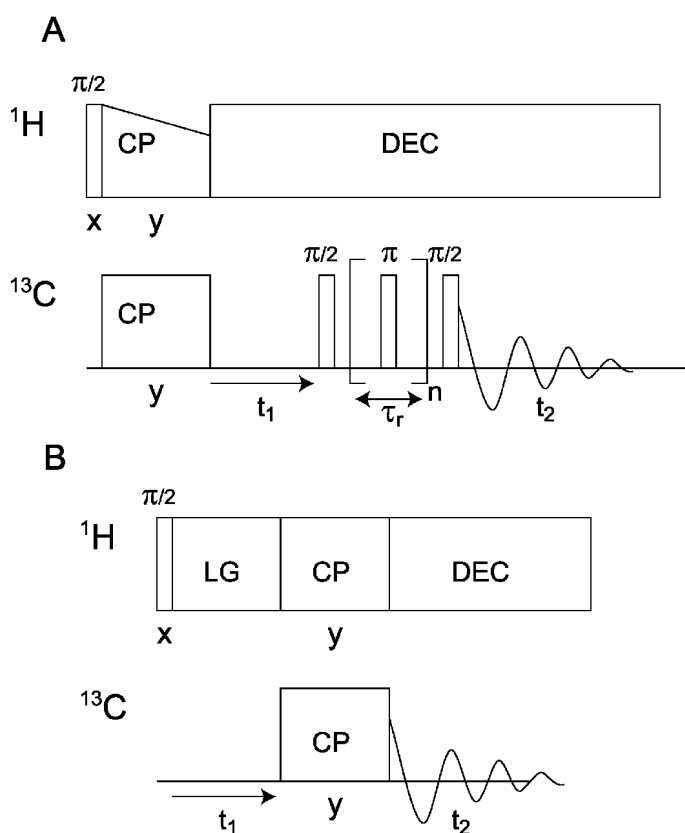
Fig. 2.1.(A) Pulse sequence of the 2D ^{13}C-^{13}C MAS NMR radio frequency-driven dipolar recoupling homonuclear correlation experiment. Following a cross polarization (CP) step, the ^{13}C spins precess freely during t_1, while heteronuclear decoupling (DEC) is applied on the ^1H spins. Subsequently, the ^{13}C-^{13}C couplings averaged by MAS are reintroduced by a rotor-synchronized train of 180° pulses. During t_2 the ^{13}C free induction decay is detected. (B) Pulse sequence of the 2D ^1H-^{13}C MAS NMR LG-CP heteronuclear correlation experiment. After ^1H excitation, the ^1H spins precess under homonuclear Lee-Goldburg (LG) decoupling during t_1. Subsequently, a CP step forms the mixing interval and the ^{13}C free induction decay is detected in t_2.

Direct ^{1}H detection is difficult in solids due to the very strong homonuclear ^{1}H dipolar interactions. Therefore, the proton signals are usually detected indirectly by correlation with less abundant nuclei. Often the ^{1}H signals are assigned in a 2D [1]H-^{13}C correlation experiment with the ^{13}C shifts obtained in the [13]C-^{13}C experiments. A straightforward [1]H-^{13}C correlation experiment consists of the CP scheme, where t_1 is inserted after the first [1]H 90° pulse and the CP interval constitutes the mixing step. This is known as Wideline Separation (WISE), since broad ^{1}H lines in the indirect dimension are separated by correlation with ^{13}C shifts in the direct dimension. In a high field and using fast MAS, the ^{1}H peaks can already be narrowed significantly [13].

Although ^{1}H signals can be assigned with the WISE technique, the ^{1}H resolution can be improved considerably if there is little inhomogeneous line broadening. In particular, the robust *Lee Goldburg* (LG) technique employs off-resonance rf irradiation to generate an effective rf field inclined at the magic angle [14, 15]. Precession of the spins around this field amounts to "magic angle spinning in spin space". With the 2D LG/MAS experiment (Fig. 2.1B), spectra can be obtained with a good resolution in both dimensions [16]. A recent version uses phase modulated *Lee Goldburg* (PMLG), which is easy to implement compared to the frequency switched LG [17].

In case of strong overlap in the ^{13}C dimension, assignment of all ^{1}H signals in a 2D [1]H-^{13}C experiment is difficult. For chlorophylls, for example, sets of ^{13}C resonances exist with very similar chemical shifts, depending on the degree of symmetry in the molecule. A full ^{1}H assignment may be obtained in a 3D [1]H-[13]C-^{13}C experiment. In this way, the ^{1}H signals are correlated to the signals of a 2D [13]C-^{13}C experiment. The 2D RFDR experiment in Fig. 2.1A can be easily extended with a third ^{1}H WISE dimension, by inserting a ^{1}H evolution interval after the first ^{1}H excitation pulse [18].

2.3   [1]H spin diffusion for structure determination

While the strong dipolar couplings between the ^{1}H spins are problematic for the resolution, these couplings can be used to transfer signals effectively over large distances

in a spin diffusion process. Analysis of ^{1}H spin diffusion has been used extensively in the past to study the morphology of polymer systems [19, 20]. In a recent biological application, the topology of a membrane-bound protein was determined using spin diffusion [21].

The recoupled ^{13}C interactions in experiments such as RFDR can also be used for ^{13}C spin diffusion. While intramolecular transfer over large distances is possible in this way, intermolecular transfer is difficult for uniformly labeled ^{13}C systems due to the different topology of the ^{1}H and the ^{13}C spins. This is depicted schematically in Fig. 2.2. The ^{1}H spins form a widely branched network with strong intra- and intermolecular couplings. In contrast, the coupling network of the ^{13}C spins is mostly limited to the directly bound neighbors, while the intermolecular couplings are weak.

The polarization transfer between the ^{1}H spins is governed by the high-field truncated Hamiltonian for the homonuclear dipolar coupling [11, 20]

$$\hat{H}_{\mathrm{II}} = \omega_{\mathrm{D}} \left(3\hat{I}_{1z}\hat{I}_{2z} - \hat{\boldsymbol{I}}_1 \cdot \hat{\boldsymbol{I}}_2 \right) \tag{2.8}$$

$$\omega_{\mathrm{D}} = -\frac{\mu_0 \gamma^2 \hbar}{4\pi} \frac{1}{r^3} \tfrac{1}{2} \left(3\cos^2\theta - 1 \right),$$
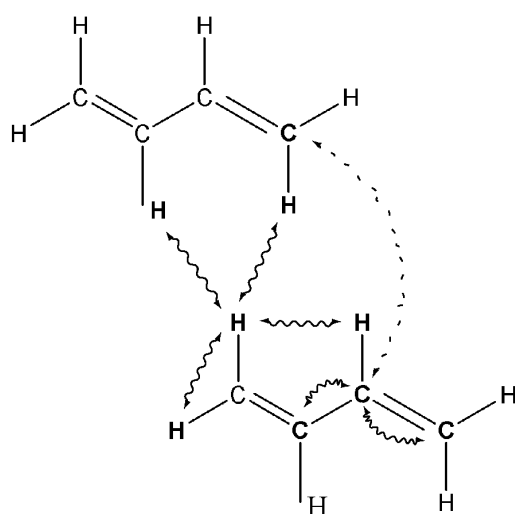

Fig. 2.2. Schematic representation of the spin-spin couplings in two adjacent organic molecules indicating the different intra- and intermolecular coupling network of ^{1}H and [13]C.

where γ is the gyromagnetic ratio, r the distance between the spins and θ the angle between internuclear distance vector and the external field. For an isolated two-spin system, starting with polarization on spin 1, the dipolar coupling induces an oscillation of the polarization between spin 1 and 2 [20],

$$\rho(t) = \hat{I}_{1z}\tfrac{1}{2}(1+\cos\omega_{\mathrm{D}}t) + \hat{I}_{2z}\tfrac{1}{2}(1-\cos\omega_{\mathrm{D}}t) + \left(\hat{I}_{1y}\hat{I}_{2x} - \hat{I}_{1x}\hat{I}_{2y}\right)\sin\omega_{\mathrm{D}}t. \qquad (2.9)$$

For large systems of many spins with varying coupling strengths, however, the polarization transfer over large distances >>1 nm behaves as classical diffusion of magnetization M, fulfilling

$$\frac{\mathrm{d}M(\boldsymbol{r},t)}{\mathrm{d}t} = D\nabla^2 M(\boldsymbol{r},t), \qquad (2.10)$$

with a diffusivity D of ca. 1 nm^2/ms in organic compounds [20]. This equation can be solved for different morphologies and used, for example, to estimate grain sizes in polymers [19, 22].

Intermolecular ^{1}H polarization transfer over ranges of ca. 3-10 Å forms an intermediate regime between the isolated 2-spin system and classical diffusion. Only for adjacent ^{1}H spins, spanning ca. <3.5 Å, distances can be estimated from the build-up of polarization transfer using a semi-classical two-spin model [23]. For longer distances relayed processes become important and prevent accurate distance determination. Hence the classical approach is only useful for a crude estimate of the distances spanned for different experimental diffusion times [24]. In addition, magic angle spinning attenuates the spin diffusion process. For moderate spinning frequencies of ca. 10-15 kHz, however, the diffusion is not quenched significantly, since the ^{1}H dipolar interactions are ca. 50 kHz in organic molecules.

To establish a strategy to resolve structures from MAS NMR distance constraints it is worthwhile to note the analogy with the structural studies in solution, in particular protein

folding using NOESY spectroscopy. The Nuclear Overhauser Effect (NOE) involves mutual transitions between dipolar-coupled spins, which is, in contrast to the polarization transfer in solids, induced by relaxation [11, 25]. The NOE exchange between resonances lead to cross-peaks in 2D NOESY spectra. As the NOE transfer depends on the distance between the spins, the NOESY signals can provide intermolecular distance constraints. An accurate quantitative analysis is also difficult for the NOE transfer due to competing processes such as spin diffusion or chemical exchange and due to variations of the relaxation times for spins within the same molecule as a result of internal motion. Instead, the signals can be roughly classified as weak, medium or strong NOE's and classified within three classes of distance restraints with varying upper limits [25, 26]. Even a simple classification of all NOE's within the category with the highest distance limit leads to a similar global structure of the protein. Recently, it has been shown that this approach is also effective for the structure determination by MAS NMR of proteins that are insoluble or difficult to crystallize, which is an intrinsic property of membrane proteins [27]. In that study, the intermolecular distance constraints were collected by ^{13}C spin diffusion in partially labeled molecules to prevent the dipolar truncation problem depicted in Fig. 2.2. Molecular modeling methods were used to generate structures which were subjected to the NMR constraints.

In this thesis, a similar strategy is adopted for the MAS NMR structure determination of aggregated chlorophylls. The intermolecular correlations obtained with ^{1}H spin diffusion are analyzed to find close intermolecular contacts. The top-down restrictions that follow from these intermolecular correlations significantly reduce the number of ways that a 3D space-filling structure can be built and serve as restraints for molecular modeling.

2.4 ^{1}H ring current shifts for structure determination

Ring current shifts result from a diamagnetic response of aromatic molecules. As a result of the secondary field from the ring current in the aromatic cycle induced by an external field, the protons attached to the outer side of an aromatic ring experience a downfield shift, while any protons within the ring center are shifted upfield. The

magnitude of the effect lies in the range of ca. 0-10 ppm. The physics of ring currents has been reviewed in detail [28]. In chemical terms, the effect can be understood from the delocalization of the π-electrons in conjugated rings as described, for example, within the molecular orbital framework [29]. For supramolecular assemblies, the ring current shifts induced in neighboring molecules can be used to obtain structural information. The ^{1}H chemical shifts are more useful to probe ring current effects, since the ^{1}H nucleus is much less sensitive to other electronic perturbations compared to [13]C [30], see also Chapter 5 of this thesis. In a recent ^{1}H NMR study of a solid hexabenzocoronene (HBC) derivative, it was shown that the ring current effects are significant over distances beyond the nearest neighbor, and the stacking of the HBC molecules was determined [31, 32]. Ring currents are also observed in systems of biological interest. In proteins, for example, the aromatic residues produce ring current shifts in adjacent residues, hence providing structural constraints [33]. In addition, in the study of chlorophyll aggregation in solution, the ^{1}H ring currents have played an important role [30].

To obtain structural information from the ^{1}H NMR data, various models have been developed to calculate the ring current shifts, in particular within the chlorophyll aggregation studies. The main purpose of those model calculations is to reproduce the spatial distribution of the ring current shifts arising from the supramolecular geometry. In particular, magnetic dipole and loop current have been used to model the ring currents. The first and crudest model consists of a single magnetic dipole in the center of a ring [34]. Later versions consider pairs of dipoles to account for the current density of the π-electrons below and above the ring [35], which was applied, for example, to study the Chl *a* dimer arrangement in solution [36]. For the early studies, the dipole models had the advantage of a few numerical evaluation steps. In addition, the models of chlorophyll ring currents can be refined by increasing the number of dipoles. An obvious disadvantage of the dipole representation is that the actual ring shape of the current density is not taken into account. Alternatively, a current loop model was proposed, which gives more accurate values close to the ring plane [37]. An examination of the BChl *c* dimer has indicated that both models are useful for structure determination,

although it is difficult to have an accurate quantitative agreement with the NMR data [38].

Computational chemistry has been used in the past to calculate the secondary fields induced by aromatic molecules [39]. With the recent advances in this field, it is now possible to calculate reliable values based on a quantum mechanical *ab initio* treatment such as the Density Functional Theory. Calculations of the Nucleus Independent Chemical Shift (NICS), for example, which probes the ring current shift induced in the center of a conjugated ring system, is now commonly accepted as a measure of aromaticity [40]. These calculations are particularly useful to obtain quantitative agreement with NMR data [32].

For solid aggregated chlorophylls, ring current shifts have provided invaluable qualitative evidence about the stacking of the molecules [18, 41]. In this thesis, a quantitative treatment of the long-distance effects of ring currents will be utilized for the determination of the structure of aggregated chlorophyll (Chapter 5 and 6). To estimate the total ring current effects in the solid aggregates, the long-range contributions from non-nearest neighbors in the microcrystalline environment are taken into account. For these long-range intermolecular contributions to the ^{1}H ring current shifts, the details near the aromatic ring are less important and a circular loop model for the spatial distribution is combined with the accuracy of a DFT calculation for the absolute ring current shift induced by a single molecule.

References

[1]   M. Mehring, "Principles of High Resolution NMR in Solids", Springer-Verlag, Berlin (1983).

[2]   E.R. Andrew, A. Bradbury and R.G. Eades, *Nature* **182**, 1659 (1958).

[3]   I.J. Lowe, *Phys. Rev. Lett.* **2**, 285-287 (1959).

[4]   M.E. Rose, "Elementary Theory of Angular Momentum", John Wiley, New York (1967).

[5]   D.M. Brink and G.R. Satchler, "Angular Momentum", Clarendon Press, Oxford (1968).

[6]   J. Herzfeld and A.E. Berger, *J. Chem. Phys.* **73**, 6021-6030 (1980).

[7]   M. Ernst, A. Samoson and B.H. Meier, *Chem. Phys. Lett.* **348**, 293-302 (2001).

[8]   M. Ernst, A. Detken, A. Bockmann and B.H. Meier, *J. Am. Chem. Soc.* **125**, 15807-15810 (2003).

[9]   S.R. Hartmann and E.L. Hahn, *Phys. Rev.* **128**, 2042 (1962).

[10]   A.E. Bennett, C.M. Rienstra, M. Auger, K.V. Lakshmi and R.G. Griffin, *J. Chem. Phys.* **103**, 6951-6958 (1995).

[11]   R.R. Ernst, G. Bodenhausen and A. Wokaun, "Principles of Nuclear Magnetic Resonance in One and Two Dimensions", Clarendon Press, Oxford (1987).

[12]   A.E. Bennett, J.H. Ok, R.G. Griffin and S. Vega, *J. Chem. Phys.* **96**, 8624-8627 (1992).

[13]   B.J. van Rossum, G.J. Boender and H.J.M. deGroot, *J. Magn. Reson. Ser. A* **120**, 274-277 (1996).

[14]   M. Lee and W.I. Goldburg, *Phys. Rev.* **A 140**, 1261 (1965).

[15]   A. Bielecki, A.C. Kolbert and M.H. Levitt, *Chem. Phys. Lett.* **155**, 341-346 (1989).

[16]   B.J. van Rossum, H. Forster and H.J.M. de Groot, *J. Magn. Reson.* **124**, 516-519 (1997).

[17]   E. Vinogradov, P.K. Madhu and S. Vega, *Chem. Phys. Lett.* **314**, 443-450 (1999).

[18]   B.J. van Rossum, D.B. Steensgaard, F.M. Mulder, G.J. Boender, K. Schaffner, A.R. Holzwarth and H.J.M. de Groot, *Biochemistry* **40**, 1587-1595 (2001).

[19]   F.M. Mulder, W. Heinen, M. van Duin, J. Lugtenburg and H.J.M. de Groot, *J. Am. Chem. Soc.* **120**, 12891-12894 (1998).

[20]   K. Schmidt-Rohr and H.W. Spiess, "Multidimensional Solid-State NMR and Polymers", Academic Press, London (1994).

[21]   D. Huster, X.L. Yao and M. Hong, *J. Am. Chem. Soc.* **124**, 874-883 (2002).

[22]   F.M. Mulder, W. Heinen, M. van Duin, J. Lugtenburg and H.J.M. de Groot, *Macromolecules* **33**, 5544-5548 (2000).

[23]   A. Lange, K. Seidel, L. Verdier, S. Luca and M. Baldus, *J. Am. Chem. Soc.* **125**, 12640-12648 (2003).

[24]   I. de Boer, L. Bosman, J. Raap, H. Oschkinat and H.J.M. de Groot, *J. Magn. Reson.* **157**, 286-291 (2002).

[25]   K. Wüthrich, "NMR of Proteins and Nucleic Acids", Wiley, New York (1986).

[26]   T.F. Havel and K. Wuthrich, *J. Mol. Biol.* **182**, 281-294 (1985).

[27]   F. Castellani, B. van Rossum, A. Diehl, M. Schubert, K. Rehbein and H. Oschkinat, *Nature* **420**, 98-102 (2002).

[28]   P. Lazzeretti, *Progress in Nuclear Magnetic Resonance Spectroscopy* **36**, 1-88 (2000).

[29]   L. Salem, "The molecular orbital theory of congugated systems", Benjamin, New York (1966).

[30]   R.J. Abraham and A.E. Rowan, in *Chlorophylls* (H. Scheer, Ed.) pp. 797-834, CRC Press, Boca Raton, FL (1991).

[31]   S.P. Brown, I. Schnell, J.D. Brand, K. Mullen and H.W. Spiess, *J. Am. Chem. Soc.* **121**, 6712-6718 (1999).

[32]   C. Ochsenfeld, S.P. Brown, I. Schnell, J. Gauss and H.W. Spiess, *J. Am. Chem. Soc.* **123**, 2597-2606 (2001).

[33]   S.J. Perkins, *Biol. Magn. Reson.* **4**, 193 (1982).

[34]   J.A. Pople, *J. Chem. Phys.* **24**, 1111 (1956).

[35]   R.J. Abraham, K.M. Smith, D.A. Goff and J.J. Lai, *J. Am. Chem. Soc.* **104**, 4332 (1982).

[36]   R.J. Abraham, D.A. Goff and K.M. Smith, *J. Chem. Soc.-Perkin Trans. 1*, 2443-2451 (1988).

[37]   C.E. Johnson and F.A. Bovey, *J. Chem. Phys.* **29**, 1012 (1958).

[38]   T. Mizoguchi, S. Sakamoto, Y. Koyama, K. Ogura and F. Inagaki, *Photochem. Photobiol.* **67**, 239-248 (1998).

[39]   C. Giessner-Prettre and B. Pullman, *J. Theor. Biol.* **31**, 287-294 (1971).

[40]   P.V. Schleyer, C. Maerker, A. Dransfeld, H.J. Jiao and N. Hommes, *J. Am. Chem. Soc.* **118**, 6317-6318 (1996).

[41]   B.J. van Rossum, E.A.M. Schulten, J. Raap, H. Oschkinat and H.J.M. de Groot, *J. Magn. Reson.* **155**, 1-14 (2002).

Chapter 3

2D ^{13}C-^{13}C MAS NMR correlation spectroscopy with mixing by true ^{1}H spin diffusion reveals long-range intermolecular distance restraints in ultra high magnetic field[§]

3.1 Abstract

An improved 2D ^{13}C-^{13}C CP^3 MAS NMR correlation experiment with mixing by true ^{1}H spin diffusion is presented. With CP^3 correlations can be detected over a much longer range than with direct ^{1}H-^{13}C or ^{13}C-^{13}C dipolar recoupling. The experiment employs an ^{1}H spin diffusion mixing period τ_m sandwiched between two cross polarization periods. An optimized CP^3 sequence for measuring polarization transfer on a length scale between 0.3 and 1.0 nm using short mixing times of 0.1 ms $< \tau_m <$ 1 ms is presented. For such a short τ_m, cross talk from residual transverse magnetization of the donating nuclear species after a CP can be suppressed by extended phase cycling. The utility of the experiment for genuine structure determination is demonstrated using a self-aggregated Chl a/H$_2$O sample. The number of intramolecular cross-peaks increases for longer mixing times and this obscures the intermolecular transfer events. Hence, the experiment will be useful for short mixing times only. For a short τ_m = 0.1 ms, intermolecular correlations are detected between the ends of phytyl tails and ring carbons of neighboring Chl a molecules in the aggregate. In this way the model for the structure, with stacks of Chl a that are arranged back-to-back with interdigitating phytyl chains stretched between two bilayers, is validated.

3.2 Introduction

For systems of biological interest, supramolecular systems, and self-assembled nano-devices, solid state NMR in conjunction with uniform isotope enrichment offers an

---

[§]This chapter was published in part in *J. Magn. Res.* **157**, 286-291 (2002).

attractive route to resolve and refine micro-structure [1]. First, a series of homonuclear and heteronuclear correlation experiments is performed to assign the NMR response to the chemical structure. During this stage, much can be learned about the electronic properties of the system and non-bonding interactions, for example by comparing the solid state shifts with solution NMR data. In a next step, hydrogen bonding interactions within the system can be investigated [2-4]. Finally, invaluable information about the structural arrangement can be obtained from a measurement of intermolecular correlations, which involves transfer over relatively large distances of ~0.5 nm. While many strategies exist nowadays for assignment studies and characterization of hydrogen bonds, intermolecular transfer in uniformly labeled systems is not yet straightforward [5-9]. In particular, detection of intermolecular ^{13}C-^{13}C correlations with dipolar recoupling techniques or proton-driven spin diffusion is very difficult, due to rapid relayed spin
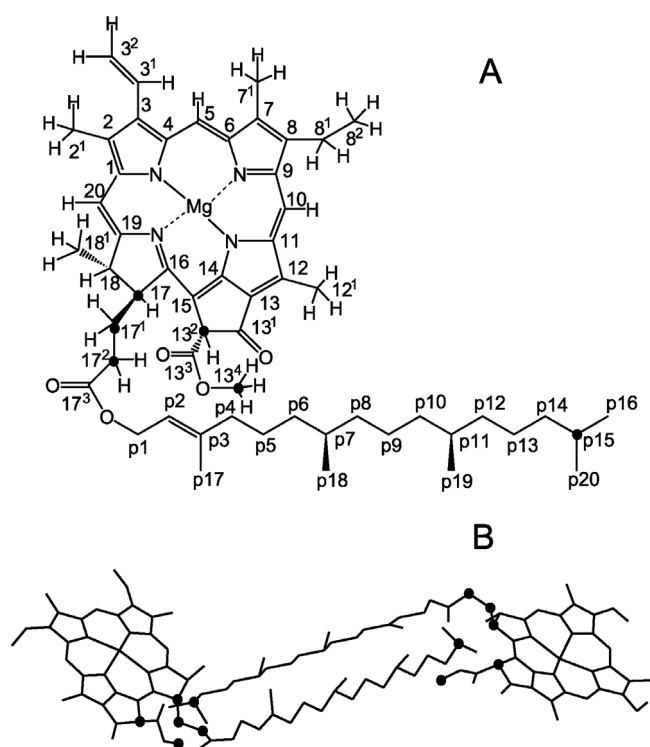
Fig. 3.1. Chemical structure of Chl a with the IUPAC numbering for the ring (A). For the phytyl tail the prefix P is used. The ^{1}H atoms are shown explicitly for the ring only. The proposed structural arrangement of the two Chl a molecules in the unit cell of self-aggregated Chl a/H$_2$O is depicted below (B). The hydrogens are left out for clarity. Solid circles indicate the carbons involved in the intermolecular correlations.

diffusion along the multispin ^{13}C labeled molecular network in uniformly enriched systems [10].

At an early stage, the use of MAS NMR correlation spectroscopy to resolve the structure of a uniformly enriched solid has been demonstrated for self-aggregated Chl a/H$_2$O [1, 11]. Chl a constitutes the green pigment in the photosynthetic apparatus of plants as well as algae and cyanobacteria. It is responsible for the absorption of light and essential for the subsequent conversion of the excitation energy into chemical energy. The chemical structure of Chl a is depicted in Fig. 3.1A. When exposed to H$_2$O it forms an aggregate. Such aggregates represent models for chlorophyll stacking in chlorosome light harvesting antennae found in some green photosynthetic bacteria [12, 13]. Thus, chlorophyll aggregates can form protein-free light-harvesting antennae, which is of potential interest for artificial photosynthesis.

To resolve a model for the 3D stacking in self-aggregated, uniformly enriched Chl a / H$_2$O with MAS NMR, ^{13}C and the ^{1}H chemical shifts were assigned by means of ^{13}C-^{13}C homonuclear and ^{1}H-^{13}C heteronuclear dipolar correlation spectroscopy [1, 11]. Shift constraints and intermolecular correlations obtained from a long-range ^{1}H-^{13}C experiment were used to construct a space filling model [11]. In this paper ^{1}H spin diffusion techniques are used to detect intermolecular ^{13}C-^{13}C correlations [14, 15]. A modified CP^3 experiment is presented, optimized for short ^{1}H mixing times 0.1 ms < τ_m < 1 ms. Correlations spanning distances between 0.1 and 1.0 nm are easily generated. Intermolecular cross-peaks are observed in the self-aggregated Chl a/H$_2$O that lead to a validation and refinement of the existing model for the stacking [1, 11].

3.3   Experimental

The preparation of uniformly labeled self-aggregated Chl a/H$_2$O has been described before [1]. The measurements were performed with a DSX-750 spectrometer and using a 4 mm triple resonance probe (Bruker, Germany), operating at a temperature of 277 K. The spinning frequency was kept constant within a few Hertz. During the ^{13}C evolution

intervals, heteronuclear TPPM decoupling [16] was applied with pulses of 7.3 µs and a phase modulation of 15°, using a rf nutation frequency of 66 kHz. Phase sensitive detection in the t_1 dimension was achieved with a TPPI scheme [17].

3.4   Results and discussion

Since protons constitute a dense network of strongly coupled spins, ^{1}H spin diffusion is an attractive route to investigate structural properties on a nm length scale [18]. The polarization exchange between ^{1}H spins is in principle a coherent process subject to relaxation [19]. However, for many spins, with varying coupling strength and sufficiently long transfer times, the spin dynamics can be described in terms of a classical diffusion model [18]. For rigid organic materials, diffusivities of ~0.8 nm^2/ms have been reported and ^{1}H spin diffusion allows the determination of the morphology of polymers over a very long range, up to ca. 200 nm [18, 20]. This value for the diffusivity has also been used for experiments employing moderate MAS frequencies [14, 15, 18, 21-23]. The favorable polarization transfer properties of ^{1}H can be combined with the superior spectral resolution of ^{13}C nuclei in a 2D [13]C-^{13}C MAS CP^3 correlation spectroscopy
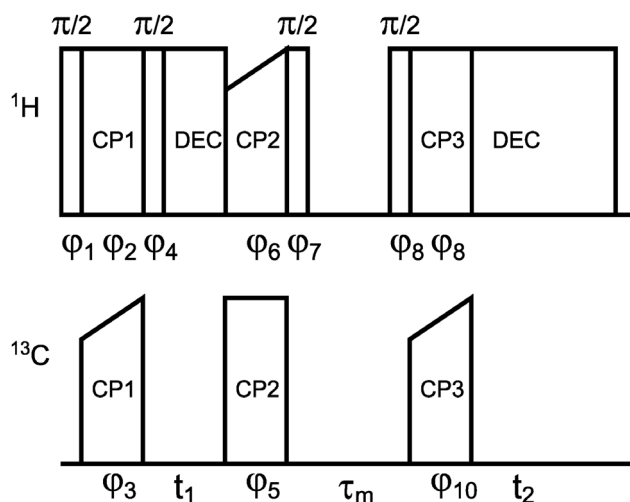
Fig. 3.2. Schematic representation of the extended CP[3] pulse sequence, suitable for the 2D ^{13}C-^{13}C MAS NMR correlation spectroscopy with a short ^{1}H spin diffusion mixing period.

experiment [14, 15]. In an early application of this method, the morphology and phase separation of ^{13}C-labeled semi-interpenetrating networks were investigated [15, 22]. In the solid state NMR of complex solid-type biological assemblies, for example membrane proteins, the same principles could be applied to probe shorter range intra- and intermolecular distances for structure determination.

Fig. 3.2 shows a CP^3 pulse scheme that is optimized for short mixing times 0.1 ms < τ_m < 1 ms. During the preparation period ^{13}C transverse coherence is established with ramped cross polarization [24]. The residual transverse ^{1}H magnetization is, ideally, rotated back to the z-axis. Next, free precession of ^{13}C is allowed during t_1, while TPPM irradiation on the ^{1}H channel is applied for heteronuclear decoupling [16]. A second CP step transfers the t_1 modulated magnetization back to the protons. The ^{1}H magnetization is subsequently stored along the magnetic field $\vec{B}_0$ by a 90º pulse. The distribution of ^{1}H z magnetization is allowed to equilibrate during a spin diffusion period τ_m. With another 90º pulse, the ^{1}H polarization is rotated back to the XY plane and a final CP is applied for high resolution ^{13}C detection.

For short mixing times $\tau_m \lesssim T_2$, a serious problem is the residual transverse magnetization from the donating nuclear species after the first two CP periods. Residual ^{1}H magnetization after the first CP interval interferes with the magnetization transfer during the second CP step. In addition, residual ^{13}C signal from the second CP interval mixes with the ^{13}C coherence created during the third CP period. These processes can give rise to strong artifacts in the 2D correlation spectrum.

The simplest way to deal with these cross talk problems is a 90º pulse to rotate the remaining coherence after the first and second CP period along the z-axis. In practice, adequate suppression of artifacts with a 90º pulse is difficult to achieve due to pulse imperfections, in particular for the ^{13}C. During rf irradiation, the effective field is tilted with respect to the z-axis by an angle θ,

$$\tan(\theta) = \frac{B_1}{\Delta B_0} \, , \tag{3.1}$$

where B_1 is the applied rf field strength, and ΔB_0 the residual z-component of the magnetic field in the rotating frame. For off-resonance irradiation, θ deviates from 90º and the effective field points out of the XY plane. For a high field spectrometer or moderate rf power and a broad chemical shift dispersion, this offset can become very significant for ^{13}C and the effect of the 90º pulse is spoiled. For example, for a spectrometer with a 750 MHz ^{1}H resonance frequency and using a moderate ~50 kHz rf power, ^{13}C spins shifted toward the extreme ends of a 300 ppm wide spectrum experience deviations (90°-θ) as high as ~30°. Due to a lower shift dispersion of ~14 ppm, this value is down to ~5° for ^{1}H spins under similar conditions.

After the first CP period, the residual ^{1}H transverse magnetization is thus only partially removed by a 90º pulse. By cycling the phase of the initial [1]H 90º pulse relative to the

Table 3.1. Phase alternation scheme corresponding with the pulse
sequence of Fig. 3.2.

φ_1	φ_2	φ_3*	φ_4	φ_5	φ_6	φ_7	φ_8	φ_9	φ_{10}	φ_{det}
+X	-Y	+Y	-X	+Y	-Y	+X	-X	+Y	+Y	-Y
+X	-Y	+Y	-X	+Y	+Y	+X	-X	+Y	+Y	+Y
-X	-Y	+Y	+X	+Y	-Y	+X	-X	+Y	-Y	-Y
-X	-Y	+Y	+X	+Y	+Y	+X	-X	+Y	-Y	+Y
+Y	+X	+Y	-Y	+Y	-Y	+X	-X	+Y	-X	+X
+Y	+X	+Y	-Y	+Y	+Y	+X	-X	+Y	-X	-X
-Y	+X	+Y	+Y	+Y	-Y	+X	-X	+Y	+X	+X
-Y	+X	+Y	+Y	+Y	+Y	+X	-X	+Y	+X	-X
-X	+Y	+Y	+X	+Y	-Y	+X	-X	+Y	-Y	+Y
-X	+Y	+Y	+X	+Y	+Y	+X	-X	+Y	-Y	-Y
+X	+Y	+Y	-X	+Y	-Y	+X	-X	+Y	+Y	+Y
+X	+Y	+Y	-X	+Y	+Y	+X	-X	+Y	+Y	-Y
-Y	-X	+Y	+Y	+Y	-Y	+X	-X	+Y	+X	-X
-Y	-X	+Y	+Y	+Y	+Y	+X	-X	+Y	+X	+X
+Y	-X	+Y	-Y	+Y	-Y	+X	-X	+Y	-X	-X
+Y	-X	+Y	-Y	+Y	+Y	+X	-X	+Y	-X	+X

* +TPPI for phase sensitive detection in t_1

phase of the ^{1}H spin lock pulse of the second CP, contributions of the residual magnetization to the magnetization transfer during this CP step are cancelled (Table 3.1). Prior versions of the CP^3 experiment use a ^{13}C lock pulse after the first CP, which allows the residual ^{1}H signal to decay during a spin lock time $\tau > {}^1$H T_2 [14, 15]. In practice, this yields a considerable loss of the ^{13}C signal due to the relaxation in the rotating frame ($T_{1\rho}$), in particular for materials with a short ^{13}C $T_{1\rho}$ and a long ^{1}H T_2. This disadvantage is avoided by the phase cycling of the initial ^{1}H 90º pulse.

The residual ^{13}C transverse magnetization after the second CP period vanishes only for a long $\tau_m \gg {}^{13}$C T_2 [15]. For shorter τ_m, the phase of the residual ^{13}C signal can be cycled relative to the phase of the ^{13}C signal detected during t_2 [14]. In this way, the ^{13}C cross talk is eliminated. The pulse scheme of Fig. 3.2 with the cycling of Table 3.1 is straightforward to implement. Given that the signal to be cancelled has a considerable intensity, the phase alternation sequence of Table 3.1 needs to be rather extensive in order to compensate for any imperfections of the phase settings, precession during pulses, etc.

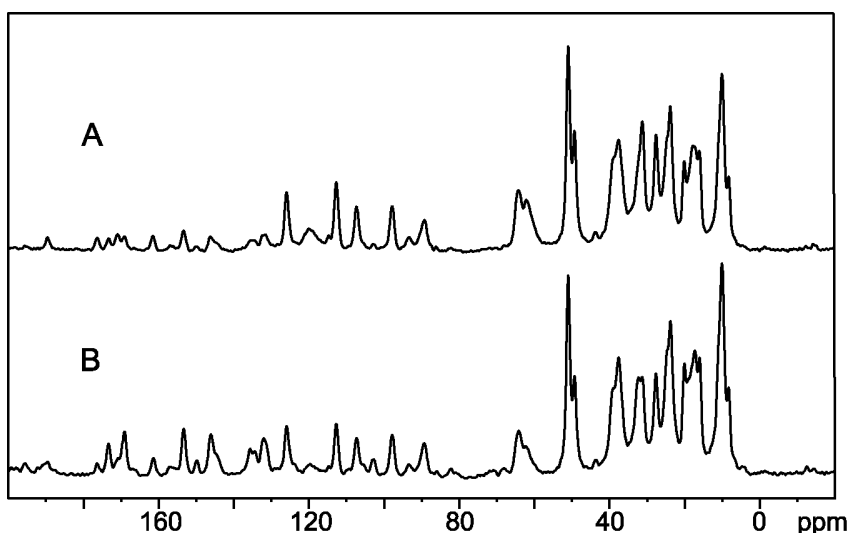*Fig. 3.3. ^{13}C CP/MAS NMR spectra of aggregated Chl a/H$_2$O recorded with a spinning speed of 12 kHz in a field of 17.6 T, using a CP time of 150 µs (A) and 1 ms (B). The signals of ^{13}C atoms bound to ^{1}H reach a maximum intensity within the short CP interval of 150 µs, while the signals of ^{13}C atoms with chemical shifts > ~130 ppm and not bound to ^{1}H require the long CP period to reach full intensity.*

For moderate MAS rates, ^{1}H spin diffusion processes can take place not only during the mixing time, but also during the CP intervals. In a static sample, the spin diffusion rate during a spin lock is effectively scaled by a factor of 1/2 [18]. Therefore, it is expected that the ^{1}H spin diffusion is slower during the CP periods. In addition, *Lee Goldburg* decoupling may be applied to further suppress the ^{1}H spin diffusion during cross polarization [2]. Here, however, the straightforward use of short CP intervals of 150 μs was found to be effective to prevent that spin diffusion during CP compromises the selectivity of the established correlations with respect to the distance (Fig. 3.3). A 2D spectrum results where only proton-bound carbons are visible (Fig. 3.4). Since these carbons usually cover a limited chemical shift range of only ~150 ppm, the spectral width can be reduced, yielding a shorter acquisition time of the 2D experiment, or a better resolution.

Using the sequence in Fig. 3.2, a series of datasets was collected from the sample of uniformly labeled self-aggregated Chl *a*/H_2O (Fig. 3.4). Each spectrum was obtained using a different mixing time in ~11 hours with a spinning frequency $\omega_r/2\pi = 14.5$ kHz. An extensive discussion of the assignment of the ^{13}C NMR response can be found elsewhere [11]. The CP transfer reaches its maximum in ~150 μs CP time. This was verified with separate 1D [1]H-^{13}C CP MAS experiments (Fig. 3.3).

Fig. 3.4. Contour plots of absorption mode 2D ^{13}C-^{13}C MAS NMR correlation spectra of aggregated Chl a/H_2O recorded with a spinning speed of 14.5 kHz in a field of 17.6 T and acquired with the sequence of Fig. 3.2. Arrows and labels are used to indicate cross-peaks, which are connected to the corresponding diagonal peaks and mirror peaks by dashed lines. Data were acquired with $\tau_m = 100$ μs (A), $\tau_m = 200$ μs (B), and $\tau_m = 700$ μs (C). For all experiments, a prescan delay of 1 s was used for a total of 192 scans for each of 200 t_1 points. A Lorentz-Gauss transformation with a line broadening of 60 Hz was applied to the datasets in the t_2 dimension prior to Fourier transformation. A sine-square apodization, phase shifted by $2\pi/3$, was used in the t_1 dimension.
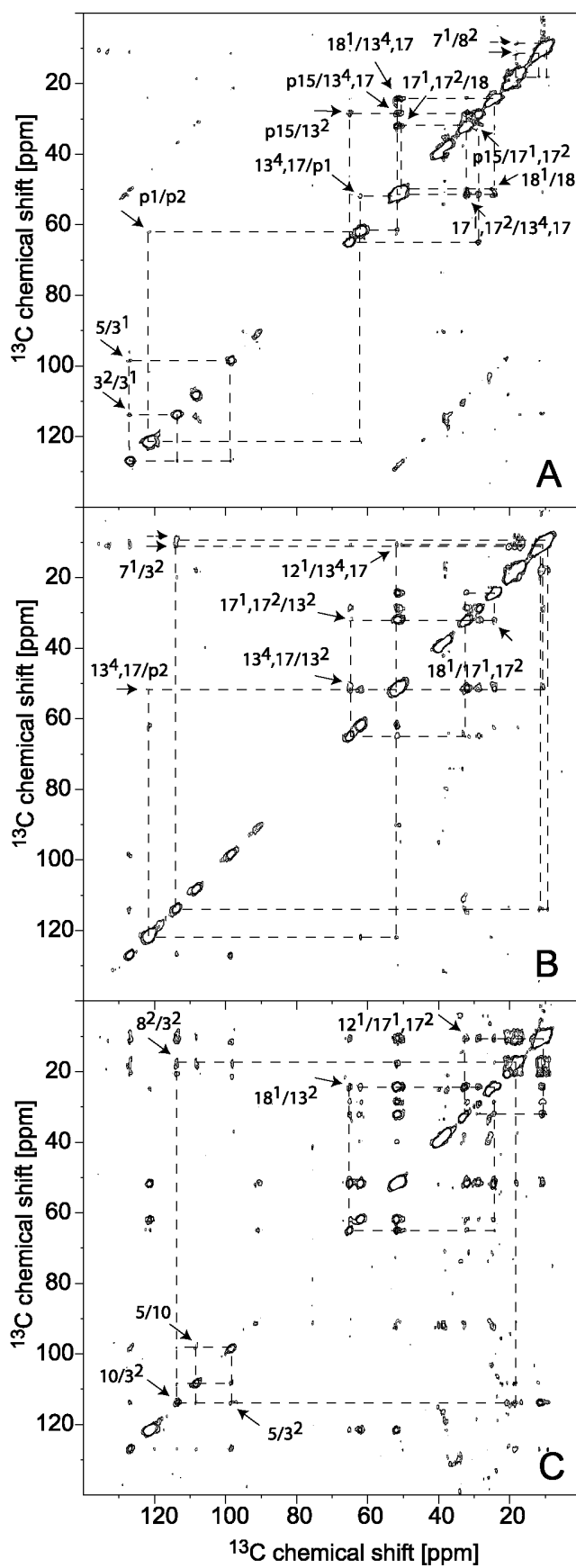
Several cross peaks in Fig. 3.4 are indicated with arrows and labels. Dashed lines indicate the symmetry-related signals via the corresponding diagonal peaks. In order to quantify the transfer range of the correlation observed with these ^{1}H spin diffusion experiments, the distances between hydrogens directly bound to the carbons assigned to the cross peaks are determined from the Chl *a* structure. For the shortest diffusion time τ_m = 100 µs (Fig. 3.4A), most of the cross-peaks involve intramolecular correlations with a ^{1}H transfer range ≲ 4 Å. The 17 and the 13^4 ^{13}C resonate with 51.7 and 51.8 ppm chemical shift, respectively [11]. Although the signals overlap in the 2D homonuclear correlation experiment, both labels are in the same region of the molecule and cross-peaks with other carbons can provide structural information. The same is true for the 17^1 and 17^2 signals, that coincide at 32.3 ppm. The 7^1 response is doubled at 8.9 and 11.5 ppm (Fig. 3.4), indicating two structurally distinct environments [11]. The p15 ^{13}C signal is shifted to 28.4 ppm [1, 11] and is well resolved in the spectrum. In Fig. 3.4A, correlations of p15 with the 13^2 and with the overlapping $17^1,17^2$, and $13^4,17$ labels are clearly observed. The p15 carbons are located at the ends of the interdigitating phytyl tails, and these correlations are attributed to intermolecular polarization transfer during τ_m.

A CP[3] experiment with a longer τ_m = 200 µs is shown in Fig. 3.4B. Some intramolecular correlations are detected that are not observed in the experiment with τ_m = 100 µs (A). Here, the ^{1}H transfer extends over ~7Å. Finally, an experiment with a mixing time of 700 µs yields many cross-peaks (Fig. 3.4C). Several of the longer range correlations are depicted in Fig. 3.4C. Selective assignment between intra- and intermolecular correlations is virtually impossible for such a long diffusion time.

In a first order approximation, the protons form a chainlike or tubular arrangement at the exterior of the molecule. During spin diffusion in one dimension, the initial magnetization located at r = 0 spreads like a Gaussian distribution with a root-mean-square distance developing as

$$\sqrt{\langle r^2 \rangle} = \sqrt{2Dt} \, .$$ (3.2)

Although a moderate spinning frequency of 14.5 kHz is used in these experiments, the characteristic diffusivity D of ~0.8 nm^2/ms is expected to be useful for a rough approximation. Eq. (3.2) yields ~4 Å and ~6 Å, for 100 μs and 200 μs mixing, respectively. Hence the actual intramolecular transfer range of ~4 Å for τ_m = 100 μs and ~7 Å for τ_m = 200 μs is in line with previous data for ¹H spin diffusion. For τ_m = 700 μs, Eq. (3.2) predicts a spin diffusion range of ~11 Å. In that case the correlations can span the entire ring and an assignment to intra- or intermolecular transfer is difficult in agreement with the data presented in Fig. 3.4C.

Based on aggregation shifts and long-range ¹H-¹³C transfer, a model for the stacking of self-aggregated Chl *a* / H_2O was proposed, where parallel Chl *a* stacks are in a sheet arrangement, similar to ethyl chlorophyllide *a* [1, 11]. In a first attempt to resolve the stacking in 3 dimensions, it was inferred from the data that the sheets form bilayers in a back-to-back arrangement with interdigitating chains, as discussed in Chapter 1. The phytyl chains were assumed to be elongated considering the linewidths of the phytyl carbons and the absence of conformational shifts.

The observed intermolecular correlations involving the p15 carbon provide a first direct experimental validation of the bilayer arrangement in the aggregate. The end of the phytyl tail of the Chl *a* molecule appears to be in close contact with the ring of a neighboring Chl *a*. From the spectra shown in Fig. 3.4, it can be concluded that the p15 proton is separated from hydrogens located near the basis of the phytyl tail by ≲ 4 Å. The only way to arrange the two Chl *a* bilayers to accommodate these distance restraints is shown schematically in Fig. 3.1B. The two Chl *a* moieties are from two adjacent bilayers and the carbons that are involved in the observable intermolecular correlations are depicted by solid circles in Fig. 3.1. According to our results, the elongated phytyl tails are somewhat closer to the other ring than suggested in the earlier work [1, 11, 25-27].

Hence, the modified CP³ experiment forms a useful complementary technique for the detection of intermolecular close contacts. It can be a valuable tool in a structure elucidation strategy. It is anticipated that the comparison of multiple datasets, recorded

with varying mixing times, can lead to sets of distance constraints that provide information about, for example, the folding of a protein.

3.5   Conclusions

The 2D CP^3 ^{13}C-^{13}C MAS NMR correlation experiment with true ^1H spin diffusion previously implemented for long range polarization transfer is successfully adapted for the detection of short range intermolecular correlations in uniformly labeled systems of biological interest. Short mixing intervals 0.1 ms < τ_m < 0.7 ms are used to detect intermolecular correlations spanning distances < 1 nm. In this way, information about the structure of self-aggregated Chl a / H_2O is obtained. There is clear evidence for a proximity of the ends of the phytyl chains Chl a rings of an opposite stack. With the phase cycling presented here, the CP^3 experiment offers an attractive method for the collection of intermolecular distance restraints and structural elucidation.

References

[1]   G.J. Boender, J. Raap, S. Prytulla, H. Oschkinat and H.J.M. de Groot, *Chem. Phys. Lett.* 237, 502-508 (1995).

[2]   B.J. van Rossum, C.P. de Groot, V. Ladizhansky, S. Vega and H.J.M. de Groot, *J. Am. Chem. Soc.* 122, 3465-3472 (2000).

[3]   X. Zhao, M. Eden and M.H. Levitt, *Chem. Phys. Lett.* 342, 353-361 (2001).

[4]   S.P. Brown, X.X. Zhu, K. Saalwachter and H.W. Spiess, *J. Am. Chem. Soc.* 123, 4275-4285 (2001).

[5]   S. Luca, D.V. Filippov, J.H. van Boom, H. Oschkinat, H.J.M. de Groot and M. Baldus, *J. Biomol. NMR* 20, 325-331 (2001).

[6]   E. Alberti, E. Humpfer, M. Spraul, S.M. Gilbert, A.S. Tatham, P.R. Shewry and A.M. Gil, *Biopolymers* 58, 33-45 (2001).

[7]   C. Ochsenfeld, S.P. Brown, I. Schnell, J. Gauss and H.W. Spiess, *J. Am. Chem. Soc.* 123, 2597-2606 (2001).

[8]   J. Pauli, M. Baldus, B. van Rossum, H. de Groot and H. Oschkinat, *Chembiochem* 2, 272-281 (2001).

[9]   M. Hong, *J. Magn. Reson.* 139, 389-401 (1999).

[10]   B.J. van Rossum, G.J. Boender, F.M. Mulder, J. Raap, T.S. Balaban, A. Holzwarth, K. Schaffner, S. Prytulla, H. Oschkinat and H.J.M. de Groot, *Spectrochim. Acta* A54, 1167-1176 (1998).

[11]   B.J. van Rossum, E.A.M. Schulten, J. Raap, H. Oschkinat and H.J.M. de Groot, *J. Magn. Reson.* 155, 1-14 (2002).

[12]   D.L. Worcester, T.J. Michalski and J.J. Katz, *Proc. Natl. Acad. Sci. U.S.A.* 83, 3791-3795 (1986).

[13]   B.J. van Rossum, D.B. Steensgaard, F.M. Mulder, G.J. Boender, K. Schaffner, A.R. Holzwarth and H.J.M. de Groot, *Biochemistry* 40, 1587-1595 (2001).

[14]   M. Wilhelm, H. Feng, U. Tracht and H.W. Spiess, *J. Magn. Reson.* 134, 255-260 (1998).

[15]   F.M. Mulder, W. Heinen, M. van Duin, J. Lugtenburg and H.J.M. de Groot, *J. Am. Chem. Soc.* 120, 12891-12894 (1998).

[16]   A.E. Bennett, C.M. Rienstra, M. Auger, K.V. Lakshmi and R.G. Griffin, J. Chem. Phys. 103, 6951-6958 (1995).

[17]   D. Marion and K. Würthrich, *Biochem. Biophys. Res. Com.* 113, 967 (1983).

[18]   K. Schmidt-Rohr and H.W. Spiess, "Multidimensional Solid-State NMR and Polymers", Academic Press, London (1994).

[19]   S. Zhang, B.H. Meier and R.R. Ernst, *Phys. Rev. Lett.* 69, 2149-2151 (1992).

[20]   J. Clauss, K. Schmidt-Rohr and H.W. Spiess, *Acta Polym.* 44, 1-17 (1993).

[21]   K. Landfester, C. Boeffel, M. Lambla and H.W. Spiess, *Macromolecules* 29, 5972-5980 (1996).

[22]   F.M. Mulder, W. Heinen, M. van Duin, J. Lugtenburg and H.J.M. de Groot, *Macromolecules* 33, 5544-5548 (2000).

[23]   K.K. Kumashiro, K. Schmidt-Rohr, O.J. Murphy, K.L. Ouellette, W.A. Cramer and L.K. Thompson, *J. Am. Chem. Soc.* 120, 5043-5051 (1998).

[24]   G. Metz, X.L. Wu and S.O. Smith, *J. Magn. Reson. Ser. A* 110, 219-227 (1994).

[25]   H.C. Chow, R. Serlin and C.E. Strouse, *J. Am. Chem. Soc.* 97, 7230-7237 (1975).

[26]   G. Donnay, *Arch. Biochem. Biophys.* 80, 80-85 (1959).

[27]   C. Kratky and J.D. Dunitz, *J. Mol. Biol.* 113, 431-442 (1977).

Chapter 4

MAS NMR Structure of a Microcrystalline Cd-bacteriochlorophyll *d* analog[§]

4.1   Introduction

Recent studies demonstrate that modern MAS NMR techniques allow the structure determination of uniformly labeled aggregates, disordered systems and polypeptides [1-4]. Similar to established methodology for structure elucidation of proteins in the dissolved state, distances or torsion angles between the nuclei can be measured and used for restricting the number of possible conformations. In solution, however, the packing of molecules is of little interest and "families" of molecular conformations are resolved. This contrasts with a genuine solid state, where the space filling arrangement is essential.
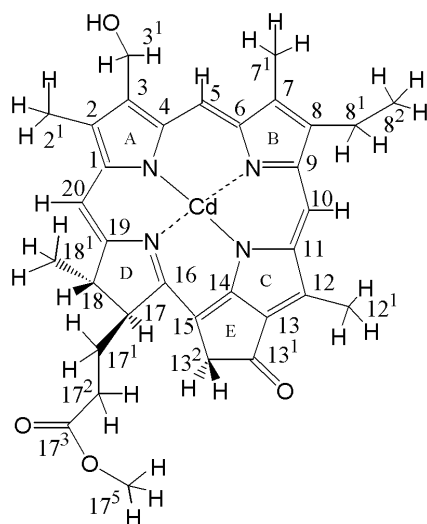
Fig. 4.1. Chemical structure of the Cd-bacteriochlorophyll d analogue.
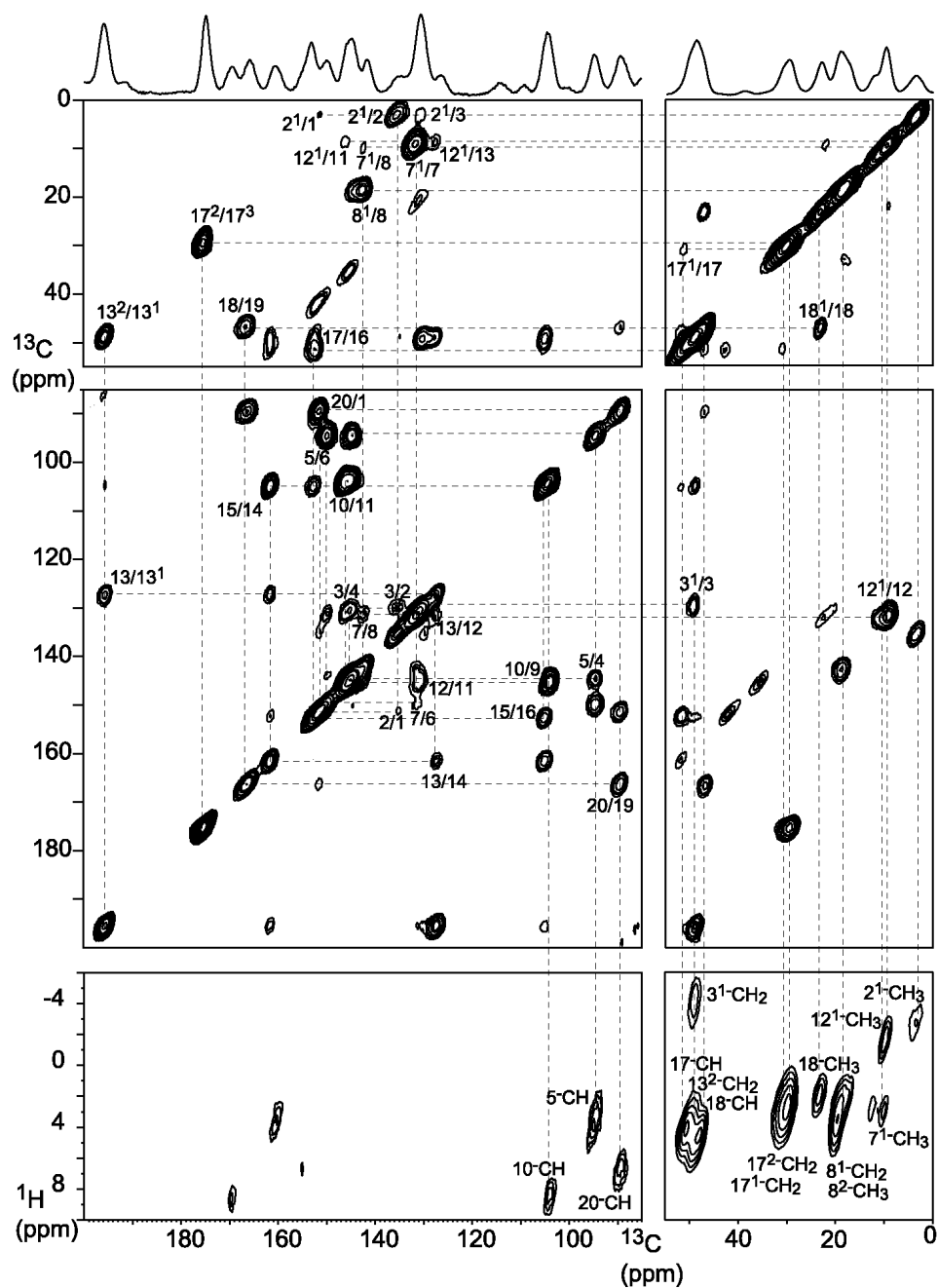
Fig. 4.2. Contour plot sections of a ^{13}C-^{13}C MAS NMR dipolar correlation spectrum of the aggregated Cd-bacteriochlorophyll d analogue recorded in a field of 9.4 T, using a spinning frequency of 11 kHz and a mixing time of 1.45 ms. The lower panels show contour plot sections of a ^{1}H-^{13}C MAS NMR PMLG dipolar correlation spectrum recorded in a field of 17.6 T employing a spinning rate of 12345 Hz. The upper trace shows parts of a 1D CP/MAS spectrum recorded in the same field using 12345 Hz MAS. The ^{13}C-^{13}C and ^{1}H-^{13}C connectivity network is indicated with dashed lines.

Thus, while the structure determination of molecules in solution can follow a strict bottom-up approach, in the microcrystalline solid state the top-down restrictions following from the requirement to fill up space in an orderly fashion have to be taken into account in the construction of a structural model from MAS NMR data [3].

Here, we acquire MAS NMR data of a uniformly ^{13}C and ^{15}N labeled Cd-bacteriochlorophyll *d* analog (Fig. 4.1), a derivative of the natural BChl *c* in the chlorosomes of green photosynthetic bacteria [5]. Ultimately, the study of these modified aggregates will help to explain the self-organization process *in vivo*. Various spectroscopic techniques have provided converging evidence for Cd•••OH•••O=C bonding, similar to the Mg•••OH•••O=C moieties in the natural system [6]. For instance, from low resolution diffraction data, a distance between the molecular planes of 6.4 Å was resolved.

4.2   Results and discussion

First, an assignment of the ^{1}H and ^{13}C resonances was obtained with 2D and 3D dipolar correlation spectroscopy. A 2D homonuclear ^{13}C-^{13}C and a heteronuclear ^{1}H-^{13}C spectrum are shown in Fig. 4.2, where the assignment is indicated with a connectivity network. The detailed chemical shift data are summarized in the Tables in chapter 5 (chlorin **1**). The ^{13}C NMR linewidths before apodization are 220-300 Hz in a magnetic field of 17.6 T and are essentially the same in a field of 9.4 T. This shows that these line widths are determined by homogeneous broadening as a result of J-couplings and residual dipolar couplings and there is little heterogeneous line broadening due to bulk susceptibility effects. In addition, a single set of peaks is detected. These observations imply local crystalline order with the same unique structural environment for every molecule.

From the MAS NMR signal of ^{113}Cd, which has a natural abundance of 12%, the chemical shift anisotropy (CSA) principal elements were extracted. The CSA shows that the Cd is strongly interacting with a fifth ligand, and the asymmetry parameter η ~0.25

reveals a non-axial coordination [7-9]. In addition, the ^{1}H and ^{13}C aggregation shifts, defined as the chemical shifts in the solid state relative to the corresponding shifts of the monomer in solution, reveal ring current effects that are very useful for structure determination [10]. The ^{1}H aggregation shifts are mainly due to ring currents and are exceptionally strong, up to 10 ppm in the upfield direction. These results can be accommodated by forming parallel stacks with the 3^1-OH groups coordinated to the Cd of the neighboring molecule and sheets due to hydrogen bonding between the 3^1-OH functionalities of one stack and the 13-C=O groups of another. The structure was optimized by the MM+ forcefield, since *ab initio* methods do not yet describe the weak interactions governing the intermolecular arrangement of this system satisfactory, while calculations at the forcefield level have been validated for large chlorophyll aggregates [11, 12]. Subsequently, a ^{1}H ring current shift calculation was done, where contributions of all macrocycles within a radius of 24 Å were added. The rings were approximated by circular loops, where the shielding of a single macrocycle was calculated by a DFT calculation at the B3LYP/6-311G(d,p) level. The calculation reproduces the experimental ring current shifts of the ^{1}H atoms with a standard deviation of the calculated versus the observed values of 1.2 ppm on a range of 11.6 ppm, while the correlation coefficient
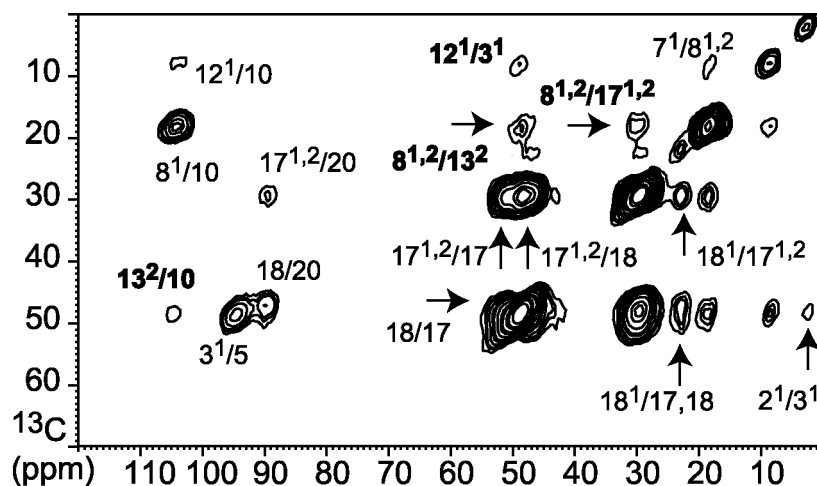

Fig. 4.3. ^{13}C-^{13}C CP^3 spectrum recorded in a field of 9.4 T using a mixing time of 200 µs. The intermolecular correlations are indicated in bold type.

58

equals 0.98. In this way, the shift data reveal a unique densely packed structure of overlapping macrocycles arranged in sheets of parallel inclined stacks (Fig. 4.4A). This structure was confirmed using the CP[3] experiment as introduced in chapter 3 (Fig. 4.3). Here ^{13}C-^{13}C correlations are generated by ^{1}H spin diffusion and close intermolecular contacts can be detected, providing direct evidence about the molecular arrangement [13]. For instance, a correlation between the 12-Me and the 3-CH$_2$OH moieties is in excellent agreement with the proposed sheet structure, since the 3^1-OH's are close to the 12-Me when sheets are formed by OH•••O=C hydrogen bonding (see also Fig. 4.4B). The CP[3] experiment also reveals close contacts between the 8-Et region and the 17-propionate region. This points to a head-to-tail arrangement of the sheets.

In a final modeling step, multiple layers were brought within van der Waals contact in a head-to-tail orientation as indicated by the NMR results. A large aggregate containing 60 molecules was optimized. Two possible arrangements emerge from the calculations that are both in accordance with the NMR, where the mutual orientation of adjacent sheets is either similar, corresponding to a triclinic structure, or with a 180° screw axis, corresponding to a monoclinic structure. Both structures were found to be stable in the modeling. The former, however, is energetically less likely due to unfavorable electric dipole interactions. According to our calculations, the electric dipole moment in the aggregates has an estimated strength of 5.1 Db and is directed ca. 30° out of the ring plane. With the screw axis, the components perpendicular to the rings are anti-parallel in neighboring sheets. In the forcefield approximation, the energy of the monoclinic structure is a modest ~0.5 kcal per molecule lower than for the triclinic structure.

From the optimized monoclinic 60-mer, the crystal cell parameters were extracted. It has space group $P2_1$ with $a = 14.3$ Å, $b = 27.3$ Å, $c = 6.4$ Å, $\beta = 147.2°$ and $Z = 2$. A projection along the b-axis is depicted in Fig. 4.4A, which corresponds to one layer of Chlide. The Cd-Cd distance is 6.4 Å, which has also been observed by electron diffraction [6]. Fig. 4.4B represents a projection along the c-axis, showing the contact between layers. The structure of a layer is well determined and the error in the position is
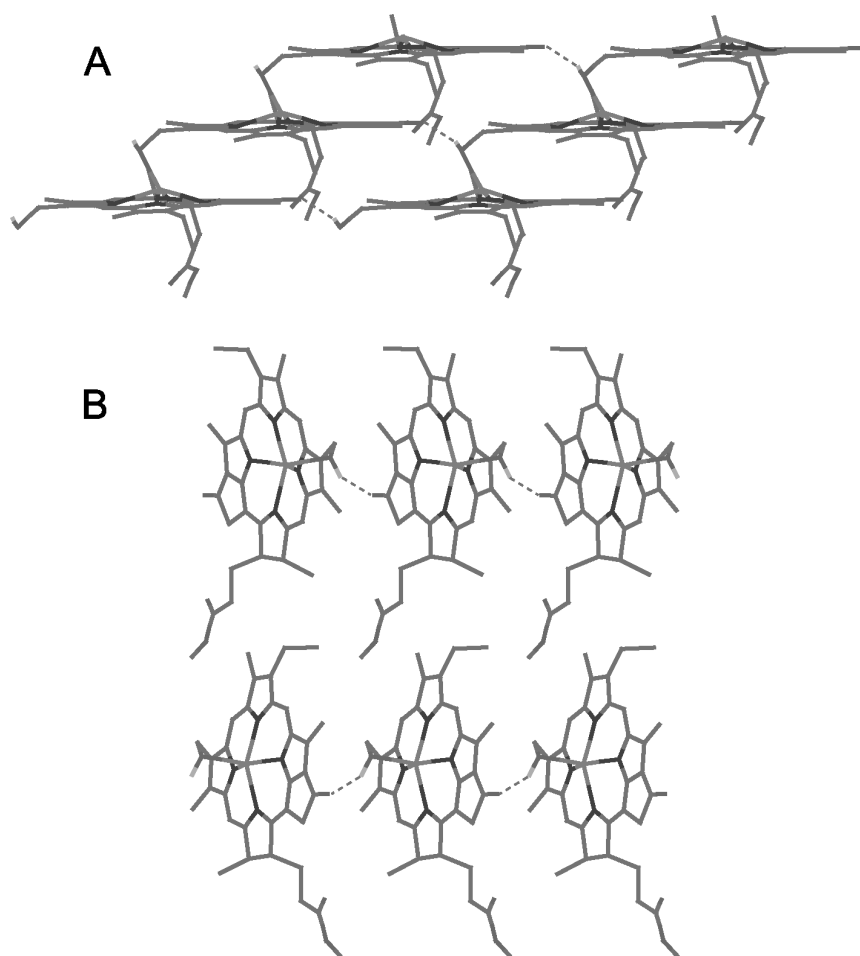
Fig. 4.4. Crystalline structure projected along the b-axis (A) and the c-axis (B).

estimated to be 0.2 Å. The error in the relative position of weakly bound neighboring layers is more difficult to quantify within the forcefield approach. A comprehensive structural model is provided as a crystallographic information (*cif*) file.[*]

The structure determined for the Cd-bacteriochlorophyll *d* analog compares well with structures of well-ordered chlorophyllide crystals that have been resolved with X-ray diffraction. For instance, in hydrated chlorophyllide *a* the rings are in a pseudo-hexagonal net, where ring A of one molecule overlaps with rings C and E of its translationally equivalent neighbor [14]. Water molecules act as cross-linkers both by coordinating to a

---

[*]The *cif* file of the crystalline structure is available at http://pubs.acs.org (DOI: 10.1021/ja0367492).

central Mg metal and by hydrogen bonding to a neighboring ring E carbonyl. Here, the 3-hydroxymethyl group introduces an additional functionality leading to the network in Fig. 4.4A. Since water is not present as a cross-linker and due to the strong interaction, the volume per molecule has the relatively small value of ~667 $\mathring{A}^3$, compared to *e.g.* 864 $\mathring{A}^3$ for ethyl chlorophyllide *a* dihydrate. In the chlorophyllide *a* crystals, the absence of long tails also results in a back-to-tail orientation, as visible in Fig. 4.4B, and twofold or threefold screw axes are observed there between the neighboring layers [14]. For self-assembled Chl *a*/H_2O, on the other hand, the sheets orient back-to-back as a result of the long farnesyl tails that interdigitate in bilayers [13].

4.3   Conclusion

  In conclusion, we have shown that a 3D structural model of a microcrystalline structure can be obtained with MAS NMR refined with molecular modeling, and we expect that this study is relevant to future applications in nanotechnology or structural research.

References

[1]   C.M. Rienstra, L. Tucker-Kellogg, C.P. Jaroniec, M. Hohwy, B. Reif, M.T. McMahon, B. Tidor, T. Lozano-Perez and R.G. Griffin, *Proc. Natl. Acad. Sci. U. S. A.* 99, 10260-10265 (2002).

[2]   F. Castellani, B. van Rossum, A. Diehl, M. Schubert, K. Rehbein and H. Oschkinat, *Nature* 420, 98-102 (2002).

[3]   B.J. van Rossum, D.B. Steensgaard, F.M. Mulder, G.J. Boender, K. Schaffner, A.R. Holzwarth and H.J.M. de Groot, *Biochemistry* 40, 1587-1595 (2001).

[4]   G.R. Goward, D. Sebastiani, I. Schnell, H.W. Spiess, H.D. Kim and H. Ishida, *J. Am. Chem. Soc.* 125, 5792-5800 (2003).

[5]   J.M. Olson, *Photochem. Photobiol.* 67, 61-75 (1998).

[6]   M. Amakawa and H. Tamiaki, *Bioorg. Med. Chem.* 7, 1141-1144 (1999).

[7]   H.J. Jakobsen, P.D. Ellis, R.R. Inners and C.F. Jensen, *J. Am. Chem. Soc.* 104, 7442-7452 (1982).

[8]   M.A. Kennedy and P.D. Ellis, *J. Am. Chem. Soc.* 111, 3195-3203 (1989).

[9]   K. McAteer, A.S. Lipton, M.A. Kennedy and P.D. Ellis, *Solid State Nucl. Magn. Reson.* 7, 229-238 (1996).

[10]   J.J. Katz, M.K. Bowman, T.J. Michalski and D.L. Worcester, in *Chlorophylls* (H. Scheer, Ed.) pp. 211-235, CRC Press, Boca Raton (1991).

[11]   A.R. Holzwarth and K. Schaffner, *Photosynth. Res.* 41, 225-233 (1994).

[12]   S. Yagai, T. Miyatake, Y. Shimono and H. Tamiaki, *Photochem. Photobiol.* 73, 153-163 (2001).

[13]   I. de Boer, L. Bosman, J. Raap, H. Oschkinat and H.J.M. de Groot, *J. Magn. Reson.* 157, 286-291 (2002).

[14]   C. Kratky and J.D. Dunitz, *J. Mol. Biol.* 113, 431-442 (1977).

Chapter 5

MAS NMR structures of aggregated Cd-chlorins reveal molecular control of self-assembly of chlorosomal bacteriochlorophylls[§]

5.1   Abstract

Magic Angle Spinning NMR has been used to investigate the self-organization of bacteriochlorophylls in chlorosomal light-harvesting antennae. Two model cadmium chlorins were studied that were uniformly ^{13}C and ^{15}N enriched in the ring moieties. The chlorin models differ from the natural BChl c in the central metal, the 3-, 12-, 17- and 20-side chains. One model system has the farnesyl tail replaced by a methyl, while the other has a stearyl tail. The ^{113}Cd MAS NMR signals indicate a five-coordination of the Cd metal. In particular, the combined NMR data show a HO•••Cd coordination, very similar to the HO•••Mg coordination in the natural system. Anomalously large ^{1}H ring current shifts up to 10 ppm reveal a very dense orderly stacking of the molecules in planar layers, for which a correlation length of at least 24 Å was determined from long-range ring current shift calculations. In addition, our model structures confirm and validate the essential role of the [$3^{1}R$]- and [$3^{1}S$]-stereoisomers in the formation of the chlorosomal antennae, since tubular structures are not formed without this chirality. The 3D arrangement of the layers is revealed by intermolecular ^{13}C-^{13}C correlations obtained from CP^{3} experiments. With the tail truncated to methyl, a microcrystalline solid is formed with favorable interactions between the planar sheets in a head-to-tail orientation. The stearyl tails lead to a considerably disordered aggregate consisting of both *syn* and *anti* layers similar to the chlorosomes, as indicated by a doubling of the N-D signal. These results reveal a balance between relatively strong local interactions and contributions to the free energy of the system associated with a longer length scale. This leads to a robust chlorosome structure, stable against thermodynamic noise and allows for fine-tuning of the structure.

5.2   Introduction

Photosynthetic green sulfur bacteria contain extra-membraneous light-harvesting antenna complexes called chlorosomes, which are ellipsoid vesicles of about 100-300 nm in length (for a review, see *e.g.* ref. [1]). Chlorosomes contain tubular antennae consisting mostly of bacteriochlorophyll BChl *c* molecules (Fig. 5.1) and BChl *d* or *e* in some bacteria, surrounded by a monolayer of lipids and some proteins. Via a BChl *a*-protein complex called baseplate, which is a part of the chlorosomal envelope facing the cytoplasmic membrane, photonic excitations are funneled into membrane bound photosynthetic reaction centers [2-4]. It has been shown that the structural organization of the chlorosomal antennae are reproduced by pure BChl *c* aggregated in hexane, which indicates that the self-assembly of BChl *c* is responsible for the tubular structure [5-7]. This is discussed in detail in Chapter 1.
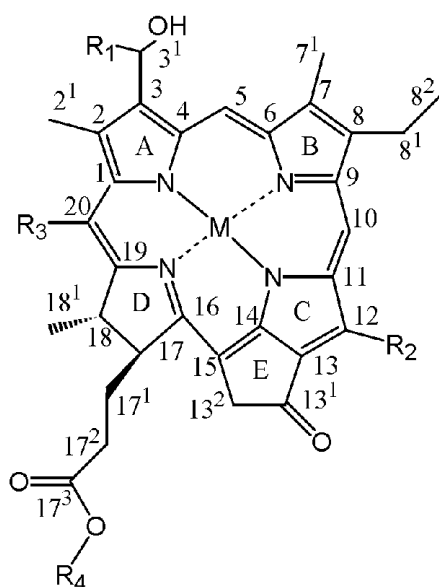
	M	R_1	R_2	R_3	R_4
BChl *c* in *C. tepidum*	Mg	Me	Et	Me	Farnesyl
Cd-Chlorin-Me (1)	Cd	H	Me	H	Me
Cd-Chlorin-stearyl (2)	Cd	H	Me	H	Stearyl

Fig. 5.1. Chemical structure of BChl c and the Cd-chlorins.

Several functionalities of the building blocks, BChl *c*, *d*, or *e*, are thought to be predominant chemical factors in steering the formation of specific supramolecular assemblies in a bottom-up process. This contrasts with the emerging and top-down thermodynamic control that is generally thought to govern mesoscopic assembly processes in most soft condensed matter systems, since these are to first order independent of the microscopic details of the molecular building blocks involved. First, a common denominator in BChl *c*, *d*, or *e* aggregates is an intermolecular 13-C=O•••HO•••Mg structural motif. Hence the molecular building blocks are kept together by coordination and H-bond interactions that are strong compared to, for instance, non-bonding van der Waals interactions. The C=O•••HO•••Mg motif can support a variety of suprastructures [8-10]. Second, chlorosomes generally contain a mixture of BChl homologues with different 8-, 12- and 20-alkyl groups [1]. The presence of different 8- and 12-substituents does not lead to significant additional line broadening in the MAS NMR data of the chlorosomes, which indicates that these homologues are in very similar structural environments [7]. On the other hand, molecular modeling of BChl *c* indicates that steric repulsion between the 2-Me and the 20-Me induces a bending of ring A. In the modeling a BChl *c* aggregate is more open than a BChl *d* aggregate possessing 20-H instead of 20-Me [11, 12]. Hence the bulkiness of the side-chains may counteract and fine-tune the dense stacking provoked by the coordination and H-bonding. The stereochemistry of the molecule appears another crucial factor for the local self-organization in the natural system. Molecular modeling predicts that BChl *c* can form stacks with different conformations with the Mg ion at the opposite side (*anti*) or the same side (*syn*) of the ring plane compared to the 17^1-C, respectively [11]. In two layers of BChl *c* with opposite curvatures, an outer *anti* layer will have ester chains pointing to the exterior, while a *syn* inner layer will have the tails filling the center of a tube [11, 13]. The [3^1R]- and [3^1S]-stereoisomers are thought to stabilize this tubular bilayer structure, where the outer *anti* layer prefers the [3^1R]- and the inner *syn* layer the [3^1S]-form. This represents another tuning mechanism where the chirality of the 3^1-position can play a pivotal role steering the free energy balance of the supramolecular assembly as a whole. Finally, the tails fill the core of the tubular micelles and provide the interface between the tubes [11, 13]. They may help to induce the formation of micelles, similar to fatty acid

molecules in an aqueous environment in synergy with the curvatures induced by the 3^1-stereochemistry.

To test for mechanisms controlling the self-organization of BChl *c* in the chlorosomes, we have studied self-assembled chlorins **1** and **2** (Fig. 5.1) with Magic Angle Spinning (MAS) NMR. These synthetic chlorins were uniformly ^{13}C- and ^{15}N-enriched with exception of the tails. In a converging strategy, several functionalities that are potentially involved in determining the size and topology of the suprastructure of the BChl aggregates, are absent or modified in parallel in chlorins **1** and **2**. To obtain insight into how the electronic and structural properties of the central metal ion affect the aggregate structure, the Mg^{2+} ion has been replaced by Cd^{2+}. ^{113}Cd, with a natural abundance of 11%, is a good NMR nucleus and has been used in the past to determine coordination properties in porphyrin compounds [14-16], heme proteins [17, 18] and photosynthetic membrane protein complexes [19]. The ionization potentials and electron affinities of the Mg^{2+} and Cd^{2+} are different. The ionic radius of Cd^{2+} in a four-coordinated environment is 0.78 Å. This is considerably larger than the 0.57 Å radius of Mg^{2+}. Second, to probe the role of the stereochemistry of the 3-substituent, the 3-(1-hydroxyethyl) is replaced by a 3-hydroxymethyl without chirality, while the chirality of the 17- and 18-side chains is unaffected. Third, the 12-side group of the chlorins is a methyl, while in the chlorosomes of *Chlorobium tepidum* an ethyl side chain is present in ca. 98% of the BChl *c* [7]. Fourth, the model molecules have a hydrogen at C-20, instead of the 20-Me, similar to BChl *d*. MAS NMR can be used to determine whether this yields a short plane-to-plane distance. Finally, the long farnesyl chains are truncated by an unlabeled Me in chlorin **1**, which is expected to influence the suprastructure of the aggregate. The chlorin **2** molecule possesses a long stearyl tail. If the tails are responsible for the micellar structure in the chlorosomes, this should transpire from the structure of self-aggregated chlorin **2**.

It will be shown that it is possible to resolve the structural arrangement of these model systems in great detail using MAS NMR combined with molecular modeling and ring current shift calculations. The results corroborate the current picture that the

stereochemistry of the 3-substituent gives a predominant contribution to the free energy balance that leads to tubular structures in the chlorosomes.

5.3   Materials and methods

[13]C, ^{15}N-Labeled chlorophyll-*a* was extracted from *Chlorella vulgaris* K-22 strain cultured in a labelled medium (Chlorella Industry Co. Ltd.) and converted to methyl ^{13}C, ^{15}N-labeled pyropheophorbide-*a* by use of unlabeled methanol [20]. Using the resulting methyl ester as the starting material, cadmium methyl ^{13}C, ^{15}N-labeled 3^1-demethyl-bacteriopheophorbide-*d* (chlorin **1**) was prepared [21]. According to related procedures [22], the methyl ester was exchanged with the unlabeled stearyl ester to produce stearyl ^{13}C, ^{15}N-labeled pyropheophorbide-*a*, followed by transformation of the 3-vinyl to 3-hydroxymethyl group. The resulting compound was metallated similar to the preparation of chlorin **1** to give the corresponding cadmium complex (chlorin **2**). Methanol-dichloromethane (1:3) solutions of the Cd-chlorins were added to excess amounts of cyclohexane, resulting in the rapid formation of the self-aggregates of both chlorins.

Solid state MAS NMR experiments were performed at a temperature of 277 K with a DMX-400 and a DSX-750 spectrometer, using 4 mm triple resonance MAS probeheads (Bruker, Karlsruhe, Germany). The spinning frequency was kept constant within a few hertz. Ramped variable amplitude cross-polarization [23] with a recycle delay of 1 s was applied in all experiments. The ^{1}H spins were decoupled during acquisition using TPPM [24]. Homonuclear [13]C-^{13}C dipolar correlation spectra were recorded using radio frequency-driven dipolar recoupling (RFDR) with phase sensitive detection in ω_1 [25]. [1]H 90° pulses of 3.5 μs were used with CP periods of 2 ms. For each of 256 steps in the indirect dimension, 8 transients were accumulated. Heteronuclear [1]H-^{13}C correlations were obtained by WISE and PMLG experiments using short cross-polarization times of 128 μs or 256 μs and a [1]H 90° pulse of 3.1 μs. The ^{1}H chemical shift scale was calibrated from a PMLG spectrum of solid tyrosine·HCl salt. For each of 128 steps in the indirect ^{1}H dimension, four ^{13}C transients were accumulated, while during the WISE experiment 64 ^{13}C transients were accumulated for each of 32 ^{1}H steps. A 3D [1]H-[13]C-[13]C

WISE/RFDR experiment was performed using a ^{1}H rf field of 81 kHz, a ^{13}C rf field of 45 kHz and a VACP interval of 128 µs. For each of 16 steps in the indirect ^{1}H dimension, and for 256 steps in the indirect ^{13}C dimension, 16 ^{13}C transients were accumulated. 1D ^{15}N CP/MAS experiments were performed with variable amplitude CP periods of 5.12 ms. For each experiment, 1024 transients were accumulated. Solid state [113]Cd shifts were referenced to 0.1 M $Cd(ClO_4)_2$ in H_2O by setting the [113]Cd response of solid $Cd(ClO_4)_2 \cdot 6H_2O$ to –9 ppm [26]. [113]Cd CP/MAS experiments employed VACP times of 2 ms acquiring ~15000 scans. [113]Cd and ^{15}N chemical shielding tensor elements were determined from the spinning sideband pattern of 1D CP/MAS spectra following the Herzfeld and Berger procedure [27]. Error margins were estimated by repeating the experiment with different spinning frequencies and by an interactive tensor analysis [28]. CP^3 experiments were performed using a ^{1}H rf field of 71 kHz and VACP periods of 64 µs [29]. For 256 indirect ^{13}C steps 16 transients were acquired. A 3D WISE/CP^3 experiment used a ^{1}H rf field of 81 kHz and three VACP periods of 96 µs. 128 scans were acquired for each of 144 indirect ^{13}C steps and 12 ^{1}H steps.

To determine the shifts of the monomer in solution, NMR experiments were performed in coordinating solvents with concentrations of ca. 0.01 M [30]. The NMR data for the monomer in dimethylsulfoxide-d_6 (DMSO) and in tetrahydrofuran-d_8 (THF) were acquired with a DMX-600 spectrometer (Bruker, Karlsruhe, Germany). The ^{15}N chemical shifts were referenced to liquid NH_3. The chemical shifts have been used to calculate the aggregation shifts $\Delta\sigma = \sigma_i - \sigma_{liq}$ for ^{1}H and [13]C. The ^{15}N and [113]Cd responses were measured in DMSO. The [113]Cd chemical shifts were referenced to 0.1 M $Cd(ClO_4)_2$ in H_2O. A single [113]Cd signal in DMSO was observed in a 1D experiment, using ~4000 scans with a recycle delay of 8 s.

Structural modeling was done using the Hyperchem version 7 software (Hypercube, Inc.). All geometry optimizations used a Polak-Ribiere conjugate gradient algorithm with a gradient convergence criterion of 0.01 kcal/mol. DFT calculations of chemical shifts were done using the Gaussian 98 (Gaussian, Inc.) software. For these calculations, a Mg
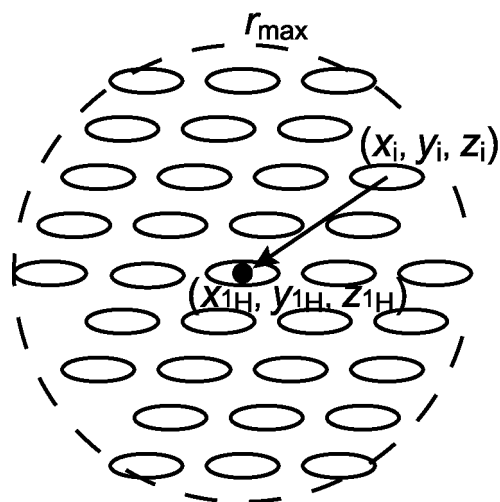
Fig. 5.2. Schematic representation of the lattice summation for the ^1H ring current shift calculation.

was used, as Cd is represented poorly compared to Mg in the DFT method, and the H_2O was removed.

To calculate the ring current effects for intermolecular distances, the macrocycles were approximated by circular loops with a 3 Å radius. The magnetic field **B** induced at a position **r** by a circular loop with current I is given by

$$\vec{B} = \frac{\mu_0 I}{4\pi} \int \frac{d\vec{l} \times \vec{r}}{r^3},$$ (5.1)

integrated around the loop in the direction of the current. For a loop with radius a in the x,y-plane and centered at the origin, the isotropic ring current shift σ_{rc} is proportional to B_z, yielding

$$\sigma_{rc}(x,y,z) = c \int_0^{2\pi} d\varphi \left(1 - \frac{x}{a}\cos\varphi - \frac{y}{a}\sin\varphi \right) \left(\left[\frac{x}{a} - \cos\varphi \right]^2 + \left[\frac{y}{a} - \sin\varphi \right]^2 + \left[\frac{z}{a} \right]^2 \right)^{-\frac{3}{2}}$$ (5.2)

The ring current of a single loop was calibrated by a nucleus independent chemical shift (NICS) DFT calculation [31] for a ghost atom placed 4.0 Å above the center of a chlorin molecule, using a B3LYP/6-311 G(d,p) level of theory. For these conditions, a ring current shift of 3.90 ppm was obtained. Using Eq. 5.2 this provides $c=2.87$ ppm as a

calibration constant. The total intermolecular ring current shift for each ^{1}H was obtained by adding the contribution from all other rings in the lattice within a maximum range $r_{max} = 24$ Å,

$$\sigma_{1H}(x_{1H}, y_{1H}, z_{1H}) = \sum_{i \neq 0}^{r < r_{max}} \sigma_{rc}(x_{1H} - x_i, y_{1H} - y_i, z_{1H} - z_i), \qquad (5.3)$$

where each σ_{rc} given by the integral in Eq. 5.2 was evaluated numerically using Maple 6[*] (Waterloo Maple, Inc.). This summation over a two-dimensional lattice is depicted schematically in Fig. 5.2.

5.4   Results

5.4.1   Assignment of the NMR responses

The chemical shifts of the aggregated chlorins were obtained using 2D and 3D MAS correlation spectroscopy. Fig. 5.3 shows a 2D ^{13}C-^{13}C RFDR spectrum of aggregated chlorin **2** recorded with a mixing time of 1.14 ms. A spectrum of aggregated chlorin **1** recorded under similar experimental conditions shows almost identical results (Fig. 4.2). The nearest neighbor connectivities of the molecular ^{13}C network lead to the assignment indicated with the dashed lines in Fig. 5.3. The spectrum of chlorin **1** has a single set of narrow peaks with line widths of 220-300 Hz in a field of 9.4 T, while the line widths are only ~10% higher in a field of 17.6 T. This provides evidence for a well-defined microcrystalline structure without major inhomogeneous broadening due to disorder. The ^{13}C line widths of aggregated chlorin **2**, however, of 200-300 Hz in a field of 9.4 T are increased by ~50% in a field of 17.6 T, which indicates a significantly increased inhomogeneous broadening and disorder in the sample. In addition, a doubling of the 15/16 correlation is resolved (Fig. 5.3).

Relayed transfer from the 2^1, 7^1 and 12^1 carbons to their second-nearest neighbors allowed the unambiguous assignment of those methyl signals. The $2^1/3$, $7^1/8$, $12^1/11$ and

---

[*]The Maple routine used for the calculation is given in the appendix of this thesis.
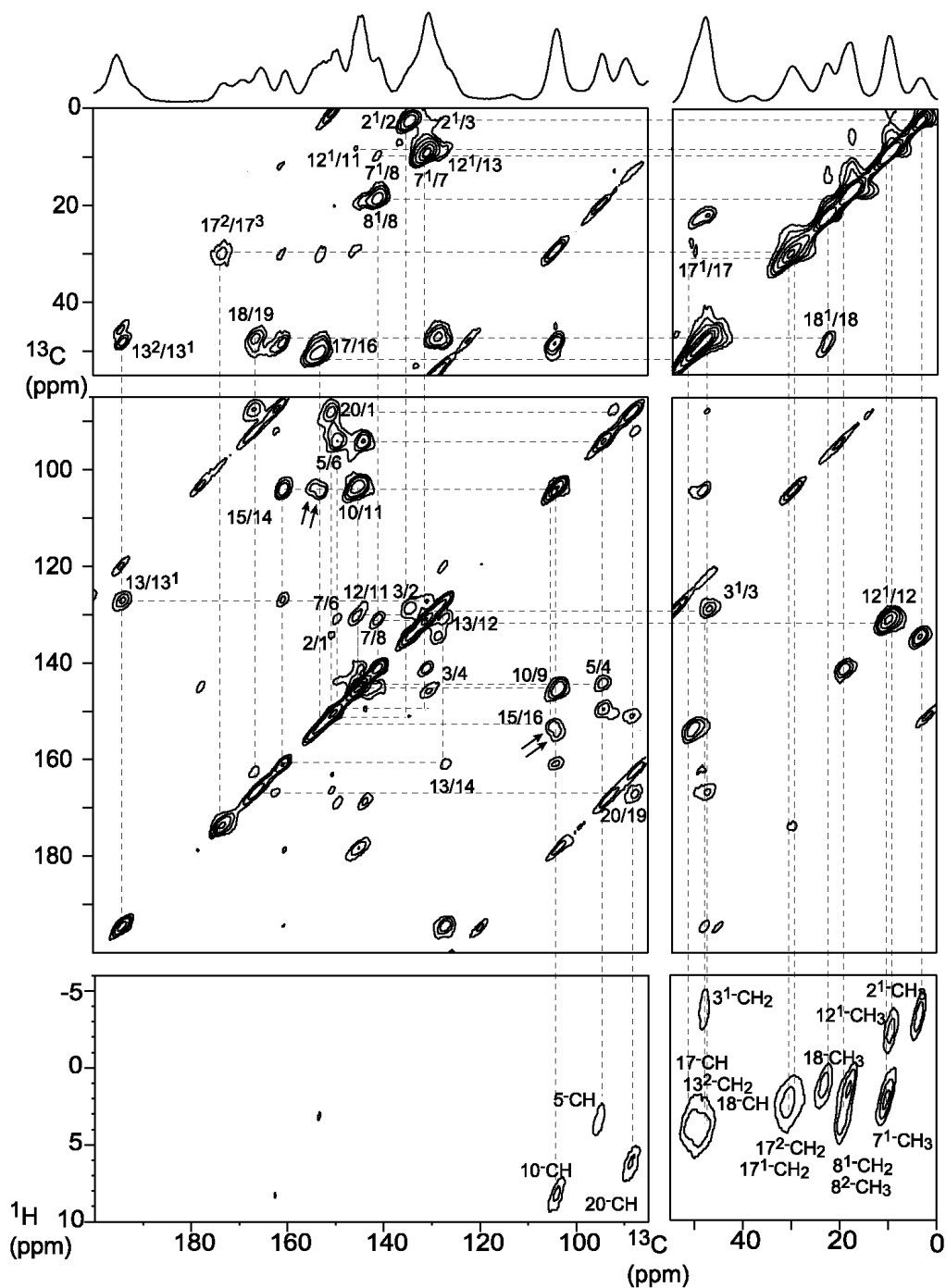
Fig. 5.3. Contour plot sections of a ^{13}C-^{13}C MAS NMR dipolar correlation spectrum of aggregated chlorin 2 recorded in a field of 17.6 T, using a spinning frequency of 14 kHz and a mixing time of 1.14 ms. The lower panels show contour plot sections of a ^{1}H-^{13}C MAS NMR PMLG dipolar correlation spectrum recorded in the same field employing a spinning rate of 11 kHz. The upper trace shows parts of a 1D CP/MAS spectrum using 12345 Hz MAS. The ^{13}C-^{13}C and ^{1}H-^{13}C connectivity network is indicated with dashed lines. The arrows indicate a doubling of the 15/16-C correlation.

$12^1/13$ correlations are weakly visible in Fig. 5.3. The 8^1 response could not be resolved from the 8^2-^{13}C signal. The 4, 6, 9 and 11 positions were assigned from relayed transfer correlations using a dataset recorded with a relatively long mixing time of 2.9 ms. The 11 carbon can be assigned from a relayed $12^1/11$ correlation in Fig. 5.3. The ^{13}C chemical shifts of the aggregated chlorins are summarized in Table 5.1, printed together with the other Tables at the end of this chapter.

For the assignment of the ^{1}H shifts, the phase-modulated Lee-Goldburg (PMLG) [32] technique was applied in a high field of 17.6 T. Using the ^{13}C data as a starting point, the ^{1}H-^{13}C signals were assigned, as depicted in the lower panels of Fig. 5.3 for chlorin **2**. The 3^1-OH proton is not observed, possibly due to some form of dynamics resulting in excessive line broadening and inefficient CP. Several signals are difficult to assign due to overlap in the ^{13}C dimension. In particular, there is overlap between the 7^1-CH$_3$ and 12^1-CH$_3$, and between the 3^1-CH$_2$ and 13^2-CH$_2$ in the ^{13}C dimension. To complete the solid state ^{1}H assignment, a 3D ^{1}H-^{13}C-^{13}C dataset was collected of chlorin **1**. A straightforward WISE step was implemented after the initial ^{1}H 90° pulse in the sequence [11]. With a short CP time of 128 μs, cross-peaks appear in the 3D spectrum that correlate a ^{1}H spin to a directly bound ^{13}C pair. In the ^{1}H WISE dimension, most peaks are already well resolved due to the truncation of the ^{1}H dipolar couplings in the high field. In Fig. 5.4A, two sections of a 2D ^{13}C-^{13}C spectrum are shown (panels I, III) together with the corresponding ^{1}H-^{13}C slices from the 3D experiment (panels II, IV). The horizontal dashed lines in the panels I and III in Fig. 5.4A correspond to the ^{13}C shifts of the ^{1}H-^{13}C slices depicted in panels II and IV. As a result of the first transfer step from ^{1}H to ^{13}C in the 3D experiment, only the bound ^{13}C is correlated to this ^{1}H signal in the ^{1}H-^{13}C-^{13}C dataset. This is illustrated with the labels in panels II and IV. With the 3D datasets all protons can be assigned unambiguously, while the 2D PMLG spectra provide the most accurate chemical shifts. The ^{1}H chemical shifts of the aggregated chlorins **1** and **2** are summarized in Table 5.2.
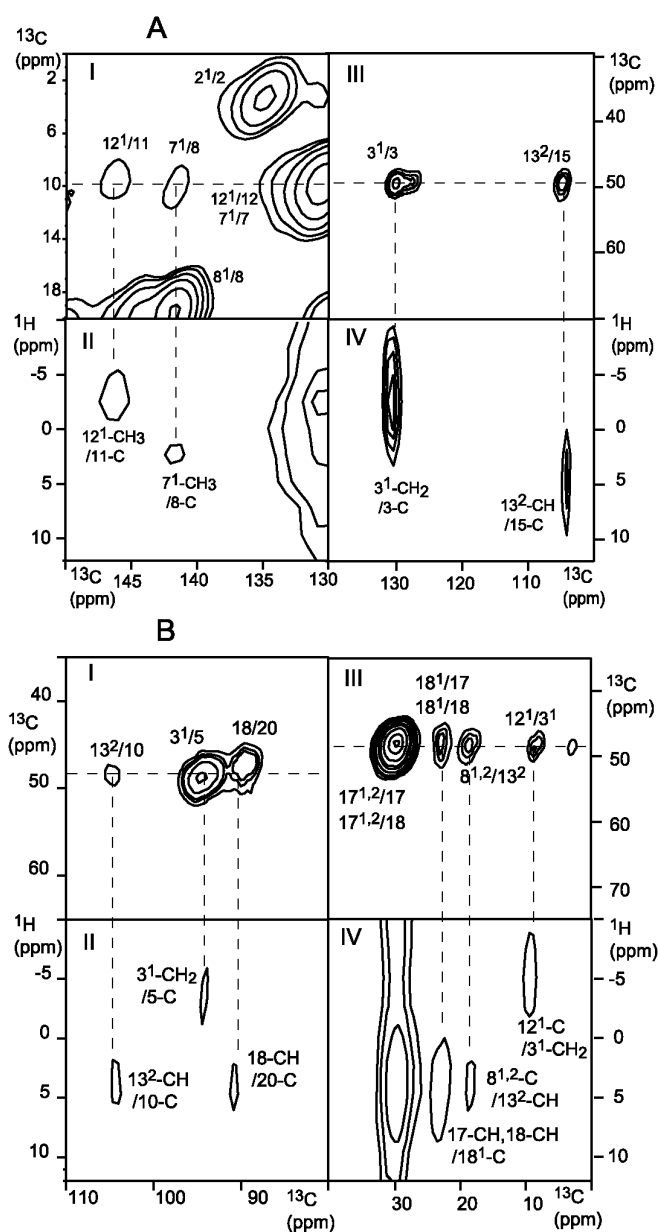
*Fig. 5.4. (A) Enlarged ^{13}C-^{13}C sections of a 2D RFDR spectrum of aggregated chlorin **1** recorded in a field of 9.4 T employing a spinning frequency of 11 kHz (I, III) and ^{1}H-^{13}C slices of a 3D ^{1}H-^{13}C-^{13}C WISE/RFDR spectrum recorded in a field of 17.6 T employing a spinning frequency of 14 kHz (II, IV). In spectrum II (IV), the ^{13}C shift in the third dimension is 9.5 (49) ppm, as indicated by the horizontal dashed line in spectrum I (III). (B) Enlarged ^{13}C-^{13}C sections of Fig. 5.7A (I, III), and ^{1}H-^{13}C slices of a 3D ^{1}H-^{13}C-^{13}C WISE/CP^{3} spectrum of aggregated chlorin **1** recorded in a field of 17.6 T using a spinning frequency of 14.5 kHz (II, IV), where the chemical shift of the indirect ^{13}C dimension is 49 ppm, as indicated by the horizontal dashed lines in spectra I and III.*
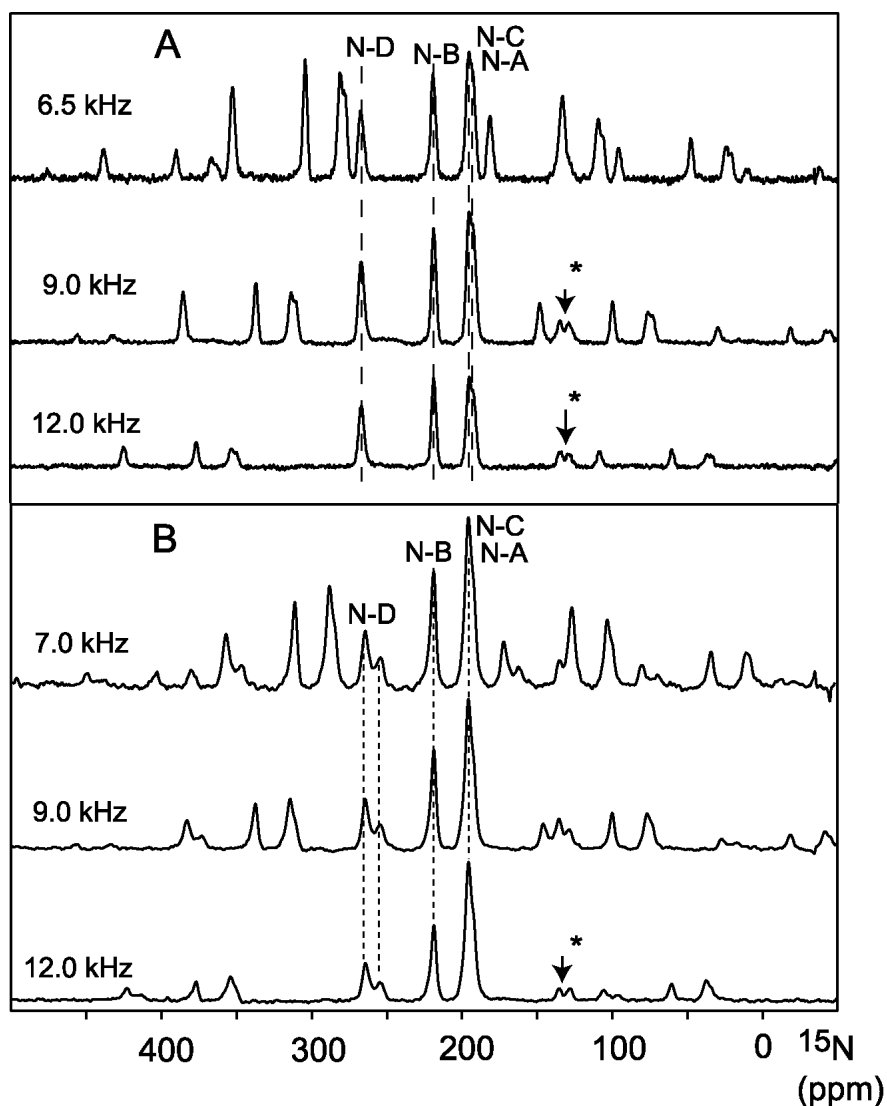
*Fig. 5.5. 1D ^{15}N CP/MAS spectra of aggregated chlorin **1** (A) and chlorin **2** (B) recorded in a field of 17.6 T employing different spinning frequencies. The isotropic contributions are connected by dashed lines. The asterisks denote small fractions of the samples, where the macrocycles do not contain Cd.*

To obtain the ^1H and ^{13}C aggregation shifts, defined as the chemical shifts in the solid state relative to the monomer shifts in solution, the chlorin **1** was dissolved in THF-d8 and DMSO-d6, which are strong coordinating solvents, while chlorin **2** was dissolved only in DMSO-d6. The ^1H and ^{13}C assignments were obtained from 1D ^1H and ^{13}C experiments, as well as 2D ^1H-^{13}C and ^{13}C-^{13}C COSY experiments. The ^{13}C and ^1H monomer shifts are listed in Tables 5.1 and 5.2, respectively.

Fig. 5.5 shows ^{15}N CP/MAS spectra of the aggregates. To assign the ^{15}N response, long-range [1]H-^{15}N heteronuclear multibond correlation (HMBC) experiments were done for the monomeric species dissolved in DMSO-d6, where the ^{15}N spins are correlated with the ^{1}H spins at the 5-, 10- and 20-*meso*-positions. The assignment of the ^{15}N signals in Fig. 5.5 is based on the response in solution (Table 5.3). The distinction between the N-A and N-C is ambiguous, since the chemical shift difference in solution is small. The ^{15}N chemical shifts and estimated tensor elements are summarized in Table 5.3. The ^{15}N spectra of aggregated chlorin **1** show a single set of peaks. In the ^{15}N MAS NMR spectra of chlorin **2**, however, a doubling of the N-D peak is observed.
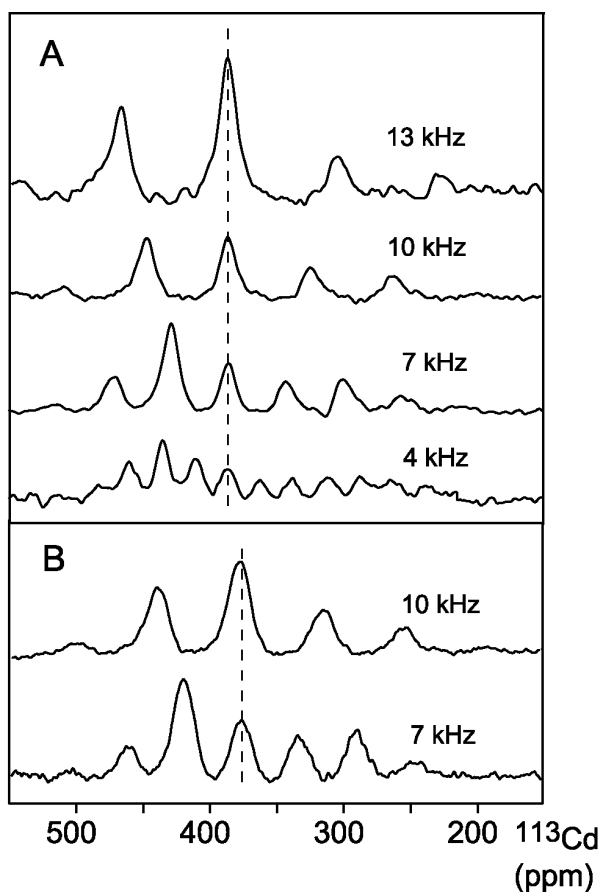
Fig. 5.6. [113]*Cd CP/MAS spectra of aggregated chlorin **1** (A) and chlorin **2** (B) recorded in a field of 17.6 T employing different spinning frequencies. The isotropic contributions are connected by a dashed line.*

In the [113]Cd CP/MAS spectra, a broad signal appears at 395 ppm for chlorin **1**, compared to 375 ppm for chlorin **2** (Fig. 5.6). The chemical shift tensor elements and anisotropy and asymmetry parameters that were estimated from the spinning side bands in Fig. 5.6 are listed in Table 5.4. Finally, the [113]Cd response in DMSO-d6 for chlorin **1** shows a single peak at 390 ppm (Table 5.4).
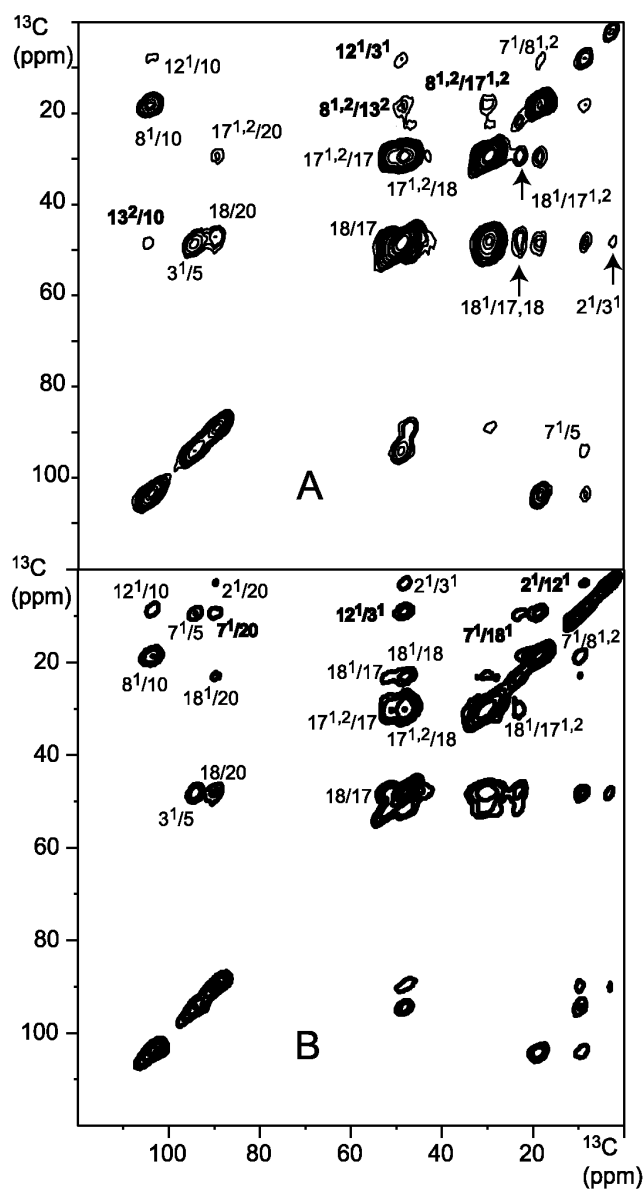
Fig. 5.7. ^{13}C-^{13}C CP^3 *spectra of aggregated chlorin **1** (A) and chlorin **2** (B) recorded in a field of 9.4 T using a spinning frequency of 11 kHz and a ^1H spin diffusion mixing time of 200 μs. The correlations labeled in bold face are assigned as intermolecular.*

Recently, it has been shown that good long range ^{13}C-^{13}C transfer can be obtained using a ^{1}H spin diffusion interval sandwiched between two additional CP steps [33, 34], as is discussed in Chapter 3. Fig. 5.7 shows 2D spectra of aggregated chlorin **1** (A) and chlorin **2** (B) recorded with a CP^3 experiment that was adapted for short mixing times [29, 35]. A ^{1}H spin diffusion interval of 0.2 ms was used to generate ^{13}C-^{13}C correlations. The assignment of the correlations in Fig. 5.7 is straightforward with the ^{13}C shifts of Table 5.1, with the exception of ambiguities due to overlap between the 3^1 and 13^2, and between the 7^1 and 12^1 carbons. To resolve these ambiguities, a 3D WISE/CP^3 experiment was implemented by including an additional ^{1}H evolution period after the initial ^{1}H 90° pulse. Fig. 5.4B shows two sections from the 2D CP^3 experiment (panels I, III) together with the corresponding ^{1}H-^{13}C slices of the 3D spectrum (panels II, IV) of chlorin **1**. With the additional information contained in the 3D dataset, the cross-peaks are assigned as indicated in Fig. 5.7A. The weak signals assigned to 7^1/8^{1,2} and 7^1/5 correlations are not detected in the 3D experiment and the assignment is tentative. Using the ^{13}C shifts from Table 5.1 and the information in Fig. 5.7A, all signals are assigned correspondingly in Fig. 5.7B for aggregated chlorin **2**.

5.4.2 Aggregation shifts

Significant upfield ^{1}H and ^{13}C aggregation shifts are observed and displayed as circles for values < -2.5 ppm in Fig. 5.8, relative to the monomer in DMSO. For chlorin **1** two sets of ^{13}C monomer shifts were determined both in DMSO and in THF. The ^{13}C shifts show significant differences when comparing the two solvents (Table 5.1). In contrast, the ^{1}H shifts are very similar for both solvents (Table 5.2). In addition, Fig. 5.9 compares the ^{1}H and ^{13}C chemical shifts for the aggregated chlorin **1** with the shifts for the monomer in DMSO. These correlation plots clearly show how pronounced the ^{1}H aggregation shifts are within the ^{1}H chemical shift range, in contrast to the ^{13}C aggregation shifts. The ^{1}H aggregation shifts are dominated by ring-current effects, in line with observations in other chlorophyll aggregates, and are more useful than the ^{13}C shifts for structure determination [30]. In particular, the ^{1}H aggregation shifts that are far from the diagonal in Fig. 5.9 are invaluable for structure determination.

In order to explain the aggregation shift patterns, structural models of coordinating chlorins were built [12, 36]. First, the modeling of sheets of molecules was done along very similar lines for chlorins **1** and **2**. The semi-empirical ZINDO/1 method suitable for transition metals [37], was used to calculate the atomic charges for subsequent MM+ force field optimization of the geometries, which was iterated until self-consistent structures were obtained. In this way, trimers were constructed by coordination of 3-hydroxymethyl oxygen to the Cd ion of the neighboring macrocycle, where the remaining third macrocycles were capped by a H_2O as a fifth ligand, and optimizedin ca. 5 iteration
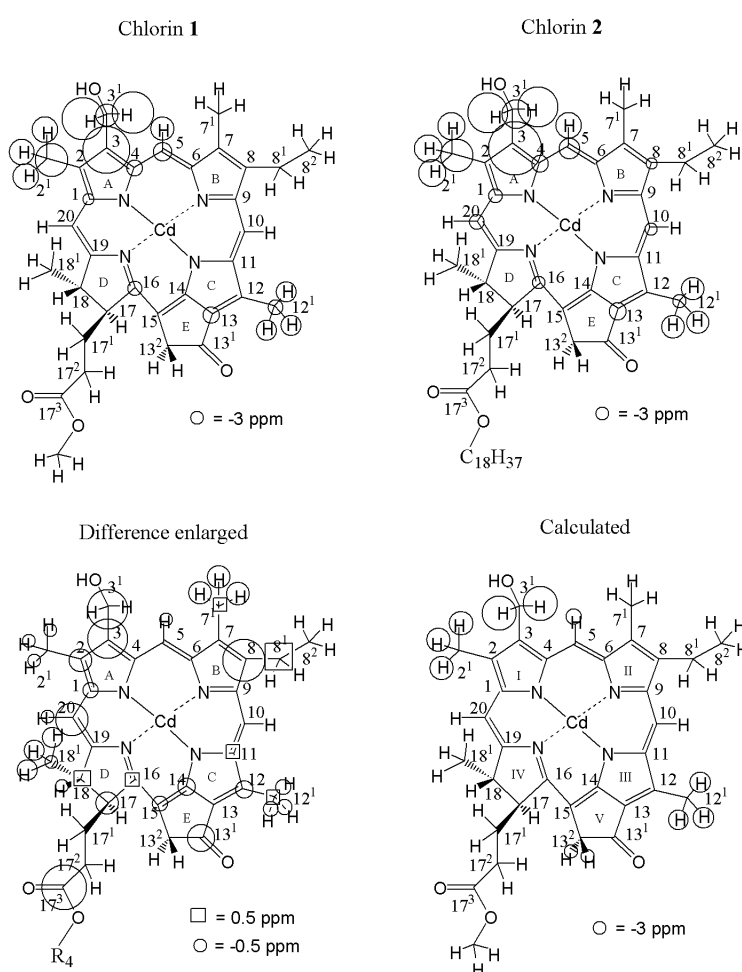
*Fig. 5.8. Detected ^1H and ^{13}C aggregation shifts of aggregated chlorin **1** and **2** relative to the monomers in DMSO-d6, the enlarged difference between the aggregates (chlorin **2** minus chlorin **1**) and calculated ^1H ring current shifts > 2.5 ppm. The circles have a radius proportional to the magnitude of the shift.*

steps. For larger structures, only the geometry was optimized with MM+. Pentamers were constructed by replacing the central molecules by three of its own copies. The charge of these molecules was negligible, the total charge thus remaining zero. Larger aggregates were built by placing multiple stacks together with the 3^1-OH groups of one stack within hydrogen bonding distance of the 13-C=O moieties of the next stack, followed by optimization with the MM+ force field. In this way, 26-mers of chlorin **1** and **2** were optimized consisting of 4 pentamer stacks and 2 trimer stacks at the outermost positions. Fig. 5.10 shows the central part of the resulting structure of chlorin **1**. The Cd-Cd distance is 6.4 Å, while the O•••H distance is approx. 2.2 Å. A Cd-Cd distance of 6.4 Å is well in line with electron diffraction data [21]. Layers of chlorin **2** are arranged similarly (see also Fig. 5.11).
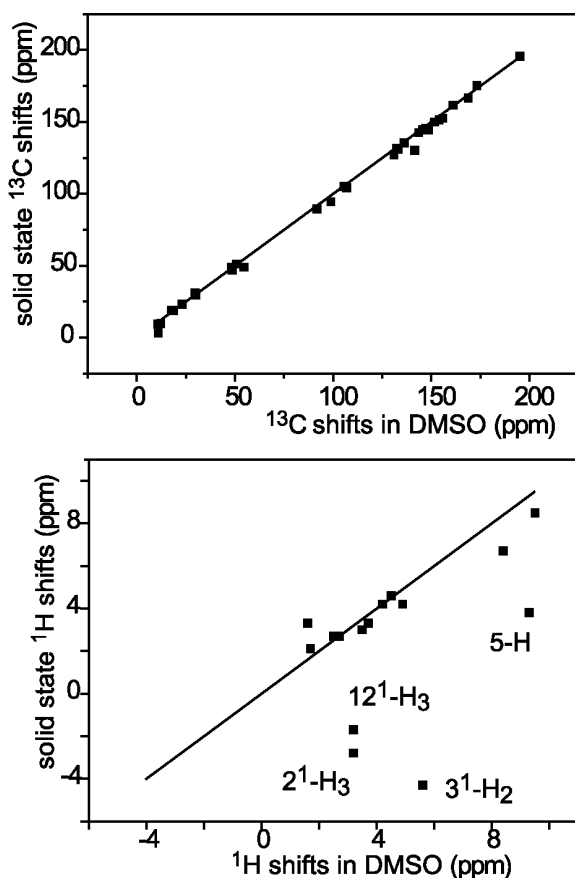
*Fig. 5.9. Chemical shift correlation plots of chlorin **1**. The ^1H and ^{13}C shifts in the solid sample are plotted against the monomer shifts in a DMSO solution. The solid lines represent the diagonals. Several ^1H signals are indicated that show a large upfield shift in the solid relative to the monomer.*

Subsequently, the layer structure of Fig. 5.10 was used for a ring current shift calculation. A molecule within the center of the 26-mer was selected and the positions of the neighboring macrocycles were used to define the unit cell of a two-dimensional lattice. The ^{1}H ring current shifts were calculated with the circular loop model and taking into account contributions within r_{max}=24 Å. The results (Fig. 5.8, Table 5.2) are in semi-quantitative agreement with the NMR measurements and reproduce the essential features, in particular the combination of very strong aggregation shifts in the 3-CH$_2$ region and significant 12-CH$_3$ shifts. About 50% of the magnitude of the observed ring current shifts can be attributed to neighbor molecules within the same stack. Another contribution of ~30% in the 3^1- and 12^1-regions originates from molecules in adjacent stacks overlapping due to the hydrogen bonding between the parallel inclined stacks (Fig. 5.10). Finally, the ring currents induced over larger distances account for the remaining ~20%. This demonstrates that the cumulative ring current effects can be very large in aggregated chlorophylls and reveal local microcrystalline order with a correlation length within the plane of a layer of at least ~24 Å.
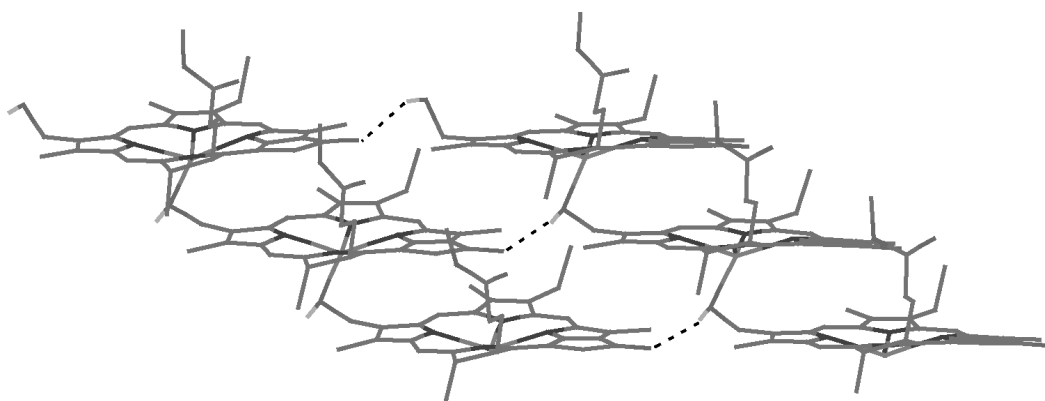
*Fig. 5.10. Structure of a layer of parallel inclined stacks of chlorin **1** used for the ring current shift calculation.*

The aggregation shift patterns for both chlorins are very similar (Fig. 5.8). The differences in aggregation shifts between the two chlorins, that are depicted enlarged in Fig. 5.8, indicate that the layer structure is marginally perturbed by the presence of the long tails. For example, the shift differences for the 3-, 3^1- and 13^1-carbons, for example, indicate that the C=O•••HO•••Cd bonding network is affected by the presence of the long stearyl tails. The overall layer structure of Fig. 5.10 is conserved, however, and induces a similar ring current shift distribution.

5.4.3 Metal bonding

Previous model studies have shown that the [113]Cd CSA tensor is very sensitive to the coordination state of the Cd^{2+} ion. For cadmium *meso*-tetraphenylporphyrin (Cd-TPP), the [113]Cd chemical shift anisotropy $\Delta\sigma = \sigma_{//} - \sigma_{\perp}$ is large, $\Delta\sigma = 341$ ppm [15]. The unique tensor element $\sigma_{33} = \sigma_{//}$ is very sensitive to the electronic environment within the plane of the macrocycle. It has a high value of 626 ppm, corresponding with a low electronic shielding. The other two elements $\sigma_{11} = \sigma_{22} = \sigma_{\perp}$ reflect the axial symmetry of the electronic system. The electronic shielding perpendicular to the porphyrin plane is relatively high with $\sigma_{\perp} = 285$ ppm. In the pyridine adduct (Py-Cd-TPP), the fifth ligand reduces the anisotropy to $\Delta\sigma = 105$ ppm. In the pyridyl adduct of cadmium protoporphyrin IX dimethyl ester (Cd-PPIXDME-PYR) the coordination is almost axial, with a [113]Cd chemical shift asymmetry $\eta = 0.32$ [17]. In Cd substituted myoglobin the Cd is coordinated by a histidine residue pulling the Cd strongly out-of-plane. This yields a crossover of $\sigma_{//}$ and $\sigma_{\perp}$ with $\Delta\sigma = -200$ ppm. These findings are supported by *ab initio* calculations [18].

The [113]Cd signals for the two aggregated chlorins (Fig. 5.6) show a very similar large negative anisotropy (Table 5.4). In the previous studies, nitrogen was considered as a fifth or sixth ligand, while here only oxygen is available. However, a similar conclusion as in Cd substituted myoglobin can be drawn. In particular, the $\sigma_{33} = 238$ ppm corresponds with a very high shielding, revealing a weak in-plane Cd-N bonding, with the Cd strongly out-of-plane and five-coordinated. For chlorin **1**, a small $\eta = 0.25$

indicates that the axial coordination is somewhat distorted to a degree comparable to Cd-PPIXDME-PYR [17]. These findings are in agreement with the layer structure of Fig. 5.10, where the Cd^{2+} ion has the 3^1-OH moiety as a fifth ligand. In addition, the 3^1-OH coordination to the Cd^{2+} ion is not axially symmetric, which explains the observed $\eta=$ 0.25 for the ^{113}Cd tensor. For chlorin **2**, the $\eta=$ 0.5 indicates that the Cd^{2+} ion is further away from the central axis.

The ^{15}N isotropic chemical shifts of chlorin **1** in solution as well as in the aggregated form (Fig. 5.5, Table 5.3) are within 10 ppm of the ^{15}N shifts of BChl *c* in methanol, except for the ^{15}N-D signals, which are shifted by up to ~15 ppm [38]. In pheophytin *a*, where the metal is replaced by H_2, the ^{15}N shifts of the N-A and N-C are decreased by ~60 ppm compared to Chl *a*, while the N-B and N-D ^{15}N shifts are increased by ~40 ppm [39]. Thus the ^{15}N data confirm that the metal is bound to the chlorin, although the ^{15}N spectra reveal a small fraction ~10% of Cd-chlorin in both samples where the Cd^{2+} ion is replaced by H_2 (Fig. 5.5) [38, 39]. The ^{15}N shifts show that the Cd-N bonding in aggregated chlorin **1** is very similar to the Mg-N bonding in BChl *c*.

The chemical shift tensor elements are also listed in Table 5.3. While the anisotropy is approximately similar for the four ^{15}N responses, the asymmetry of N-B and N-D is significantly higher than for N-A and N-C, which appears to correspond to a stronger Cd-N bonding.

The ^{15}N shifts of chlorin **2** are very similar with the exception of the ^{15}N-D signal that appears to be doubled in the aggregate with a difference of 10 ppm between the two components, while a single component is observed in DMSO (Table 5.3). For the formation of BChl *c* dimers in CCl_4 solution, it was found that the ^{15}N-D is most sensitive and shows a change of 4 ppm [38]. In the chlorosomes, the *syn* and *anti* layers are thought to give very similar ring current shifts, since they form mirror images with respect to the overlap between the macrocycles [11]. To explore the possibility that the ^{15}N signals are different between *syn* and *anti* configuration, a DFT calculation was performed at the BLYP/6-31G(d,p) level. To estimate the geometries, two monomers of chlorin **1** were optimized by the iterative ZINDO/1 and MM+ method with H_2O as a fifth

ligand in either the *syn* or the *anti* configuration. The metal-nitrogen distances are very similar for both configurations, while the structure of the macrocycle is perturbed. For these approximate *syn* and the *anti* geometries, a DFT calculation of the chemical shift was performed.

Table 5.5 summarizes the calculated ^{15}N shifts for the *syn* and the *anti* structures. The ^{15}N-D shift differs by ~5 ppm between the two structures, while the other three ^{15}N shifts differ by less than 1.5 ppm. Although the absolute calculated ^{15}N shifts agree only moderately with the observed shifts, they clearly show that the ^{15}N-D signal is much more sensitive to the *syn* or *anti* configuration than the other ^{15}N signals. In addition, according to the calculation several ^{13}C signals are also doubled with differences of 1-2 ppm, primarily in the ring D region (Table 5.5). Such splittings are difficult to resolve. However, the C-16 resonance in aggregated chlorin **2** is indeed doubled with a difference of 1.3 ppm (Table 5.1). Thus the theoretical results are in line with the NMR data and indicate that the aggregated chlorin **2** consists of a mixture of *syn* and the *anti* layers.

5.4.4   Intermolecular contacts

The correlations in Fig. 5.7 are the first to appear for increasing τ_m = 0.1-0.2 ms and are between nearby substituents of chlorin **1** and **2** spanning intramolecular ^{1}H distances $\lesssim$ 6 Å. A build-up rate in this range has also been found for the Chl *a*/H$_2$O aggregate in chapter 3 [40]. Many correlations in Fig. 5.7 involve one methyl group in line with the distribution of substituents around the chlorin ring, and span short ^{1}H distances $\lesssim$ 3 Å. Spin diffusion involving methyls is less efficient due to their fast rotation, which attenuates the dipolar couplings. In contrast, intramolecular correlations between two groups other than methyl are strong and can be observed over distances $\lesssim$ 6 Å. In particular the region near the 17-position has several protons forming a network where the spin diffusion proceeds rapidly. Thus a cross-peak in the CP^3 experiments indicates an efficient diffusion pathway between the two spins in a network of protons.
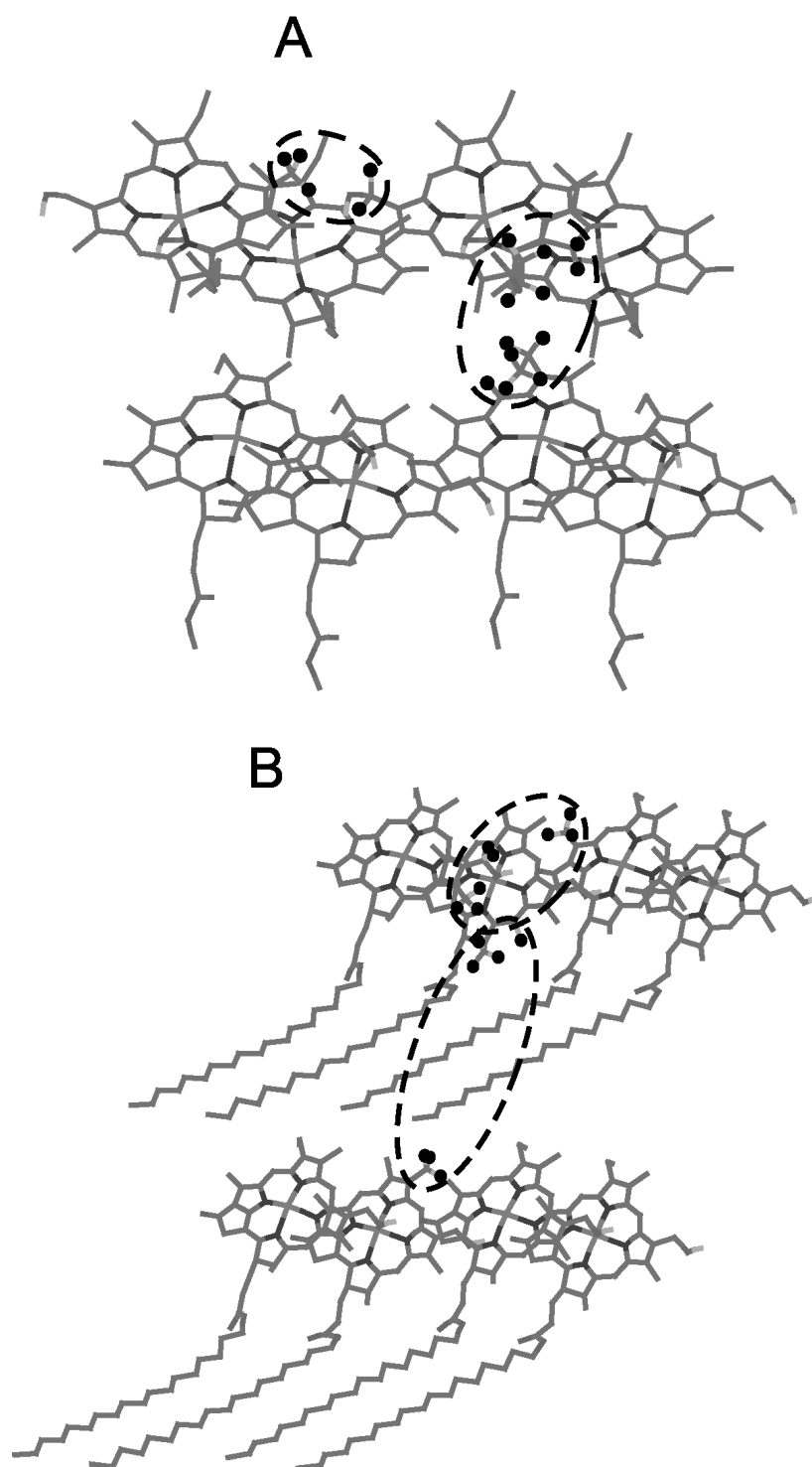
*Fig. 5.11. Calculated structure of aggregated chlorin **1** (A) and schematic structure of aggregated chlorin **2** (B) showing two sheets, containing two stacks of two molecules each. The black dots represent ^{13}C atoms involved in the intermolecular correlations.*

Several correlations in Fig. 5.7 are attributed to intermolecular transfer, since there is no intramolecular pathway in the proton network that can serve to correlate the resonances for $\tau_m = 0.2$ ms. While the differences between chlorins **1** and **2** are marginal for the intramolecular peaks, more significant differences can be observed for the intermolecular correlations. The $12^1/3^1$ intermolecular correlation in Fig. 5.7A is in excellent agreement with the layer structure in Fig. 5.10, since there are close contacts of ~2.5 Å between the nearest protons of these side chains (Fig. 5.11). This observation confirms the OH•••O=C hydrogen bonding between the stacks. In the chlorin **2** aggregate additional transfer between the 12^1- and 2^1-carbons is observed, which confirms the perturbation of the C=O•••HO•••Cd bonding network in the layers. The remaining intermolecular correlations are between the ring-B and ring-D regions located at the opposite sides of a layer. Hence, these correlations involve transfer between adjacent layers in a head-to-tail orientation. The specific correlations between adjacent layers are different between the two aggregates. This is attributed to the presence of the stearyl tails between the layers of chlorin **2**.

In a final step, 3D space-filling structures of the chlorin aggregates can be constructed as a result of these intermolecular correlations. For the microcrystalline chlorin **1** aggregate, multiple layers were brought within van der Waals bonding distance and optimized with the force field. The local crystal structure was described in chapter 4 [41]. Fig. 5.11A shows the arrangement of two neighboring layers. The energy of this arrangement was found to be 11 kcal/mole lower for the contact between two molecules in adjacent sheets than for a structure where the layers are isolated. This indicates favorable van der Waals interactions between the layers. The arrangement in Fig. 5.11A displays a network of strongly coupled ^{1}H spins where the 17 and 8 regions are in close contact, in accordance with the observed intermolecular correlations.

According to the NMR data, the aggregated chlorin **2** is more disordered than chlorin **1**. This resembles the chlorosomes, where a significant line broadening is also observed [11]. In the chlorosomes of *Chlorobium tepidum*, however, a splitting pattern around ring-B is observed that is associated with the bilayers [11]. In addition, the observed

transfer between the ring-B and ring-D regions in the aggregated chlorins is not consistent with the bilayer structure. In *Chloroflexus aurantiacus*, a monolayered tube with the tails on the exterior side and a central hole was proposed [42, 43]. In that case, the cavity should be filled with another low molecular weight compound, while the *in vitro* aggregated chlorins form a pure and dry sample. Hence the experimental evidence strongly favors planar sheets over tubular structures for both Cd-chlorins. The force field method is limited with respect to accurate modeling of the long tails in a large aggregate of chlorin **2**. Fig. 5.11B shows a schematic structure of two adjacent layers of chlorin **2**. The protons of the saturated stearyl chains form a dense three-dimensional network of very strongly coupled ^{1}H spins, which can explain the intermolecular transfer over a relatively large distance. A possible arrangement of bilayers with interdigitating tails, such as in Chl *a*/H_2O [40, 44], was also explored. In the Chl *a*/H_2O aggregate, however, the H_2O molecules form a hydrogen bonding network within a Chl *a* layer, which makes the layer structure much more open. The chlorin **2** layers are very dense, making it difficult for the tails to interdigitate. In addition, a doubling of the NMR response of the 7- and 8-substituents is observed in the Chl *a*, that is associated with conformational changes at the interface between adjacent bilayers, while the NMR results of chlorin **2** show single resonances for the 7- and 8-side chains. These contribute to the converging evidence for a head-to-tail arrangement of the layers.

5.5   Discussion

The organization of layers of BChl *c* in the chlorosomes, that is built upon the C=O•••HO•••Mg network [7, 11, 12] is conserved in the aggregated Cd-chlorins. This is also supported by other spectroscopic methods. In particular, the Q_y band is red-shifted, relative to the monomer in a polar solution, by 87 nm for chlorin **1** [21], while chlorin **2** is shifted by 91 nm. This compares well with the shifts of 85 nm and 88 nm observed for BChl *c* in the chlorosomes and BChl *c* precipitated from hexane [1]. The stretching frequencies of the 3^1-O-H and the 13-carbonyl C=O at 3140 and around 1640 cm^{-1}, respectively, are from the C=O•••HO•••Cd network in the aggregated chlorin **1** [21]. Thus the ligation and H-bond structural motif that is keeping the individual molecules

together in the chlorosomal antennae is robust, in the sense that the five-fold coordination and how it supports the intermolecular bonding network survives the substitution of Mg^{2+} by Cd^{2+}. The density of the layers depends on the bulkiness of the side chains. In particular, the natural BChl *c* has additional 3^1-Me and 20-Me substituents instead of hydrogens and in most cases a 12-Et instead of a 12-Me side group. Due to the less bulky substituents in the Cd-chlorins compared to the Mg forms, the stacking is more dense, which is evident from the exceptionally large aggregation shifts (Fig. 5.8). The plane-to-plane distance is ~3.5 Å, while a distance of ~4.5 Å was found for BChl *c* [11]. This is corroborated by a recent spectroscopic and molecular modeling study of Zn-chlorins, where the effect of various 3^1 substituents was investigated [36]. It was found that the Zn-substitute of the Cd analogue has a visible absorption band that is red-shifted to 740 nm compared to 705 nm for the corresponding (3^1R) type. Modeling of the latter Zn analogue yielded a plane-to-plane distance of ~4.1 Å, instead of ~3.5 Å without the 3^1-Me, which indicates a denser packing if the 3^1-Me is absent.

While the stacking is essentially similar to the chlorosomal antennae, the differences in molecular structure lead to a different self-organization on the supramolecular scale. In chapter 4 it was found that the chlorin **1** self-aggregates with a microcrystalline order and layers of chlorin are arranged in a head-to-tail orientation, in contrast with the tubular structures in the chlorosomes. The NMR data suggest that aggregated chlorin **2** is more disordered and both layers with *syn* and with *anti* stacking are found.

These differences of global self-organization reveal the essential factors controlling the tubular organization in the chlorosomes. First, in the chlorosomes, the 3^1-Me introduces the $[3^1R]$ and $[3^1S]$ stereoisomers. For various bacteriochlorophylls it has been found that the formation of higher aggregates and the degree of structural similarity to the chlorosomes depends on the 3^1-epimeric composition of the solution [45-57]. In the chlorosomes of *C. tepidum*, the 3^1-stereoisomers interact with the *syn* and *anti* configuration of the metal ion in the sense that a $[3^1S]$-*syn* inner layer surrounded by a $[3^1R]$-*anti* outer layer is thought to stabilize the tubular micelles [11]. In addition, in a study of the aggregation of BChl *e*, it was found that a minimal amount of the $[3^1S]$

stereoisomer is required for the formation of aggregates resembling the chlorosomal antennae [13, 49]. In particular, upon addition of the [3^1S] stereoisomer to a [3^1R] BChl *e* aggregate, the Q_y absorption band shifts from 706 nm to 717 nm indicating the reorganization from a lower aggregate to a chlorosome-like aggregate. The subtle interplay between the [3^1R] and [3^1S] stereoisomers that appears essential for the formation of the tubular micelles is absent in the Cd-chlorins. Without the 3^1-Me the Cd-chlorin molecules have C_s mirror symmetry with respect to the ring plane, with the exception of the ring D substituents, that are less important for the intermolecular binding. This points to the critical role for the 3-side chain, and the changes in the suprastructure are primarily attributed to the substitution of the 3-(1-hydroxyethyl) moiety with a 3-hydroxymethyl group lacking the 3^1-chirality.

The tails constitute another factor that is of interest to the suprastructure. In chlorin **1** the tails are truncated by a methyl. The structural modeling results suggest favorable weak interactions between the layers oriented head-to-tail, where the truncated tails perfectly fill the space between the 8-Et and 7-Me groups of the neighboring layer. In this way a microcrystalline solid can be formed. In the aggregated chlorin **2**, the suprastructure is different as a result of the tails. Although the stearyl tail does not have any significant interaction with the other substituents in a single molecule, it contributes to the entropic and interfacial energy terms in the free energy balance. The tails alone are apparently not sufficient for tubular micelles. In this respect the chlorosomal antennae are different from micelles of fatty acids. On the other hand, the tails induce structural disorder in the aggregate. As a result of this disorder, layers with both *syn* and *anti* stacking are formed, which resembles the chlorosomes.

5.6   Conclusions

Synthetic Cd-chlorins **1** and **2** are self-aggregated in cyclohexane and studied to gain insight into how key functionalities can steer the suprastructure of BChl *c* aggregation in the chlorosomes. With various MAS NMR experiments in combination with molecular modeling and ring current shift calculations, local structures are found that are similar to

the stacking of BChl *c* in the chlorosomes at the molecular level, while the supramolecular structure of tubular micelles is not formed. The aggregate chlorin **1** with the truncated tails appears to be microcrystalline with a monoclinic local symmetry. The aggregate chlorin **2** with the long stearyl tails is more disordered and the NMR response suggests the presence of both *syn* and *anti* layers. With these structures, several key factors controlling the self-organization in the chlorosomes can be designated. The Cd···OH···O=C motif induces self-organization in a robust bottom-up process in essentially the same fashion as the Mg···OH···O=C moieties in the chlorosomes. The packing of the molecules in sheets is more dense than for the chlorosomes and gives rise to very strong ring current shifts. The high density is attributed mainly to the 3^1- and 20-substituents, which are less bulky than in the chlorosomes. A quantitative analysis of the ring currents, including non-nearest neighbor effects, validates the layer structure that was built by molecular modeling. Intermolecular ^{13}C-^{13}C correlations provide a conclusive validation of the space-filling model structures. Sheets of chlorin are oriented head-to-tail in the aggregates. The model structures identify the 3-moiety in BChl *c* as a prerequisite for tubular suprastructure. It is envisaged that the $[3^1R]$- and $[3^1S]$-stereoisomers in the chlorosomes break the symmetry of the planar sheets and give rise to terms in the free energy balance that favor a tubular structure. The truncated tails in chlorin **1** lead to a microcrystalline structure. In contrast, the stearyl tails of chlorin **2** induce structural effects that resemble the chlorosomal antennae, in particular the presence of *syn* and *anti* layers. This suggests that the long tails are also needed for the formation of the antennae, probably due to the many weak interactions between the hydrogens of adjacent chains or the contribution of the flexible chains to the entropy of the system. In conclusion, this study shows how a balance of strong local interactions in a bottom-up process and terms in the free energy balance associated with a longer distance scale is responsible for this supramolecular assembly, which provides a view on evolutionary selection and may be of interest to future design of artificial structures.

*Table 5.1. ^{13}C chemical shifts of chlorins **1** and **2**.*

Position	$\sigma_{1,THF}$	$\sigma_{1,DMSO}$	$\sigma_{1,i}$	$\sigma_{2,DMSO}$	$\sigma_{2,i}$
12^1	12.5	12.2	9.2	12.2	9.4
2^1	11.4	10.9	3.3	10.8	3.2
7^1	11.3	10.7	9.8	10.7	10.3
8^2	18.1	17.6	[18.7]	17.5	[19.1]
8^1	20.3	18.7	18.7	18.8	19.7
18^1	23.8	23.0	23.1	23.1	22.6
17^1	31.3	29.6	31.0	29.7	30.6
17^2	31.3	30.2	29.6	30.5	30.1
13^2	49.7	48.3	48.7	48.3	48.6
18	50.6	48.5	47.0	48.5	47.7
17	53.0	50.7	51.2	50.8	50.3
3^1	56.9	54.5	49.0	54.6	47.4
20	92.3	91.7	89.6	91.8	88.3
5	100.3	98.8	94.4	98.9	94.3
15	107.2	105.5	105.0	105.6	103.7; 104.4
10	107.6	106.8	104.1	106.8	104.0
13	131.8	131.0	127.2	131.1	127.0
12	134.2	132.5	131.5	132.5	130.8
7	134.3	133.1	131.1	133.0	130.8
2	136.9	136.3	135.3	136.2	134.2
3	142.6	141.5	130.3	141.4	128.7
8	144.4	143.6	142.6	143.5	140.9
9	147.2	145.6	144.6	145.5	144.7
11	149.3	147.2	145.3	147.2	145.8
4	149.4	148.4	144.6	148.4	144.5
6	152.8	151.5	150.0	151.6	149.6
1	155.4	154.0	151.4	154.0	150.8
16	156.7	155.9	152.5	155.9	152.8; 154.1
14	162.8	161.1	161.6	161.0	160.9
19	169.2	168.8	166.7	168.7	166.7
17^3	173.8	173.2	175.2	172.8	173.7
13^1	195.1	195.2	195.5	195.1	194.4

Table 5.2. ^{1}H chemical shifts of chlorins 1 and 2 and calculated ring current shifts (ppm).

Position	$\sigma_{1,THF}$	$\sigma_{1,DMSO}$	$\sigma_{1,i}$	$\sigma_{2,DMSO}$	$\sigma_{2,i}$	σ_{calc}
12^1-H$_3$	3.6	3.5	-1.7	3.5	-2.3	-4.8
2^1-H$_3$	3.3	3.2	-2.8	3.2	-3.3	-5.6
7^1-H$_3$	3.2	3.2	3.0	3.2	2.1	-0.1
8^2-H$_3$	1.7	1.6	3.3	1.6	1.5	0.1
8^1-H$_2$	3.8	3.7	3.3	3.7	3.4	-0.1
18^1-H$_3$	1.7	1.7	2.1	1.7	4.1	-0.3
17^1-H$_2$	2.4	2.7	2.7	2.7	2.4	-1.4
17^2-H$_2$	2.4	2.5	2.7	2.5	2.4	0.0
13^2-H$_2$	4.9/5.2	4.9/5.2	4.2	4.9/5.2	3.9	-3.2
18-H	4.6	4.5	4.6	4.5	4.1	-0.3
17-H	4.2	4.2	4.2	4.2	3.9	-0.9
3^1-H$_2$	5.7	5.6	-4.3	5.6	-3.9	-8.1
20-H	8.4	8.4	6.7	8.4	6.2	-1.5
5-H	9.4	9.3	3.8	9.3	3.3	-3.6
10-H	9.5	9.5	8.5	9.5	8.1	-1.6

Table 5.3. ^{15}N chemical shifts and tensor elements (ppm) with the associated anisotropy and asymmetry parameters of chlorins 1 and 2.

Position	σ_{DMSO}	σ_i	σ_{11}	σ_{22}	σ_{33}	δ (kHz)	η
(1) N-A	192.7	193.0[a]	324	278	-22	-25	0.21
(1) N-B	221.6	219.3	421	265	-28	-28	0.63
(1) N-C	197.6	195.5[a]	347	265	-24	-25	0.37
(1) N-D	264.2	267.2	500	304	-3	-31	0.73
(2) N-A	193.3	192.8[b]	353	251	-18	-24	0.48
(2) N-B	222.2	218.8	406	266	-16	-27	0.60
(2) N-C	198.2	195.5[b]	353	251	-18	-24	0.46
(2) N-D	265.0	254.3;	472;	280;	10;	-28;	0.79;
		264.3	496	290	8	-29	0.80

[a] N-A and N-C could be interchanged. [b] N-A and N-C not fully resolved.

Table 5.4. ^{113}Cd chemical shifts (ppm) with the associated anisotropy and asymmetry parameters.

Chlorin	σ_{DMSO}	σ_i	σ_{11}	σ_{22}	σ_{33}	δ (kHz)	η
1	390	395 ± 3	494 ± 15	454 ± 15	238 ± 15	-39 ± 5	0.25 ± 0.13
2	n.d.	375 ± 3	484 ± 15	414 ± 15	228 ± 15	-37 ± 5	0.50 ± 0.16

Table 5.5. Calculated chemical shifts (ppm) for the syn and anti isomers, see text for details.

Position	*Syn*	*Anti*
N-A	185.6	184.1
N-B	198.5	199.3
N-C	196.4	196.0
N-D	232.0	227.4
C-10	107.7	106.7
C-16	150.0	151.0
C-17	64.4	62.9
C-18	58.9	60.0
C-20	93.3	94.3
C-17^1	43.8	41.7
C-17^2	44.2	45.6

References

[1]   J.M. Olson, *Photochem. Photobiol.* **67**, 61-75 (1998).

[2]   M.G. Müller, K. Griebenow and A.R. Holzwarth, *Biochim. Biophys. Acta* **1144**, 161-169 (1993).

[3]   M. Mimuro, Y. Nishimura, I. Yamazaki, M. Kobayashi, Z.Y. Wang, T. Nozawa, K. Shimada and K. Matsuura, *Photosynth. Res.* **48**, 263-270 (1996).

[4]   R. van Grondelle, J.P. Decker, T. Gillbro and V. Sundstrom, *Biochim. Biophys. Acta* **1187**, 1-65 (1994).

[5]   K. Griebenow, A.R. Holzwarth, F. van Mourik and R. van Grondelle, *Biochim. Biophys. Acta* **1058**, 194-202 (1991).

[6]   L.A. Staehelin, J.R. Golecki and G. Drews, *Biochim. Biophys. Acta* **589**, 30-45 (1980).

[7]   T.S. Balaban, A.R. Holzwarth, K. Schaffner, G.J. Boender and H.J.M. de Groot, *Biochemistry* **34**, 15259-15266 (1995).

[8]   R.E. Blankenship, J.M. Olson and B. Miller, "Anoxygenic Photosynthetic Bacteria", Kluwer, Dordrecht (1995).

[9]   P. Hildebrandt, H. Tamiaki, A.R. Holzwarth and K. Schaffner, *J. Phys. Chem.* **98**, 2192-2197 (1994).

[10]   D.C. Brune, T. Nozawa and R.E. Blankenship, *Biochemistry* **26**, 8644-8652 (1987).

[11]   B.J. van Rossum, D.B. Steensgaard, F.M. Mulder, G.J. Boender, K. Schaffner, A.R. Holzwarth and H.J.M. de Groot, *Biochemistry* **40**, 1587-1595 (2001).

[12]   A.R. Holzwarth and K. Schaffner, *Photosynth. Res.* **41**, 225-233 (1994).

[13]   D.B. Steensgaard, H. Wackerbarth, P. Hildebrandt and A.R. Holzwarth, *J. Phys. Chem. B* **104**, 10379-10386 (2000).

[14]   P.D. Ellis, R.R. Inners and H.J. Jakobsen, *J. Phys. Chem.* **86**, 1506-1508 (1982).

[15]   H.J. Jakobsen, P.D. Ellis, R.R. Inners and C.F. Jensen, *J. Am. Chem. Soc.* **104**, 7442-7452 (1982).

[16]   P.F. Rodesiler, E.A.H. Griffith, N.G. Charles, L. Lebioda and E.L. Amma, *Inorg. Chem.* **24**, 4595 (1985).

[17]   M.A. Kennedy and P.D. Ellis, *J. Am. Chem. Soc.* **111**, 3195-3203 (1989).

[18]   K. McAteer, A.S. Lipton, M.A. Kennedy and P.D. Ellis, *Solid State Nucl. Magn. Reson.* **7**, 229-238 (1996).

[19]   J. Matysik, Alia, G. Nachtegaal, H.J. van Gorkom, A.J. Hoff and H.J.M. de Groot, *Biochemistry* **39**, 6751-6755 (2000).

[20]   H. Tamiaki, M. Amakawa, Y. Shimono, R. Tanikaga, A.R. Holzwarth and K. Schaffner, *Photochem. Photobiol.* **63**, 92-99 (1996).

[21]   M. Amakawa and H. Tamiaki, *Bioorg. Med. Chem.* **7**, 1141-1144 (1999).

[22]   T. Miyatake, H. Tamiaki, A.R. Holzwarth and K. Schaffner, *Photochem. Photobiol.* **69**, 448-456 (1999).

[23]   G. Metz, X.L. Wu and S.O. Smith, *J. Magn. Reson. Ser. A* **110**, 219-227 (1994).

[24]   A.E. Bennett, C.M. Rienstra, M. Auger, K.V. Lakshmi and R.G. Griffin, *J. Chem. Phys.* **103**, 6951-6958 (1995).

[25]   A.E. Bennett, J.H. Ok, R.G. Griffin and S. Vega, *J. Chem. Phys.* **96**, 8624-8627 (1992).

[26]   J.J.H. Ackerman, T.V. Orr, V.J. Bartuska and G.E. Maciel, *J. Am. Chem. Soc.* **101**, 341 (1979).

[27]   J. Herzfeld and A.E. Berger, *J. Chem. Phys.* **73**, 6021-6030 (1980).

[28]   HBA 1.4, K. Eichele and R.E. Wasylishen, Dalhousie University.

[29]   I. de Boer, L. Bosman, J. Raap, H. Oschkinat and H.J.M. de Groot, *J. Magn. Reson.* **157**, 286-291 (2002).

[30]   R.J. Abraham and A.E. Rowan, in *Chlorophylls* (H. Scheer, Ed.) pp. 797-834, CRC Press, Boca Raton, FL (1991).

[31]   P.V. Schleyer, C. Maerker, A. Dransfeld, H.J. Jiao and N. Hommes, *J. Am. Chem. Soc.* **118**, 6317-6318 (1996).

[32]   E. Vinogradov, P.K. Madhu and S. Vega, *Chem. Phys. Lett.* **314**, 443-450 (1999).

[33]   F.M. Mulder, W. Heinen, M. van Duin, J. Lugtenburg and H.J.M. de Groot, *J. Am. Chem. Soc.* **120**, 12891-12894 (1998).

[34]   M. Wilhelm, H. Feng, U. Tracht and H.W. Spiess, *J. Magn. Reson.* **134**, 255-260 (1998).

[35]   A. Lange, S. Luca and M. Baldus, *J. Am. Chem. Soc.* **124**, 9704-9705 (2002).

[36]   S. Yagai, T. Miyatake, Y. Shimono and H. Tamiaki, *Photochem. Photobiol.* **73**, 153-163 (2001).

[37]   W.P. Anderson, W.D. Edwards and M.C. Zerner, *Inorg. Chem.* **25**, 2728-2732 (1986).

[38]   Z.Y. Wang, M. Umetsu, M. Kobayashi and T. Nozawa, *J. Am. Chem. Soc.* **121**, 9363-9369 (1999).

[39]   S.G. Boxer, G.L. Closs and J.J. Katz, *J. Am. Chem. Soc.* **96**, 7058-7066 (1974).

[40]   I. de Boer, L. Bosman, J. Raap, H. Oschkinat and H.J.M. de Groot, *J. Magn. Reson.* **157**, 286-291 (2002).

[41]   I. de Boer, J. Matysik, M. Amakawa, S. Yagai, H. Tamiaki, A.R. Holzwarth and H.J.M. de Groot, *J. Am. Chem. Soc.* **125**, 13374-13375 (2003).

[42]   L.A. Staehelin, J.R. Golecki, R.C. Fuller and G. Drews, *Arch. Mikrobiol.* **119**, 269-277 (1978).

[43]   V.I. Prokhorenko, D.B. Steensgaard and A.F. Holzwarth, *Biophys. J.* **79**, 2105-2120 (2000).

[44]   B.J. van Rossum, E.A.M. Schulten, J. Raap, H. Oschkinat and H.J.M. de Groot, *J. Magn. Reson.* **155**, 1-14 (2002).

[45]   M. Umetsu, J. Hollander, Z.Y. Wang, T. Nozawa and H.J.M. de Groot, *J. Phys. Chem. B* **108**, 2726-2734 (2004).

[46]   H. Tamiaki, S. Takeuchi, S. Tsudzuki, T. Miyatake and R. Tanikaga, *Tetrahedron* **54**, 6699-6718 (1998).

[47]   H. Tamiaki, M. Kubo and T. Oba, *Tetrahedron* **56**, 6245-6257 (2000).

[48]   T. Miyatake, T. Oba and H. Tamiaki, *ChemBioChem* **2**, 335-342 (2001).

[49]   Y. Saga, K. Matsuura and H. Tamiaki, *Photochem. Photobiol.* **74**, 72-80 (2001).

[50]   S. Sasaki, M. Omoda and H. Tamiaki, *J. Photochem. Photobiol. A-Chem.* **162**, 307-315 (2004).

[51]   S. Sasaki and H. Tamiaki, *Bull. Chem. Soc. Jpn.* **77**, 797-800 (2004).

[52]   H. Tamiaki, H. Kitamoto, A. Nishikawa, T. Hibino and R. Shibata, *Bioorg. Med. Chem.* **12**, 1657-1666 (2004).

[53]   T. Mizoguchi, Y. Saga and H. Tamiaki, *Photochem. Photobiol. Sci.* **1**, 780-787 (2002).

[54]   M. Kunieda, T. Mizoguchi and H. Tamiaki, *Photochem. Photobiol.* **79**, 55-61 (2004).

[55]   T.S. Balaban, A.R. Holzwarth and K. Schaffner, *J. Mol. Struct.* **349**, 183-186 (1995).

[56]   J. Chiefari, K. Griebenow, N. Griebenow, T.S. Balaban, A.R. Holzwarth and K. Schaffner, *J. Phys. Chem.* **99**, 16194-16194 (1995).

[57]   H. Tamiaki, S. Takeuchi, R. Tanikaga, S.T. Balaban, A.R. Holzwarth and K. Schaffner, *Chem. Lett.*, 401-402 (1994).

Chapter
6

General discussion and future outlook

6.1   Structure determination

The specific aim of the work described in this thesis is to study the molecular control of the self-assembly of pigment in the chlorosomes by resolving space-filling structures of model systems of aggregated chlorophyll. To achieve this goal the experimental methodology for MAS NMR structure determination was further developed. The MAS NMR investigations of the chlorosomes are reviewed in Chapter 1 and the development of experimental techniques, which forms the prelude to the work of this thesis, is summarized in Chapter 2.

A complete assignment of the ^{1}H and ^{13}C signals in the aggregated chlorophyll models was possible with 2D and 3D correlation spectroscopy. For the 3D experiment, a straightforward implementation of the ^{1}H free precession interval without radio-frequency decoupling was used, since the high magnetic field of 17.6 T combined with fast MAS of 15 kHz yields a sufficient resolution for an unambiguous assignment.

In aggregated chlorophylls the ^{1}H shifts relative to the monomer in solution are predominantly due to ring currents. This contrasts with the ^{13}C data. Here, the ring current effects are more difficult to interpret due to significant additional electronic perturbations of the ^{13}C shifts. The ^{1}H NMR data are reproduced well by ring current shift calculations for model structures, and the arrangement of the Cd-chlorins in layers as obtained from molecular modeling can be validated. This is described in detail in Chapter 5. Here, the spatial distribution of the induced ring currents is approximated by circular loops, while the magnitude of the ring current in a molecule is calibrated by a DFT calculation. The circular loop approximation is most probably the predominant

source of error in the calculation, and can be improved upon in the future, for example by using a 3D grid of ghost atoms around a chlorin molecule in a DFT calculation of the chemical shifts. In addition, the configuration space can be screened by an automated procedure in an efficient way and by obeying the restrictions imposed by the symmetry of the microcrystalline state for solutions that match the measured ^{1}H data. In this way, the ring current shift information is exploited maximally, and it is possible in principle to demonstrate the uniqueness of the structure with respect to the ^{1}H NMR data.

The strong dipolar couplings in the network of ^{1}H spins have enabled the observation of intermolecular contacts in aggregated chlorophylls in Chapters 3, 4 and 5. While many intermolecular constraints are required to determine *e.g.* folding conformations of proteins in solution, the supramolecular structure of chlorophylls is already restricted by the rigidity of the molecules and the top-down restrictions of the symmetry of a 3D space-filling structure. Hence, although the information from intermolecular correlations is not very precise due to the inhomogeneous distribution of the ^{1}H spins, the few additional global constraints can complete a space filling structure. For the solid Chl a/H$_2$O, for example, detailed structural information about the local arrangement in layers was known from previous studies [1]. It was shown in Chapter 3 with the CP^3 CHHC correlation experiment that the phytyl tails are fully stretched within bilayers, thus completing the description of the space-filling structure. For the aggregated Cd-chlorin models, the intermolecular contacts confirm the hydrogen bonding between adjacent stacks and provide the orientation of adjacent layers. Using these structural restraints, a local crystal structure was determined for the first time using MAS NMR, as described in Chapter 4. The CP^3 CHHC experiment can also provide structural restraints for the folding of a protein [2]. This is of interest, since these studies provide the first long-range intermolecular ^{13}C-^{13}C distance restraints in uniformly ^{13}C labeled systems.

Finally, other NMR nuclei, in particular ^{113}Cd and ^{15}N, have also been useful for the structural study of the chlorin aggregates. First, the chemical shift anisotropy of the ^{113}Cd signal provides convincing evidence for the five-coordination of the Cd^{2+} ion. This shows that the ^{113}Cd NMR can be used successfully to answer the first basic question about a

chlorophyll molecule in a solid environment, how the metal is coordinated. Second, the ^{15}N chemical shifts in conjunction with DFT chemical shift calculations have provided evidence for the co-existence of *syn* and *anti* layers. It is anticipated that experimental ^{15}N data, including the full CSA tensors, will be useful in the future to obtain information about the electronic or geometrical structure as a result of the increasing reliability and accuracy of chemical shift calculations.

6.2   Self-assembly

The detailed structural information of the aggregated chlorins obtained by MAS NMR reveals various contributions to the molecular control of the self-organization of BChl *c* in the chlorosomal antennae (Chapter 5). First, local interactions that are relatively strong, such as hydrogen bonding and metal coordination, lead to a network of molecules. In addition, the bulkiness of the 3- and 20-substituents regulates the density and induces curvature of the aggregate due to steric hindrance. These mechanisms constitute a bottom-up causal relation from the microscopic level to the mesoscopic level, since the details of the building blocks affect the suprastructure of the assembly. In contrast, there appear to be emerging factors controlling the global structure of the supramolecular assembly that can be understood only as a result of the collective interaction of many molecules in a downward causal relation steering the microscopic arrangement of the building blocks. For the BChl *c* aggregate in the chlorosomes, the net outcome is an organization into cylindrical elements, which is thought to facilitate the light-harvesting biological function of the chlorosomes [3].

The model studies confirm that the stereochemistry of the 1-hydroxyethyl moieties is a crucial factor for obtaining the tubular micelles. In the models the chiral 3-substituent is not present, and their aggregates form linear structures. In the model chlorins the symmetry of the ring is also broken at ring D, by the 17^1 and 18^1 side chains. For chlorin **1** this leads to a preference for the *anti* conformer. Evidently the energetic effects of the symmetry breaking at ring D are only moderate. They are ineffective when long tails are present, since the chlorin **2** aggregate comprises a mixture of the *syn* and *anti* conformers.

The structure of a supramolecular assembly is governed by the free energy change upon formation of the aggregate from the monomer elements,

$$\Delta G = \Delta H - T\Delta S. \tag{6.1}$$

The enthalpy change ΔH consists of the interactions between the chlorin molecules in the aggregate, minus the interaction between the monomer and the solvent that are broken. Several interactions were investigated by the model studies in this thesis: intermolecular metal coordination as well as the H-bonding, alignment of electric dipole moments, non-bonding steric interactions due to the bulkiness of side chains, interactions between the tails and steric hindrance involving the chiral 3-, 17- and 18-substituents.

The main conclusion of the model studies is that the bacteriochlorophyll aggregates in the chlorosomes form a supramolecular structure that is stable and robust against thermodynamic fluctuations by a balance between molecular bottom-up control and thermodynamic top-down control of the suprastructure. There appears to be an interplay between the thermodynamic phase behavior of the bulk and the molecular functionalities, providing a handle for evolutionary selection, and leading to biologically functional and stable chlorosome light-harvesting antennae. The interplay between the molecular control and the phase behavior at longer length scales leads to a classification in terms of a ΔG_{mol} and ΔG_{bulk} in the free energy balance of Eq. [6.1], according to

$$\Delta G = \Delta G_{\text{mol}} + \Delta G_{\text{bulk}} \tag{6.2}$$

The first term in this free energy change ΔG_{mol} comprises the enthalpy contributions predominantly involved in the molecular control over the suprastructure:

$$\Delta G_{\text{mol}} = \Delta H_{\text{HO}\cdots\text{M}} - \Delta H_{\text{steric}} + \Delta H_{\text{H-bond}} - \Delta H_{\text{R/S}} \tag{6.3}$$

The enthalpy gain $\Delta H_{\text{HO}\cdots\text{M}}$ due to coordination of the hydroxyl group to the metal ion of a neighboring molecule, leads to linear stacks, while the distance between the molecules

in the stack can be mediated by non-bonding steric interactions involving ring moieties described by the enthalpy cost ΔH_{steric}. Hydrogen-bond interaction $\Delta H_{H\text{-bond}}$ between adjacent stacks leads to the stabilization of layers that are strained by the interaction $\Delta H_{R/S}$ of the chiral $[3^1R]$ or $[3^1S]$ moieties with their structural environment. In parallel the symmetry breaking due to the 3-side chain produces a preference for *syn* or *anti* stacking, leading to two possible directions of curvature of a chlorin plane to minimize the strain $\Delta H_{R/S}$ that may help to establish a bilayer tube in chlorosomes. On the other hand, the bulk phase behavior is primarily governed by the interactions between the monomer and the solvent, the arrangement of electric dipole moments and the entropic term, according to

$$\Delta G_{bulk} = -\Delta H_{solvent} \pm \Delta H_{surface} + \Delta H_{dipole} - T\Delta S. \qquad (6.4)$$

The enthalpic part of ΔG_{bulk} also contains a global contribution $\Delta H_{surface}$ to the free energy difference that results from many weak surface interactions at interfaces other than the solvent interactions, such as the hydrophobic interactions between the tails of the chlorin molecules. Depending on the nature of these interactions, this term can be either positive or negative. The entropic part $T\Delta S$ is by definition, as a statistical concept, related to a large number of molecules and may be important in controlling the supramolecular structure of amphiphilic molecules, primarily since the entropy is affected by the conformations and degree of order of the long hydrophobic tails [4]. In this way, ΔG_{mol} represents the bottom-up driving force of the self-organization, while the other contribution, ΔG_{bulk}, contains the terms that become increasingly important for a larger number of molecules. Although these terms may be neglected in first order for the local organization of the aggregate into stacks or layers, they will be essential for the long-range organization of the supramolecular assembly and can become predominant over the molecular terms. For instance, it is thought that a minimal fraction of $[3^1R]$ or $[3^1S]$ will impose an overall curvature in a mixture of epimers. This illustrates how the free energy balance between molecular control and bulk phase behavior leads to robustness of the biological structure.

In the future, the various terms in Eqs. [6.3] and [6.4] can be quantified and phase diagrams for chlorophyll aggregation can be determined. In particular, details of how the chirality of the 3-substituent affects the structure in the chlorosomes may be provided by future MAS NMR studies of aggregates of pure [3^1R] and [3^1S] stereoisomers, together with epimeric mixtures, to distinguish between tubular and possibly other supramolecular structures.

References

[1]   B.J. van Rossum, E.A.M. Schulten, J. Raap, H. Oschkinat and H.J.M. de Groot, *J. Magn. Reson.* **155**, 1-14 (2002).

[2]   A. Lange, S. Luca and M. Baldus, *J. Am. Chem. Soc.* **124**, 9704-9705 (2002).

[3]   V.I. Prokhorenko, D.B. Steensgaard and A.R. Holzwarth, *Biophys. J.* **85**, 3173-3186 (2003).

[4]   A. Ben-Shaul, I. Szleifer and W.M. Gelbart, *Proc. Natl. Acad. Sci. U. S. A.* **81**, 4601-4605 (1984).

Appendix

This is the Maple routine that was used for the calculation of the ^{1}H ring currents.

```
> restart:
> #The formula for the secondary field
> m:=(-y*sin(psi)-x*cos(psi)+1)/((x-cos(psi))^2+(y-
sin(psi))^2+z^2)^(3/2);
> #The unit vectors of the 2D lattice in units of loop radius):
> a1:=-0.99;
> a2:=1.48;
> a3:=1.13;
> b1:=-2.46;
> b2:=4.06;
> b3:=-0.09;
> Bt:=0;
> #Generate 2D lattice vectors in nested loop:
> q:=-10;
> r:=-8;
> for i from 0 to 19 do
> q:=q+1;
> r:=-8;
> for j from 0 to 15 do
> r:=r+1;
> #Add unit vectors to 1H coordinates (in units of loop radius, origin
is ring center):
> x:=<x1H>+q*a1+r*b1;
> y:=<y1H>+q*a2+r*b2;
> z:=<z1H>+q*a3+r*b3;
> R:=sqrt(x^2+y^2+z^2);
> #Add to total if contribution within 2.4 nm sphere:
> if R<8 then
> #Calibration constant=2.87 ppm
> Bz:=evalf(Int(m,psi=0..6.2831853)*2.87);
```

```
> Bt:=Bt+Bz;
> end if;
> end do;
> end do;
> #Correct for intramolecular contribution:
> q:=0;
> r:=0;
> x:=<x1H>+q*a1+r*b1;
> y:=<y1H>+q*a2+r*b2;
> z:=<z1H>+q*a3+r*b3;
> Bz:=evalf(Int(m,psi=0..6.2831853)*2.87);
> Bt-Bz;
```

Summary

This thesis describes the self-assembly process of bacteriochlorophyll in the chlorosomes by experimental modeling, aiming for fundamental understanding of the organization of biological systems. In addition, the study of how self-assembly processes can be controlled by manipulating molecular building blocks is a central theme in nanotechnology, an important core technology for the near future. Two ^{13}C, ^{15}N labeled self-aggregated Cd-chlorin model systems for the chlorosomal antennae were studied, where several key chemical functionalities are modified with respect to the natural BChl, predominantly BChl *c*, in the chloromes. It is shown that the structural arrangement of these aggregates can be resolved in great detail using magic angle spinning (MAS) NMR. To achieve this, novel MAS NMR methodology for structure determination was developed.

In **chapter 1**, the context of the work of this thesis is summarized. Many of the existing MAS NMR techniques for structure determination of chlorophyll aggregates were developed using a microcrystalline Chl *a*/H$_2$O system. Therefore, the recent MAS NMR results in resolving the supramolecular structure of this aggregate are reviewed. In addition, the structural model of the chlorosomal antennae of *Chlorobium tepidum* is described. The bilayer tubular structure is an important point of reference for interpreting the results of the model studies that are presented in this thesis. In addition, **chapter 2** provides a theoretical background for the MAS NMR techniques that are used in this thesis.

The MAS NMR technology for structure determination of solids is rapidly developing, where most attention for biological applications is directed towards the folding of proteins in a solid environment, such as membrane proteins. Although this is obviously an essential topic, another challenge is to determine 3D space-filling structures of biological systems, including the intermolecular arrangement. The detection of long-range intermolecular ^{13}C-^{13}C correlations providing direct structural information is

difficult for uniformly ^{13}C labeled systems. **Chapter 3** introduces a MAS NMR experiment that is derived from a technique for the morphological characterization of polymers, where ^{1}H spin diffusion is an effective way to produce long-range magnetization transfer. The CP^3 CHHC transfer experiment employs a ^{1}H spin diffusion interval sandwiched between two additional CP steps. The details of the novel experiment are worked out for very short ^{1}H diffusion times of ca. 0.1-0.7 ms, which corresponds to a transfer range of ca. 3-10 Å. In particular, thorough phase cycling is necessary to prevent cross-talk artifacts. With this CP^3 experiment intermolecular ^{13}C-^{13}C correlations are detected for the Chl a/H$_2$O aggregate. These results refine the existing structural model and demonstrate that the long phytyl tails are stretched and interdigitating in the bilayers.

The MAS NMR structure determination is taken one step further in **chapter 4**, where it is shown that it is possible to establish a local crystal structure of a microcrystalline solid (chlorin **1**). The ring current shifts that are observed in the chlorin aggregates relative to the monomers in solution provide invaluable information about the stacking of the molecules. In particular the ^{1}H shifts are an accurate probe of the secondary fields induced by the aromatic rings. The ring current effects are calculated for the structural model that is obtained by force field calculations, using a circular loop approximation for the spatial part, while the magnitude of the effect is calibrated with a quantum mechanical DFT calculation. The calculations include the significant long-range contributions of non-nearest neighbors to the ^{1}H ring current shifts. The results show a good quantitative agreement with the experimental values and indicate a dense packing of the molecules in layers. In addition, the CP^3 experiment reveals a head-to-tail orientation of adjacent planar layers, thus completing the 3D structural model. The structure is ordered and is described by the local crystal parameters.

Chapter 5 presents the MAS NMR study of the chlorin **1** and **2** model aggregates and discusses the self-assembly of BChl c in the chlorosomes. The Cd-chlorin molecules differ from the natural BChl c in the central metal, the 3-, 12- and 20-side chains. Chlorin **1** has the tail truncated with methyl, while chlorin **2** has a stearyl tail. The detailed data

106

Summary

that is obtained from various 1D, 2D and 3D MAS NMR experiments include the ^{1}H and ^{13}C isotropic chemical shifts of the aggregates and of the monomers in solution, the ^{15}N and ^{113}Cd chemical shifts anisotropies of the aggregate and the isotropic shifts in solution. In addition, intermolecular ^{13}C-^{13}C correlations are observed using the CP^3 technique. The aggregates share a similar local arrangement of the molecules consisting of parallel inclined stacks. An essential element in the process of self-organization is formed by the C=O⋯HO⋯Cd intermolecular bonding network, very similar to the C=O⋯HO⋯Mg axis in the natural system. This indicates a robust bottom-up control of the local structure by these chemical functionalities. Anomalously large ring current shifts up to 10 ppm reveal a very dense stacking of the molecules in layers. From this dense stacking it is deduced that the bulkiness of the 3- and 20-side chains determine the overall density of the chlorophyll stacking. In addition, these model systems confirm and validate the essential role of the [3^1 *R*]- and [3^1 *S*]-stereoisomers in the formation of the chlorosomal antennae, since planar layers instead of tubular structures are formed without this chirality. With the tail truncated by methyl, a microcrystalline solid is formed, which is summarized in the previous chapter. The stearyl tails lead to a more disordered aggregate consisting of both *syn* and *anti* layers similar to the chlorosomes, as indicated by a doubling of the ^{15}N-D signal.

These results reveal a balance between local interactions and contributions to the free energy of the system associated with a longer distance scale, which is discussed in **chapter 6**. On the one hand, the details of the molecular building blocks lead to a supramolecular structure, such as the layers formed by the intermolecular bonding network. On the other hand, the suprastructure is controlled by factors with a collective thermodynamic nature. In particular, the symmetry breaking effect of the chiral 3-substituent and the disorder induced by the long tails allowing both the *syn* and *anti* conformations emerge from this study.

Samenvatting

Dit proefschrift beschrijft het proces van zelf-assemblage van bacteriochlorofyl in chlorosomen aan de hand van experimentele modellen. Enerzijds is dit van belang voor een fundamenteel begrip van de organisatie van deze biologische systemen. Anderzijds is het onderzoek naar hoe zelf-assemblageprocessen gestuurd kunnen worden door het manipuleren van moleculaire bouwstenen een centraal thema in de nanotechnologie, een belangrijke basistechnologie voor de nabije toekomst. Twee ^{13}C, ^{15}N gelabelde zelf-geaggregeerde Cd-chlorin-modelsystemen voor de chlorosomen zijn bestudeerd, waarbij verscheidene essentiële chemische functionaliteiten anders zijn in vergelijking met het natuurlijke BChl, vooral BChl *c*, in de chlorosomen. Er is aangetoond dat de structurele opbouw van deze aggregaten tot in detail opgelost kan worden met behulp van "magische hoek tollende" oftewel *magic angle spinning* (MAS) NMR. Om dit te bereiken zijn tevens nieuwe MAS-NMR-methoden ontwikkeld.

In **hoofdstuk 1** wordt de context geschetst van het werk van dit proefschrift. Veel van de bestaande MAS-NMR-technieken voor de structuurbepaling van chlorofylaggregaten zijn ontwikkeld met gebruik van een microkristallijn Chl *a*/H$_2$O-systeem. Daarom worden de recente resultaten wat betreft het ophelderen van de supramoleculaire structuur van dit aggregaat behandeld. Verder wordt het structurele model van de chlorosoomantenne's van *Chlorobium tepidum* beschreven. De bilaag-buisvormige structuur is een belangrijk referentiepunt voor het interpreteren van de resultaten van de modelstudies die in dit proefschrift gepresenteerd worden. Voorts geeft **hoofdstuk 2** een theoretische achtergrond voor de MAS-NMR-technieken, die in dit proefschrift gebruikt worden.

De MAS-NMR-technologie voor de structuurbepaling van vaste stoffen is snel in ontwikkeling, waarbij de meeste aandacht voor biologische toepassingen uitgaat naar de vouwing van eiwitten in een vaste omgeving, zoals membraaneiwitten. Hoewel dit uiteraard een essentieel onderwerp is, is een andere, minstens zo grote, uitdaging het

bepalen van 3D-ruimtevullende structuren van biologische systemen, dus inclusief de intermoleculaire opbouw. De detectie van intermoleculaire ^{13}C-^{13}C-correlaties over grote afstanden verschaft directe structurele informatie. De mogelijkheid hiertoe is echter tot nu toe beperkt geweest voor uniform ^{13}C-gelabelde systemen. **Hoofdstuk 3** introduceert een MAS-NMR-experiment dat aangepast is vanuit een techniek voor de morfologische karakterisering van polymeren, waarbij ^{1}H-spindiffusie een effectieve manier is om overdracht van magnetisatie over een lange afstand te genereren. Het CP^3-experiment gebruikt een ^{1}H-spindiffusie interval omsloten door twee extra CP-stappen. De details van het nieuwe experiment worden uitgewerkt voor zeer korte ^{1}H-diffusietijden van ca. 0.1-0.7 ms, wat overeenkomt met een overdracht over ca. 3-10 Å. Grondige filtering van signalen door middel van fase afwisseling is met name vereist om artefacten door doorspraak te voorkomen. Met dit CP^3-experiment worden intermoleculaire ^{13}C-^{13}C-correlaties waargenomen van het Chl *a*/H$_2$O-aggregaat. Deze resultaten verfijnen het bestaande structurele model en tonen aan dat de lange fytyl-staarten gestrekt zijn en in elkaar grijpen in de bilagen.

De MAS NMR structuurbepaling wordt in **hoofdstuk 4** nog een stap verder gebracht, waarbij wordt getoond dat het mogelijk is om een lokale kristalstructuur van een microkristallijne vaste stof (chlorin **1**) vast te stellen. De chemische verschuivingen door ringstromen, die worden waargenomen in de aggregaten ten opzichte van de monomeren in oplossing bieden zeer waardevolle informatie over de stapeling van de moleculen. Met name de ^{1}H verschuivingen vormen een zuivere maat voor de secundaire velden, die opgewekt worden door de aromatische ringen. De ringstroomeffecten worden berekend voor het structurele model, dat is opgesteld door middel van mechanische krachtveld (*force field*) berekeningen, waarbij een cirkelvormige ringstroom benadering is gebruikt voor het ruimtelijke deel in combinatie met een kwantummechanische DFT kalibratie voor de absolute sterkte van het effect. De berekeningen nemen ook de aanzienlijke bijdragen over langere afstanden mee van de niet-naaste buren aan de ringstroom verschuivingen. De resultaten vertonen een goede kwantitatieve overeenkomst met de experimentele waarden en wijzen op een dichte pakking van de moleculen in lagen. Verder laat een CP^3-experiment een kop-staart-oriëntatie zien van naburige vlakke lagen,

waarmee het 3D-model compleet is. De structuur is geordend en wordt beschreven door de locale kristalparameters.

Hoofdstuk 5 presenteert het MAS-NMR-onderzoek van de chlorin **1** en **2** model-aggregaten en behandelt de zelf-assemblage van BChl *c* in de chlorosomen. De Cd-chlorinmoleculen verschillen van het natuurlijke BChl *c* wat betreft het centrale metaalion, de 3-, 12- en 20-zijketens. Chlorin **1** heeft een staart die gekort is tot een methyl, terwijl chlorin **2** een stearylstaart heeft. De gedetailleerde data, die verkregen zijn door verscheidene 1D-, 2D- en 3D-MAS-NMR-experimenten, omvatten de ^{1}H- en ^{13}C-isotrope verschuivingen van de aggregaten en van de monomeren in oplossing, de ^{15}N- en ^{113}Cd-anisotrope verschuivingen in de aggregaten en de isotrope waarden van de monomeren in oplossing. Bovendien zijn intermoleculaire ^{13}C-^{13}C-correlaties waargenomen met de CP^{3}-methode. De aggregaten hebben een vergelijkbare locale ordening van de moleculen, die bestaat uit parallelle scheef gestapelde kolommen. Een essentieel onderdeel in het process van zelf-aggregatie wordt gevormd door het C=O⋯HO⋯Cd intermoleculaire bindingsnetwerk, analoog aan de C=O⋯HO⋯Mg as in het natuurlijke systeem. Dit duidt op een robuuste bottom-up-sturing van de locale structuur door deze chemische functionaliteiten. Anomaal grote ringstroom-verschuivingen tot 10 ppm onthullen een zeer dichte stapeling van de moleculen in lagen. Uit deze dichte stapeling wordt afgeleid dat de grootte van de 3- en 20-zijketens de globale dichtheid van de chlorofylpakking bepalen. Verder bevestigen en valideren deze modelsystemen de essentiële rol van de [3^{1}*R*]- en [3^{1}*S*]-stereoisomeren voor de vorming van de antenne's in de chlorosomen, omdat vlakke lagen in plaats van buisvormige structuren gevormd worden zonder deze chiraliteit. Met de korte methylstaart wordt een microkristallijne vaste stof gevormd zoals samengevat in hoofdstuk 4. De stearylstaarten leiden tot een meer wanordelijk aggregaat bestaande uit zowel *syn*- als *anti*-lagen zoals in de chlorosomen, wat wordt aangeduid door een opsplitsing van het ^{15}N-D-signaal.

Deze resultaten laten een balans zien tussen locale interacties en bijdragen tot de vrije energie van het systeem die geassocieerd worden met een langere afstandschaal. Dit wordt besproken in **hoofdstuk 6**. Aan de ene kant leiden de details van de moleculaire

bouwstenen tot een supramoleculaire structuur, zoals de lagen die gevormd worden door het intermoleculaire bindingsnetwerk. Aan de andere kant wordt de suprastructuur gestuurd door factoren met een collectief thermodynamisch karakter. Met name het symmetrie brekende effect van de chirale 3-substituent en de wanorde geïnduceerd door de staarten, die de beide *syn* en *anti* conformaties toelaat, komen naar voren uit dit onderzoek.

Publications

I. de Boer, L. Bosman, J. Raap, H. Oschkinat and H. J. M. de Groot, "2D ^{13}C-^{13}C MAS NMR correlation spectroscopy with mixing by true ^{1}H spin diffusion reveals long-range intermolecular distance restraints in ultra high magnetic field", *J. Magn. Reson.* **157**, 286-291 (2002).

I. de Boer, J. Matysik, M. Amakawa, S. Yagai, H. Tamiaki, A. R. Holzwarth and H. J. M. de Groot, "MAS NMR structure of a microcrystalline Cd-bacteriochlorophyll *d* analogue", *J. Am. Chem. Soc.* **125**, 13374-13375 (2003).

Alia, J. Matysik, I. de Boer, P. Gast, H. J. van Gorkom and H. J. M. de Groot, "Heteronuclear 2D (^{1}H-^{13}C) MAS NMR resolves the electronic structure of coordinated histidines in light-harvesting complex II: Assessment of charge transfer and electronic delocalization effect", *J. Biomol. NMR* **28**, 157-164 (2004).

I. de Boer and H. J. M. de Groot, "MAS NMR of the chlorosomes", accepted for publication in *Chlorophylls*, 2nd ed. (H. Scheer Ed.), Kluwer.

I. de Boer, J. Matysik, K. Erkelens, S. Sasaki, T. Miyatake, S. Yagai, H. Tamiaki, A. R. Holzwarth and H. J. M. de Groot, "MAS NMR structures of aggregated Cd-chlorins reveal molecular control of self-assembly of chlorosomal bacteriochlorophylls", *J. Phys. Chem. B*, in press.

I. de Boer, J. Matysik, S. Sasaki, T. Miyatake, S. Yagai, H. Tamiaki, A. R. Holzwarth, H. J.M. de Groot, "Self-organization of BChl *c* in chlorosomes studied by MAS NMR of aggregated Cd-chlorins", *Proceedings of the 13th International Congress of Photosynthesis*, in press.

Curriculum vitae

Het VWO heb ik doorlopen aan het Stedelijk Gymnasium Leiden, waarna ik in september 1994 begonnen ben aan de studie Technische Natuurkunde aan de TU Delft. Mijn afstudeeronderzoek naar luminescente fosfors voor Plasma Display Panels heb ik verricht onder leiding van dr. P. Dorenbos en prof. C. W. E. van Eijk in de groep Instrumentatie Stralingsonderzoek aan het Interfacultair Reactor Instituut. Mijn ingenieursbul heb ik behaald in 2000. Tevens heb ik dat jaar de prodedeuse psychologie afgerond aan de Universiteit Leiden. In september van dat jaar ben ik mijn promotieonderzoek begonnen in de groep Biofysische Organische Chemie van prof. H. J. M. de Groot. Tijdens mijn onderzoek heb ik vaste-stof-NMR-methoden ontwikkeld voor de structuurbepaling van chemische modelsystemen voor biologische antennesystemen. Door toepassing van deze methoden is inzicht verkregen in de moleculaire zelf-assemblage van deze antenne's. De resultaten van dit onderzoek heb ik kunnen presenteren met posters tijdens verscheidene internationale conferenties: "The 2nd (3rd) Alpine Conference on Solid-State NMR," Chamonix-Mont Blanc, Frankrijk (sept. 2001 (2003)) en "The XXth International Conference on Magnetic Resonance in Biological Systems," Toronto, Canada (aug. 2002) en als voordracht tijdens andere conferenties: "The NMR Discussion Group," Vlaardingen (okt. 2002), "The Dutch Polymer Days," Lunteren (feb. 2004), "The International Workshop on Supramolecular Nanoscience of Chemically Programmed Pigments," Kusatsu, Japan (juni 2004) en "The 13th International Congress of Photosynthesis," Montréal, Canada (aug. 2004).

Nawoord

Bij het totstandkomen van dit proefschrift hebben velen een rol van betekenis gespeeld. Om te beginnen is al mijn praktische ervaring met MAS-NMR opgebouwd door de grote hulpvaardigheid van Johan Hollander, Kees Erkelens en Fons Lefeber. Daarnaast waren inhoudelijke discussies met Jörg Matysik, Suzanne Kiihne, Francesco Buda en Johan van der Maarel van belang voor de ontwikkeling van methoden en het interpreteren van resultaten.

My appreciation for the valuable discussions goes to Alfred Holzwarth, Silviu Balaban and Hitoshi Tamiaki,

共同研究者としての指導のみならず、日本での講演の機会をいただいた民秋均教授、ならびに有益な議論と観光案内をしてくれた佐々木真一博士に感謝いたします。

Frans Hulsbergen ben ik erkentelijk voor het aanleveren van de ideale foto voor de omslag van dit proefschrift. Liesbeth van der Velden vormde de altijd vriendelijke en ondersteunende bezetting van het secretariaat. Een onvergetelijke tijd dank ik aan iedereen bij SSNMR en de BOF groep van Johan Lugtenburg, met name mijn mede-promovendi Prasad, Sylvia, Adriaan, Shipra, Prashant, Anna, Esha, Eugenio en Richard voor de gezelligheid in het lab en daarbuiten. De steun van Mechteld, mijn ouders, familie en vrienden was onontbeerlijk om dit wonderbaarlijke en emotioneel afwisselende project tot een goed einde te brengen. Tenslotte wil ik dit proefschrift opdragen aan de onlangs overleden Leon Bosman, die als afstudeerder een bijdrage heeft geleverd aan het ontwikkelen van de experimentele technieken en wiens pure fascinatie voor wetenschappelijk onderzoek mij scherp voor de geest staat.

Leiden, september 2004   Ido de Boer